University of Kentucky

UKnowledge

2023

CONSERVED NOVEL INTERACTIONS BETWEEN POST-REPLICATIVE REPAIR AND MISMATCH REPAIR PROTEINS HAVE DIFFERENTIAL EFFECTS ON DNA REPAIR PATHWAYS

Anna K. Miller
University of Kentucky, akmil2048@gmail.com
Author ORCID Identifier:
 https://orcid.org/0000-0001-7329-9996
Digital Object Identifier: https://doi.org/10.13023/etd.2023.422

Right click to open a feedback form in a new tab to let us know how this document benefits you.

STUDENT AGREEMENT:

I represent that my thesis or dissertation and abstract are my original work. Proper attribution has been given to all outside sources. I understand that I am solely responsible for obtaining any needed copyright permissions. I have obtained needed written permission statement(s) from the owner(s) of each third-party copyrighted matter to be included in my work, allowing electronic distribution (if such use is not permitted by the fair use doctrine) which will be submitted to UKnowledge as Additional File.

I hereby grant to The University of Kentucky and its agents the irrevocable, non-exclusive, and royalty-free license to archive and make accessible my work in whole or in part in all forms of media, now or hereafter known. I agree that the document mentioned above may be made available immediately for worldwide access unless an embargo applies.

I retain all other ownership rights to the copyright of my work. I also retain the right to use in future works (such as articles or books) all or part of my work. I understand that I am free to register the copyright to my work.

REVIEW, APPROVAL AND ACCEPTANCE

The document mentioned above has been reviewed and accepted by the student's advisor, on behalf of the advisory committee, and by the Director of Graduate Studies (DGS), on behalf of the program; we verify that this is the final, approved version of the student's thesis including all changes required by the advisory committee. The undersigned agree to abide by the statements above.

<div align="right">

Anna K. Miller, Student

Dr. Eva M. Goellner, Major Professor

Dr. Isabel Mellon, Director of Graduate Studies

</div>

CONSERVED NOVEL INTERACTIONS BETWEEN POST-REPLICATIVE REPAIR AND MISMATCH REPAIR PROTEINS HAVE DIFFERENTIAL EFFECTS ON DNA REPAIR PATHWAYS

_____

DISSERTATION

_____

A dissertation submitted in partial fulfillment of the
requirements for the degree of Doctor of Philosophy in the
College of Medicine
at the University of Kentucky

By

Anna Kristin Miller

Lexington, Kentucky

Co- Directors: Dr. Eva Goellner, Assistant Professor of Toxicology and Cancer Biology

And Dr. Isabel Mellon, Associate Professor of Toxicology and Cancer Biology

Lexington, Kentucky

2023

ABSTRACT OF DISSERTATION

CONSERVED NOVEL INTERACTIONS BETWEEN POST-REPLICATIVE REPAIR
AND MISMATCH REPAIR PROTEINS HAVE DIFFERENTIAL EFFECTS ON DNA
REPAIR PATHWAYS

DNA mismatch repair (MMR) is the DNA repair mechanism that repairs base-base mispairs and small insertions and deletions remaining after replication. MMR is also required for apoptosis after certain types of exogenous DNA damage that result in damage-associated mispairs. The basic MMR mechanism is well understood; however, proteins associated with MMR continue to be identified. The roles of these interacting proteins in MMR are largely unknown. We have identified the yeast protein Rad5 as a novel interactor of the critical MMR proteins Msh2 and Mlh1. Rad5 is a DNA helicase and E3 ubiquitin ligase involved in post-replicative repair. However, to date, Rad5 has no known role in MMR despite interacting with both MMR factors. We show that the deletion of yeast *RAD5* does not have the mutation rate or mutation spectrum associated with defective canonical MMR. Rad5's interactions with MMR are conserved throughout evolution and split between its human homologs, HLTF and SHPRH.

Human MSH2 interacts with HLTF regardless of damage, whereas human MLH1 interacts with SHPRH in an MMR-specific damage-dependent manner. Loss of HLTF or SHPRH, alone or in tandem, does not affect canonical MMR. SHPRH knockdown or knockout induces a moderate resistance to MMR-mediated apoptosis; however, loss of HLTF does not affect MMR-mediated apoptosis. We recently confirmed that our HLTF and SHPRH knockout cells affect survival after exposure to DNA-damaging agents that are substrates for post-replicative repair. Loss of MSH2, but not MLH1, also confers a resistance to apoptosis when treated with DNA damage related to post-replicative repair.

This study defines a novel accessory factor that binds with MMR proteins and is conserved from yeast to humans. This study also provides a deeper understanding of how MMR accessory factors may provide a mechanistic distinction between canonical and non-canonical MMR and how MMR influences post-replicative repair pathways. Understanding the interplay between MMR and other repair pathways is essential for cancer development and treatment implications.

Anna Kristin Miller
_____
(Name of Student)

10/19/2023
_____
Date

CONSERVED NOVEL INTERACTIONS BETWEEN POST-REPLICATIVE REPAIR AND MISMATCH REPAIR PROTEINS HAVE DIFFERENTIAL EFFECTS ON DNA REPAIR PATHWAYS

By
Anna Kristin Miller

Dr. Eva Goellner
Co-Director of Dissertation

Dr. Isabel Mellon
Co-Director of Dissertation

Dr. Isabel Mellon
Director of Graduate Studies

10/19/2023
Date

DEDICATION

This dissertation is dedicated to my family.

ACKNOWLEDGMENTS

me to this day, and I am so grateful for that. Dr. Blackburn, you welcomed me into your lab as an undergraduate and showed me the potential to do research that will help others. You taught and continue to be a valued mentor for me, and I enjoy getting to catch up with you and talk about graduate school and what's going on in life. I am also thankful that you were willing to be my outside examiner, being able to have you involved in this process is something that I treasure.

To all of those at Procter and Gamble – thank you all for giving me the opportunity of a lifetime. Each of the people I met during my short time there were so kind and willing to teach and I am looking forward to joining the team and working with you all.

I also want to thank my family for all their support – you have pushed me and encouraged me to pursue my passions, even when I was figuring it out. Mom and Dad – thank you for loving me and instilling a Christian faith in me that has carried me throughout graduate school and life. Kelsey and Maggie – thanks for being the best sisters I could have and talking with me through good times and bad. I also want to thank all of my grandparents and extended family – your unwavering support and faith in me is something I will always cherish. And to my in-laws: Dave and Carol, Aaron and Rebekah, Jacob, and all the others – thank you for bringing me in and treating me like family. Without all my family, there is no way I would be where I am now.

Last but definitely not least, I have to thank my husband, Michael. I don't know what I would have done without your support in this process. You push me to be my best self both with research and throughout life and have always believed in me. You were a huge part of this process and for that I say thank you.

And to all those I have not mentioned but have helped me in some way, shape, or form (there are too many to count) – thank you all.

TABLE OF CONTENTS

LIST OF TABLES

LIST OF FIGURES

CHAPTER 1. INTRODUCTION

1.1   DNA Damage and Repair

A vital component of every living thing is the presence of DNA, which is conserved during replication and passed down from parent to offspring. As a result, the conservation of DNA sequences is essential to maintaining function within cells and our body as a whole. As such, DNA replication fidelity is crucial, and the utilization of highly selective polymerases with exonuclease proofreading ability paired with mismatch repair results in a mutation rate of approximately 1×10^{-9}, or one error in every billion base pairs [1]. Our body – and consequently DNA – is constantly being exposed to stressors that cause damage to the DNA. There are two main origins for DNA damage: endogenous and exogenous DNA damage [2]. Endogenous DNA damage can result from replication errors, reactive oxygen species (ROS), methylation, abasic sites, and base deamination [2]. Exogenous damage can result from ionizing radiation, ultraviolet radiation, chemotherapeutics, and environmental agents such as alkylating agents, aromatic amines, and polycyclic aromatic hydrocarbon [2].

The presence of a wide variety of mechanisms and agents that can damage DNA causes a wide range of damage to the DNA, including but not limited to mispairs, insertions/deletions, base adducts, intra- and inter-strand crosslinks, single-stranded DNA breaks, and double-stranded DNA breaks [3]. Due to varying types of DNA damage, multiple DNA repair pathways are specialized for the different DNA damages that occur. There are five major DNA repair pathways: base excision repair (BER), nucleotide excision repair (NER), homologous recombination (HR), non-homologous end joining (NHEJ), and mismatch repair (MMR) [2]. In addition, pathways are present that bypass DNA

lesions that can cause replication fork collapse and genomic instability. Post-replicative repair (PRR) helps to bypass DNA lesions through its use of lower fidelity DNA polymerases through two branches, error-free and error-prone PRR [2]. Utilizing these pathways helps prevent genomic instability and, ultimately, disease development and progression. Although DNA repair and damage tolerance pathways may each specialize in a specific type of DNA damage, previous publications have shown an overlap between DNA repair pathways [4–7]. This review will focus on DNA mismatch repair and its accessory factors to highlight the interplay between mismatch repair and other DNA repair pathways.

1.2 DNA Mismatch Repair

DNA mismatch repair (MMR) is one of the major DNA repair pathways – it focuses on repairing mismatches and insertions and deletions left in the DNA after replication [3,8]. The steps for canonical MMR are as follows: mispair recognition by the MSH2-MSH6 or MSH2-MSH3 heteroduplex, recruitment of MLH1-PMS2 (Mlh1-Pms1 in humans), nicking of the daughter strand by MLH1's endonuclease activity, recruitment of EXO1 to excise before and past the mispair, DNA gap filling by DNA polymerases with PCNA, and finally, ligation which leaves a DNA strand that is now error free [9–11]. Utilizing the canonical role of the MMR pathway substantially increases replication fidelity, up to 1000-fold, making the error rate approximately one mismatch for every 10^9 bases [1]. MMR also has a non-canonical role of initiating apoptosis in the presence of certain types of DNA-damaging agents, such as MNNG [12,13]. MNNG is an alkylating agent that creates an O6-methylguanine, which is often mispaired with a thymidine during the next round of replication [13]. MMR recognizes that a mispair is present but cannot resolve the damage,

resulting in the initiation of cell cycle arrest and apoptosis [13]. Both the canonical and non-canonical MMR pathway prevents the accumulation of mutations, which can ultimately lead to genomic instability and diseases such as cancer [8,12,14].

Mismatch repair defects can be seen in the clinic by measuring a phenotype known as microsatellite instability, or MSI, where there is an accumulation of insertions and deletions in several repeat sequences known to be prone to sporadic expansions and contractions that require DNA MMR to maintain sequence fidelity [15,16]. Approximately 15% of sporadic colorectal cancers are identified to have MSI [17,18]. Other sporadic cancers can also have an MSI phenotype, and patients with MSI cancers are now being recognized as candidates for immunotherapy treatment due to the high tumor mutation burden and accumulation of neoantigens in MMR-defective tumors [19]. Defective MMR has also been associated with the familial cancer predisposition syndrome Hereditary Nonpolyposis Colorectal Cancer (HNPCC), also known as Lynch syndrome [13,20–23]. Most of the mutations found in Lynch syndrome have been identified in the MMR proteins, primarily MLH1 and MSH2; however, some cases do not have mutations in known MMR proteins [9,10,21,22]. Understanding the role of proteins in the MMR pathway can be crucial in identifying additional players that could be important in disease detection and treatment.

The general mechanism for canonical mismatch repair is well known and has essential MMR proteins, specifically MSH2 and MLH1. Although there are key players, accessory factors also play an important role in the MMR mechanism, as shown by the overlap in the functions of some accessory factors. Many accessory factors interact with at least one of the critical mismatch repair proteins. Interactors of the integral MMR protein MLH1 often have an MLH1-interacting peptide (MIP) box or an MLH1-interacting

motif (MIM) [24,25]. A site present on multiple MSH2 interacting partners and has

conservation in different species has also been recently identified and coined the MSH2-

interacting peptide (SHIP) box [26]. These conserved sites have been utilized to identify

multiple proteins that interact with the critical MMR proteins and play a role in the MMR

pathway [24,26–29]. Identifying novel accessory factors of MMR has provided further insight

into the nuances of the MMR mechanism, and many of these proteins have also been

associated with cancer.

1.3   Accessory Factors in Yeast

1.3.1   *MMR Homologs as Accessory Factors*

Much of the groundwork in identifying the mechanism of MMR has been

performed in the yeast *Saccharomyces cerevisiae*. Because of the techniques developed to

understand MMR, interacting partners can be identified, and their role can be MMR

investigated. One of the MMR accessory factors identified was Mlh2, a MutL homolog

that complexes with Mlh1 [30]. The role of the Mlh1-Mlh2 complex was less understood

than the Mlh1-Pms1 or Mlh1-Mlh3 heterodimers [30]. It was found that Mlh2 and Pms1

formed similar foci, with foci formation occurring with downstream MMR inhibition and

loss of foci occurring with MMR mispair recognition defects [31]. The role of Mlh2 as an

accessory factor is supported since the loss of Mlh2 individually does not affect mutation

rates, but loss of Mlh2 in conjunction with loss of Msh6 or Pms1 has a synergistic increase

in mutation rate [31]. Overexpression of Mlh2 did increase in mutation rate, likely due to

outcompeting Pms1 binding to Mlh1 while not having the endonuclease activity present

in Pms1 [31]. Loss of Mlh2 not having a mutator phenotype of its own in addition to the

similar foci formation to Pms1 while lacking endonuclease activity indicates that Mlh2 is an accessory factor for MMR, likely enhancing Pms1-Mlh1 MMR activity.

1.3.2   *DNA Repair Proteins as MMR Accessory Factors*

Strengthening the argument of overlap between the various DNA repair mechanisms, *S. cerevisiae* Ntg2 was identified as an interactor of Mlh1 [24,32]. Ntg2 is a DNA N-glycosylase/AP lyase that has a role in BER by removing the damaged base and DNA backbone after oxidative damage [32]. Ntg2 was not known to be a player in MMR since the loss of Ntg2 did not have a mutator phenotype; however, overexpression of Ntg2 had an increased mutator phenotype, although not to the extent of defective Mlh1 [32]. This established the hypothesis that Ntg2 could be an accessory factor for MMR since the overexpression of Ntg2 could act in a manner similar to Mlh2, which is proposed to outcompete Mlh1's primary interactors.

1.3.3   *Identification of a Conserved Mlh1 Binding Region*

Identifying Ntg2 as an MMR accessory factor allowed a conserved amino acid motif to be distinguished on numerous Mlh1 interacting proteins. Gellon established that Ntg2 had a sequence similarity to other Mlh1 interactors, Exo1 and Sgs1, and mutation of some of the amino acids within the conserved region decreased the interaction between Ntg2 and Mlh1 [32]. Building on this paper, Dherin characterized the Mlh1 binding motif in the interacting proteins and named the motif an Mlh1-interacting protein, or MIP, box [24]. The MIP box was present in the yeast Mlh1 interacting proteins Exo1, Ntg2, and Sgs1, with mutations in the MIP box disrupting interactions with both yeast Mlh1 and human MLH1 [24]. The MIP box may also be important for an interacting protein's role in MMR, with Exo1's MIP region corresponding to a role in MMR but not post-replicative repair [33].

The MIP box was conserved in human MLH1 interactors, many of which are homologs to the yeast Mlh1 interactors [24,25,28]. Dherin also identified a region on Mlh1, coined the S2 site, which was shown to be essential for proteins that interacted with MLH1 via the MIP box. This site also affects Exo1-dependent MMR since Exo1 interacts with Mlh1 via its MIP box [24]. The presence of the MIP box was further supported by looking at the crystal structure of Mlh1 and its MutLα partner, Pms1. Looking at the structure of Mlh1 gave more insight into how the MIP box and S2 sites interacted between Mlh1 interactors and Mlh1, respectively [34]. The S2 site of Mlh1 did not seem to have a conformational change after binding with the MIP box containing proteins; however, it did confirm the location of the S2 site that was previously stated and strengthened the argument that the serine and two aromatic residues are essential in the MIP box motif [34].

Another protein identified as an accessory factor is the *S. cerevisiae* helicase protein Sgs1. MMR was shown to have a role in suppressing homeologous recombination, and Sugawara set to establish the role of MMR in heteroduplex rejection through the single-strand annealing (SSA) pathway [35]. This paper identified that *msh2Δ* and *msh6Δ* have a decrease in heteroduplex rejection, and it determined that *sgs1Δ* also decreases the heteroduplex rejection [35]. Goldfarb expanded on this work by showing that the MMR activity of Msh2 and Msh6 and the helicase activity of Sgs1 are important for heteroduplex rejection [36]. This strengthened the argument that Msh2-Msh6 was interacting with Sgs1, mainly since a mutation of Sgs1 that left the helicase domain intact also affected heteroduplex rejection, indicating that it may disrupt the interactions between these proteins [36]. Sugawara hypothesized that Sgs1 interacts with the MMR proteins Msh2 and Msh6 since a previous study showed that Sgs1 was found to have a potential physical

interaction with Msh6 [35,37]. This was supported by a recent study that used a co-immunoprecipitation of Msh2-Msh6 to show that Sgs1 does interact with the MMR proteins [38]. Sgs1 also has a MIP motif, and mutation of the MIP box proved a loss of interaction with Mlh1 [24]. These studies suggest that Sgs1 interacts with Msh2-Msh6 to play a role in MMR's response to heteroduplex rejection but point to a potential role in MMR since Sgs1 also interacts with Mlh1.

1.3.4 *Identification of a Conserved Msh2 Binding Region*

A conserved interaction motif between Exo1 and Msh2 has also been recently identified, which is present in other Msh2 interacting proteins. Exo1 is a protein involved in the MMR pathway that is known to interact with both critical MMR proteins, Mlh1 and Msh2. Exo1 was found to interact with Mlh1 through the presence of an MIP box [24], but interaction with Msh2 was previously only known to be on the unstructured C-terminal end [39]. Goellner identified two regions on Exo1 that, when deleted, abolished interaction with Msh2 [26]. These two regions had amino acid sequence similarities and despite the overall lack of conservation in the unstructured C-terminal tail of Exo1, the Msh2 binding regions were found to be conserved through multiple eukaryotic species and present in additional *S. cerevisiae* proteins [26]. They termed this region the Msh2-interacting peptide (SHIP) box [26]. This paper also helped to understand the role of Exo1 in MMR further since SHIP box mutations lost interaction with Msh2 but did not affect the other functions of Exo1 [26]. New potential MMR interactors, Fun30 and Dpb3, were identified by the presence of putative SHIP motifs [26].

Fun30 and Dpb3 were confirmed to interact with Msh2 via yeast-two-hybrid analysis, and Fun30 was suggested to have a partial role in Exo1-dependent MMR

[26]. In another study, the Xenopus Fun30 homolog, Smarcad1, was presented to be an MMR accessory factor, with the loss of Smarcad1 having a slight MMR defect alone but synergistically increasing the MMR defect with MutSα and MutSβ loss [40]. Goellner et. al also determined a potential binding site for interaction of the SHIP-containing proteins on Msh2 [26]. Mutation of the yeast Msh2 M470 site to isoleucine disrupted interaction with the SHIP motif containing proteins Exo1, Fun30, and Dpb3 [26]. The SHIP box is also likely conserved in human proteins – with potential SHIP boxes identified in human EXO1, SMARCAD1 (Fun30 in yeast), MCM9, and WDHD1 [26]. The Msh2 M470 site is also conserved in humans as MSH2 M453I and disrupts interactions with proteins containing the SHIP box motif [41]. Identification of a site for Msh2 interactions allowed for further identification of Msh2 interacting proteins.

Identification of a SHIP box also allowed for separation-of-function experiments to studying MMR and other repair pathways. The identification that Rad27 is a player in MMR could be reviewed because of the recognition of the SHIP box in Exo1 [27]. The *rad27Δexo1Δ* strain was lethal, so Rad27's function in MMR couldn't be studied. However, deleting the regions containing Exo1's MIP and SHIP boxes allowed Rad27 to be identified as an additional Exo1-independent sub-pathway [11,27]. Rad27-mediated MMR has similar kinetics to Exo1 in MMR, and the *rad27Δ exo1Δ440-702* double mutant showed a synergistic increase in MMR [27]. Rad27 was found to utilize strand displacement and polδ to repair mismatches in an Exo1-deficient manner[27]. This study gave evidence for at least three MMR sub-pathways – one being Exo1-dependent and the others being Exo1-independent. Recognizing and understanding the differences in MMR sub-pathways can help us understand the role the MMR plays canonically and in response to exogenous

damage and its role in other DNA repair pathways. A summary of the MMR-interacting partners in *Saccharomyces cerevisiae* is found in Figure 1.1A.

1.4   Accessory Factors in Humans

1.4.1   *Human Homologs with Conserved Interactions*

Many of the interacting proteins identified in *S. cerevisiae* have been conserved in humans, with the homologs retaining their interaction and role in MMR. Many helicases have been studied relating to MMR since UvrD is the helicase in methyl-directed prokaryotic MMR but does not have a known homolog. RECQ1 is a human homolog of yeast Sgs1 and a member of the RecQ family, helicases that play a role in DNA replication and repair and help maintain genomic stability [42]. RECQ1 was found to interact with EXO1 and stimulate EXO1's nuclease activity [43]. RECQ1 was also found to directly interact with MLH1 and the MutSα proteins MSH2 and MSH6, where the presence of MutSα stimulates the helicase activity of RECQ1[43]. This evidence strengthens the hypothesis that yeast Sgs1, and its homolog RECQ1, play some role in the MMR pathway.

Another yeast protein, Fun30, was found to be an MMR accessory factor and has a human homolog, SMARCAD1 [26]. SMARCAD1 is a chromatin remodeler that plays a role in HR and was found to interact with MSH2 constitutively and with MLH1 in a damage-dependent manner [44–46]. A study aimed at understanding the role of SMARCAD1 in MMR-mediated apoptosis found that loss of SMARCAD1 does not affect MMR protein levels, but loss of SMARCAD1 causes resistance to MMR-mediated apoptosis [46]. The ATPase domain was identified as a crucial part of MMR-mediated apoptosis and the interaction between SMARCAD1 and MMR was also found to be important in HR [29,46]. MutSβ has been implicated in HR and SSA[47], and MutSβ was

identified as a player in end resection based on its interaction with EXO1 [29]. SMARCAD1 likely recruits the MutSβ complex to the site of damage, which then recruits EXO1 for end resection [29]. Interaction between these two proteins affects both MMR and HR, further supporting that interaction between different repair pathway proteins could be significant in regulating and differentiating which repair pathway to choose.

1.4.2 *Utilization of Conserved MLH1 Binding Sequences in Humans*

Identification of the MIP box was utilized in *S. cerevisiae* to identify novel interactors of Mlh1 [24]. During this study, human BLM was found to have an MIP box that mediates the BLM-MLH1 interaction [24]. BLM is another member of the RECQ helicase family, whose defects cause Bloom's syndrome, which increases cancer susceptibility [48,49]. In an attempt to understand more about the biology behind BLM that may lead to Bloom's syndrome, it was identified that BLM directly interacts with MLH1 and they are localized in the same area of the cell [50,51]. BLM is involved in the response to DSB, primarily through HR, and MMR has been implicated in HR [52,53]. BLM was also found to interact with MSH6 directly, and their co-localization increases in the presence of irradiation damage; however, they reported no role of MutSα on BLM helicase activity [54]. Another publication reported that MutSα stimulated BLM X-junction binding and helicase activity and is blocked by p53 [55]. The reported differences could be due to different conditions in the helicase assay, such as the amount of MutSα complex added to the reaction. The role of MutSα in HR related to BLM is shown with the loss of MutSα increasing the amount of Rad51 foci with damage like p53; BLM, p53, and RAD51 increase their complex in the absence of MutSα [55]. The interaction of MMR proteins with helicases involved in HR reinforces the idea that

MMR proteins have some role in HR, HR proteins may have a role in MMR, and these interactions regulate the activity of repair efficiency.

Another protein identified as an interactor with an MIP box is FAN1/KIAA1018[56], an interstrand crosslink (ICL) repair protein. FAN1 was identified to interact with MLH1 via a MIP box and a novel region coined the MLH1-interacting motif (MIM) [25,28]. The interaction between FAN1 and MLH1 is essential in both MMR and ICL repair [25,28]. FAN1 interacts with MLH1 independent of DNA damage and FAN1 was found to interact with MSH2 in an MMR-specific damage-dependent manner [57]. With MMR-associated damage, FAN1 binds to chromatin with the help of MLH1, and likely uses its nuclease activity in processing mispairs after exogenous damage, making it an accessory factor in MMR-mediated apoptosis [57]. The FAN1-MLH1 interaction was also important in survival from ICL damage and in stabilizing CAG/CTG trinucleotide repeats, which are associated with Huntington's disease [25,28].

1.4.3 *Utilization of Conserved MSH2 Binding Sequences in Humans*

It was recently identified that the SHIP box was present in yeast Exo1, and this motif was used to identify new yeast Msh2 interacting proteins, one of which has a human homolog [26]. As mentioned in 1.4.1, yeast Fun30 has a human homolog, SMARCAD1, and both are considered MMR accessory factors [40,46]. A SHIP box has also been identified in another protein, SLX4 [41]. SLX4 is a tumor suppressor that acts as a nuclease scaffold to regulate their activity and target them to the correct locations [58]. SLX4 has been identified as an interactor of MutSα and MutSβ, and the interaction between SLX4 and MutSβ has been associated with resolving Holliday junctions [41,59–63]. The MSH2-SLX4 interaction influenced the response to MMR damaging agents, with SLX4

suppressing MMR activity and damage signaling [41]. Since SLX4 was found to have a SHIP box, which is present in other MSH2 interacting proteins, it could potentially compete with the other interacting proteins to reduce MMR activity [41]. This provides further evidence of MMR accessory factors playing a role in regulating MMR activity.

1.4.4 *Effect of Nucleosome Remodeling and Assembly on MMR*

MMR proteins are expressed throughout multiple cell cycle stages; however, MMR's activity is coupled to the S phase of the cell cycle [64–66]. Since MMR occurs during the S phase and DNA is being packaged rapidly after replication, MMR has a short timeframe to repair mismatches left after replication[67] and may interact with chromatin remodelers to be able to access the DNA (review on chromatin remodeling and MMR by Goellner[68]). One chromatin remodeler that was found to play a role in MMR is SMARCAD1. In *Xenopus*, it was identified that when mismatches are present in DNA, more nucleosome exclusion occurs, dependent on the critical MMR protein Msh2, not Mlh1 [40]. This study suggested that Smarcad1 may assist in nucleosome exclusion and repair by MMR, with its ATPase domain being an important factor in MMR, and may act as an antagonist to the histone chaperone protein CAF-1 [40].

Histones are present in the nucleus, and MMR proteins are also primarily located in the nucleus. CAF-1 is a histone chaperone protein also found in the nucleus; CAF-1 decreases MMR-related DNA degradation when added to the nucleus [69]. CAF-1 and histones were found to deposit on nicks present with a mispair, potentially to protect from excessive degradation by MMR. MutS suppresses the deposition of CAF-1 and histones, likely to allow for DNA repair after replication [69]. This is supported by evidence that MMR initially delays nucleosome assembly; however, nucleosome assembly after

DNA repair is efficient [70]. The delay in nucleosome assembly is due to the MMR process since the loss of MMR function decreases nucleosome assembly delay [70]. The interaction between CAF-1, MMR, and nucleosome assembly suggests that MMR interacts with chromatin-related proteins to access DNA for efficient repair. CAF-1 also has a potential role in suppressing MMR-mediated apoptosis, showing that this interplay affects multiple MMR functions [71].

1.4.5   *Role of Epigenetics on MMR*

Epigenetic changes alter the structure of chromatin to affect gene expression and allow different DNA functions to occur, such as replication, transcription, and translation. Histone modification, an epigenetic process, has been connected to MMR. The PWWP domain was identified in MSH6, which is a mark for interaction with the histone mark H3K36me3, is evidence that reinforces the connection between MMR and epigenetics [72]. Li confirmed that MSH6 binds to H3K36me3 histone octamers, which is not essential for MMR activity, but the interaction is necessary for MSH6 foci formation [72]. SETD2 is responsible for the trimethylation of H3K36, and although it is not physically involved in MMR, loss of SETD2 and, subsequently, H3K36me3 leads to MSI and a mutator phenotype *in vitro* [72]. Additionally, SETD2-deficient cancer cell lines were studied and showed the presence of MSI and a loss of MSH6 foci formation [72]. This study indicates that trimethylation of H3K36 by SETD2 could recruit the MutSα complex to enhance MMR efficiency.

In addition to the methylation of histones, the demethylation of histones could also play a role in MMR, with members of the KDM4 lysine demethylase family involved in the MMR pathway. There are five members of the KDM4 family, with

KDM4A-C being involved in the demethylation of H3K36me2/3 [73]. Overexpression of KDM4A-C, but not the other KDM4 family members, decreased MSH6 foci formation, induced MSI, and increased mutation frequency [74]. Alternatively, loss of demethylase activity results in less MSI and a mutation frequency similar to controls [74]. The findings from Awwad and Ayoub support Li's findings that regulation of H3K36me3 plays a role in MMR and give more insight into the proteins and methylases/demethylases involved in MMR. The dynamic regulation of methylation/demethylation could be significant in balancing MMR activity.

1.4.6 *Other DNA Repair Proteins in MMR*

DNA methyltransferases (DNMTs) have been identified as epigenetic factors that methylate DNA; additionally, some have also been identified as players in DNA repair [75]. DNMT1 deficiency was previously found to cause MSI in mice, and a connection between DNMT1 and MLH1 in trinucleotide instability has been made [76–78]. Loss of DNMT1 in normal cells was also found to have a potential MMR defect, with an increased resistance to 6-thioguanine and an increased mutation rate [79]. Loss of DNMT1 also caused a slight decrease in expression of the MutLα proteins MLH1 and PMS2, which could contribute to the MMR defect seen previously [79]. MutSα was also found to recruit DNMT1 to oxidative damage potentially by protein-protein interaction [80]. The interaction of proteins involved in DNA binding and methylation, in addition to methylation of MMR proteins in some cancers[81], strengthens the evidence that epigenetics could play a role in MMR.

DNMT1 was found to interact with MED1, a methyl-CpG binding endonuclease and N-glycosylase involved in BER [82–84]. MED1, also known as MBD4,

and MLH1 play a role in apoptosis in DNMT1-depleted Xenopus [85,86]. MED1 was found to interact with MLH1, and the methyl-binding domain of MED1 has a potential role in the MMR efficiency in an MMR-proficient cell line [83]. The methyl-binding domain of MED1 has a YF amino acid sequence also found in the mouse and rat homologs, which could indicate a potential MIP box, although it has not been studied. The presence of multiple proteins involved in BER and the utilization of MMR in response to alkylating agents in the absence or defect of the BER protein O^6-methylguanine methyltransferase (MGMT) further support the interplay between these DNA repair pathways.

1.4.7   *Additional Proteins Related to MMR*

The interacting proteins described have various roles in the cell, such as helicases, chromatin remodelers, or nucleases. These proteins also have roles in epigenetic changes and different DNA repair pathways. Because of the presence of UvrD as a helicase in prokaryotic MMR, the focus on identifying additional helicases has been extensively studied. Other helicases have also been identified as interactors of MMR, and they have a role in both MMR and their original repair pathway. FANCJ, also known as BRIP1, is a helicase involved in the FA pathway and was found to be an interactor of the MutL complexes; disruption of the FANCJ-MutL interaction decreased the repair efficiency of ICLs [56,87]. MCM9, a helicase involved in HR[88], was also identified as an accessory factor of MMR based on interactions with many MMR proteins and a deficiency in MCM9 associated with decreased MMR efficiency and MSI [89]. It was hypothesized that MSH2 recruits MCM9 to the chromatin, which then recruits MLH1, and MCM9 uses its helicase activity to stimulate MMR [89].

A few other MMR-interacting proteins that will be discussed have a DNA binding function. Orc6 is part of the origin replication complex (ORC), where it binds to DNA and assists in ORC-dependent and independent functions [90,91]. Orc6 was found to be important in MMR and MMR-mediated apoptosis [92]. A portion of the role in MMR-mediated apoptosis could be the importance of Orc6 in ATR activation, a downstream damage signal associated with MMR-mediated apoptosis. Orc6 binds to MutS, which could help facilitate the complexing of MutS and MutL to enhance MMR [92]. The importance of Orc6 in DNA binding and replication and the importance of MMR and replication timing also strengthens the argument that Orc6 is an accessory factor of MMR.

The final interacting proteins mentioned in this section will be proteins containing the HMG box, which occur in DNA-binding proteins and can help with protein interactions and damage recognition [93]. In a reconstitution of MMR, HMGB1 was purified and was found to interact with MutSα but not MutLα [94]. HMGB1 enhanced MMR activity, potentially by enhancing MMR initiation and excision [94]. WDHD1 is another protein found to interact with MSH2 that contains an HMG box. A proteomic study was utilized to look at potential MMR interactors, and WDHD1 was found to interact with the MutSα and MutSβ components [95]. Loss of WDHD1 was found to increase resistance to MMR-mediated apoptosis, a characteristic of defective non-canonical MMR [95]. In this study, the authors define the MSH2 binding site on WDHD1 and found a short amino acid sequence that we now know represents a SHIP box motif [95].

The presence of multiple DNA binding proteins that interact with the critical MMR proteins and have a role in canonical and non-canonical MMR indicates that these proteins are also accessory factors in MMR. Additionally, the presence of MMR

accessory factors involved in different DNA repair pathways with different roles in these pathways emphasizes the overlap of numerous DNA repair pathways – these pathways play a role in MMR and MMR plays a part in the other repair pathways. A summary of the human interactors and their connection to MMR can be found in Figure 1.1B.

1.5   Research Objective

This study investigated the possibility of new mismatch repair interacting proteins that act as MMR accessory factors. We identified an MMR interacting protein in *Saccharomyces cerevisiae* that is conserved in humans, where one homolog has a role in non-canonical MMR, and the interactions of the other homolog have a potential role in post-replicative repair.

In Chapter Two, we demonstrate that *S. cerevisiae*'s Rad5 interacts with Mlh1 and Msh2, although it does not seem to have a role in canonical MMR. The interaction was split between Rad5's human homologs, HLTF and SHPRH, where HLTF interacts with MSH2 and SHPRH interacts with MLH1 in a damage-dependent manner. SHPRH was found to be a potential player in MMR-mediated apoptosis.

In Chapter Three, we report that the human interactions seen in Chapter Two are also observable in the cellular environment via microscopy. We also identified how HLTF interacts with MSH2 and that MSH2 likely plays a role in post-replicative repair. Although we could not determine how SHPRH interacts with MLH1, we found that loss of MMR proteins, MLH1 and MSH2, affect SHPRH's cellular localization, further supporting the role of SHPRH in MMR.

The results from this study provide a novel insight into new MMR accessory factors and another role of MSH2 in a DNA damage response pathway.

Moreover, identifying additional MMR accessory factors can further the understanding of the MMR mechanism and its role in disease development and progression.
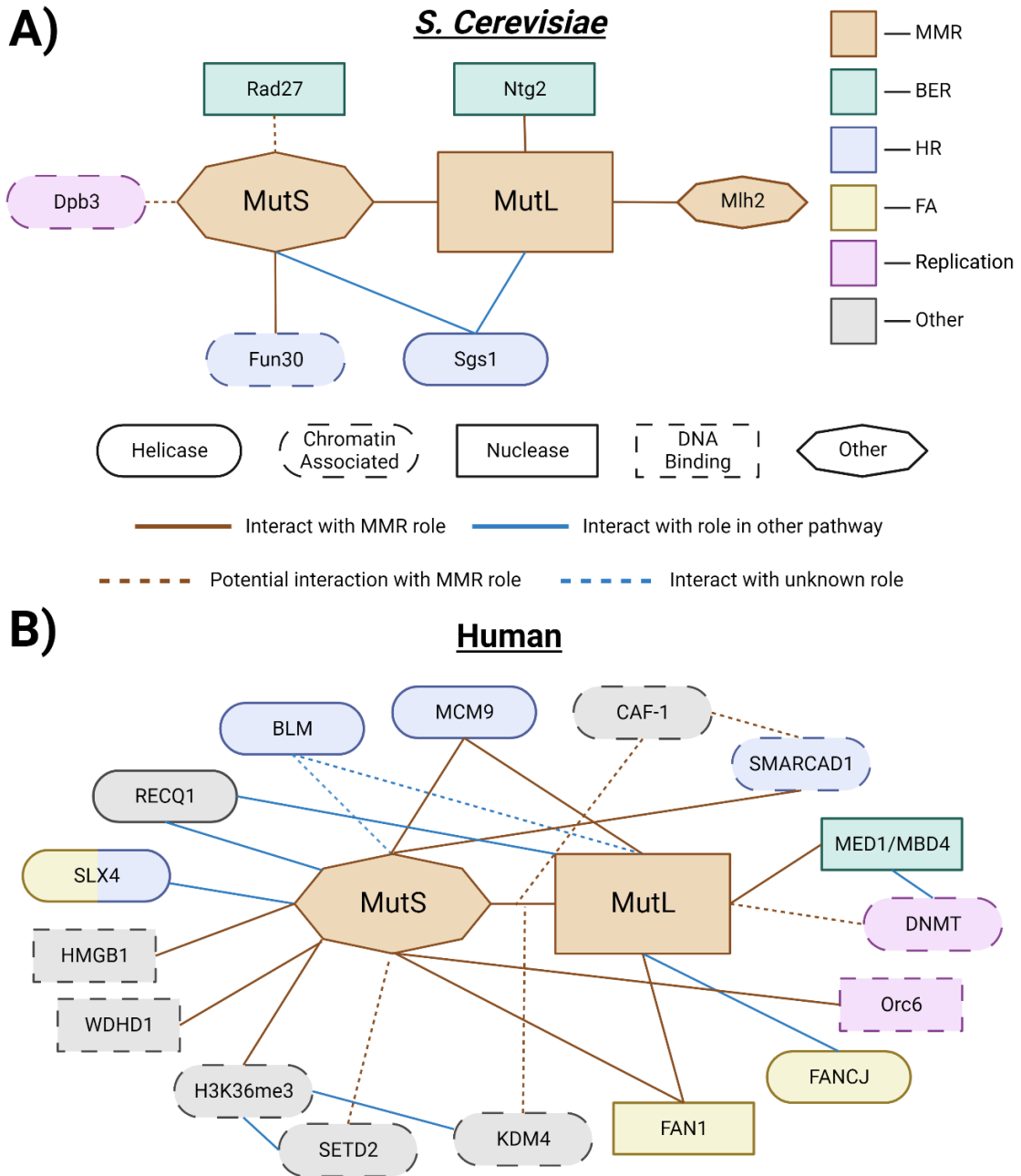
Figure 1.1 Interaction Map of Accessory Factors in MMR.
A) Proteins found to be involved or interacting with MMR proteins in *Saccharomyces cerevisiae*. The color of the proteins indicates the associated DNA repair pathway, and the shape/outline of the proteins indicates their role in the cells. The lines connecting to the MMR proteins indicate interaction and role in MMR or another repair pathway. B) Proteins

found to interact with MMR proteins in humans. The description of proteins in A is the same in part B.

CHAPTER 2. Rad5 and Its Human Homologs, HLTF and SHPRH, Interact with Critical Mismatch Repair Proteins

2.1   Citation

2.2   Introduction

DNA mismatch repair (MMR) is the post-replicative repair pathway that repairs base-base mispairs and small insertion/deletion mispairs arising from DNA replication errors [8,9]. MMR also induces apoptosis after recognizing mispairs caused by exogenous DNA damaging agents, such as O^6-methylguanine:thymidine mispairs that occur after exposure to S_N1 alkylators [12,13]. MMR cannot repair these regions as the O^6-methylguanine lesion is on the template strand. Defects in the MMR result in an accumulation of mutations, which can result in altered cellular function and the development of cancers [23]. Germline mutations in MMR genes are the underlying cause of familial cancer predisposition syndrome, Lynch syndrome [21,97], and constitutional mismatch repair deficiency [98]. Lynch syndrome predisposes individuals to several cancer types, primarily colorectal, stomach, endometrial, and ovarian cancers [99,100], and constitutional mismatch repair deficiency is associated with many cancer types in pediatric patients [98]. In MMR genes, somatic mutations and epigenetic silencing are also found in a significant subset of sporadic cancers of the same subtypes [81,101].

Mutation avoidance by eukaryotic MMR involves several steps: 1) mispair recognition by the heterodimeric MutS homologs, MSH2-MSH6 or MSH2-MSH3, 2) recruitment of the MutL homolog, MLH1-PMS2 (called Mlh1-Pms1 in *Saccharomyces*

cerevisiae), 3) removal of the mispaired DNA from the daughter strand through either Exonuclease 1 (Exo1)-dependent, Rad27-dependent or Exo1- and Rad27-independent MMR, and 4) gap-filling by the replicative polymerases, PCNA, and RFC and 5) nick ligation [8,9,11,27].

While the core machinery of eukaryotic DNA MMR is well-defined, new MMR-interacting proteins are still being identified [26,27,40,57,72,89,94]. Remarkably, short peptide sequences have been identified that mediate interactions with Mlh1 (the Mlh1-interacting peptide motif or MIP box; [24]) and, more recently, Msh2 (the Msh2-interacting peptide motif or SHIP box; [26]). Together, these motifs are involved in the interaction of *S. cerevisiae* Mlh1 with Ntg2, Sgs1, and Exo1, *S. cerevisiae* Msh2 with Exo1, Fun30, and Dpb3, and likely human MSH2 with SMARCAD1 (*S. cerevisiae* Fun30), WDHD1, and MCM9 [24,26,34,89,95]. Identifying novel MMR accessory proteins and elucidating the mechanisms by which they interact with MMR will be critical to understanding mechanisms suppressing cancer development and potentially guiding cancer therapies involving DNA-damaging agents.

Here, we identify another novel MMR interacting partner, Rad5, that we predict to have both SHIP and MIP box motifs. Rad5 is a helicase and E3 ubiquitin ligase involved in post-replication repair (PRR) pathways, which allow tolerance of template strand lesions that would otherwise lead to replication fork stalling [102,103]; however, Rad5 has no known role in MMR. PRR bypasses DNA template lesions via error-prone translesion synthesis (TLS) and error-free template switching (TS) branches [104], the choice of which is in part controlled by the ubiquitination status of proliferating cell nuclear antigen (PCNA) [102]. The Rad5 E3 ligase has been associated with TS through the activity

of Mms2-Ubc13-Rad5 in forming a lysine 63-linked polyubiquitination chain on PCNA [105]. However, recent studies have also identified Rad5 as a player in TLS through its interaction with the TLS protein Rev1 [103], which is consistent with the lack of epistasis of *rad5Δ* and *ubc13Δ* mutations observed in assays for genome instability [106].

Rad5 has two known human homologs, helicase-like transcription factor (HLTF) and SNF2 Histone Linker PHD Ring Helicase (SHPRH). Both HLTF and SHPRH share the SNF2 helicase and RING finger domains with Rad5, and HLTF additionally shares the HIRAN (HIP116, Rad5 N-terminal) domain that is present N-terminal to the SNF2 helicase domain [107]. HLTF and SHPRH have E3 ubiquitin ligase ability, both can polyubiquitinate PCNA, and HLTF can complement the UV sensitivity of a *rad5Δ S. cerevisiae* strain [108–110]. HLTF and SHPRH also have direct but distinct roles in directing TLS- and TS-mediated PRR. HLTF and SHPRH deletion mutants have different sensitivities to agents that cause DNA lesions [111]. HLTF enhances TLS and inhibits SHPRH following UV damage, but MMS treatment causes SHPRH response and HLTF degradation instead [112]. Loss of HLTF expression has been associated with several cancer types, including colorectal cancer [113]. Loss of SHPRH has also been associated with multiple cancers via 1) loss of heterozygosity of the long arm of chromosome 6, where SHPRH resides, 2) accumulation of SHPRH point mutations in melanoma and ovarian cancer-derived cell lines [114], and 3) through the protective action of a circular RNA encoding a 146 amino acid fragment of SHPRH in glioblastoma [115,116].

In this study, we confirm the predicted interactions in *S. cerevisiae* between Msh2 and Rad5 and Mlh1 and Rad5 and verify that an MIP box mediates the Mlh1-Rad5 interaction. These interactions are conserved with human homologs HLTF and SHPRH.

Interestingly, the Msh2-Rad5 and Mlh1-Rad5 interactions have split between the two homologs, with HLTF binding only to human MSH2 and SHPRH binding to human MLH1. We also show that loss of SHPRH results in moderate resistance to alkylating agents. Together, these data identify novel interacting partners of MMR in both yeast and humans and suggest that the SHPRH-MLH1 interaction is partially involved in an apoptotic response to damage-induced mispairs.

2.3   Materials and Methods

2.3.1   *Chemicals and Reagents*

Antibodies used in this study include anti-MLH1 (Cell Signaling Technologies 3515S), MSH2 (Cell Signaling Technologies 2017S), HLTF (Fisher PA5-30173), SHPRH (Santa Cruz sc-514395), IgG (Santa Cruz sc-2025). 6-Thioguanine (6TG) was obtained from TCI America (T0212-1G) delivered by VWR, and MNNG was obtained from Sigma-Aldrich (Cat #129941).

2.3.2   *Yeast-Two-Hybrid Assay*

Plasmids expressing fusion proteins for yeast two-hybrid analysis were generated by Gateway cloning (Invitrogen) the gene of interest without its start codon into either the Gateway-modified bait vector, pBTM116, which encodes the LexA DNA binding domain and Trp1, or the Gateway-modified prey vector, pACT2, which encodes the GAL4 activation domain and Leu2. Bait and prey plasmids were co-transformed into the L40 *S. cerevisiae* reporter strain L40 (MATa trp1-901 leu2-3112 his3Δ200 LYS2::(4lexAop-HIS3) URA3::(8lexAop-lacZ)), in which a positive interaction of the bait and prey fusion proteins results in expression of HIS3 and hence complementation of the his3Δ200 mutation [117]. Colonies were grown overnight in a complete synthetic medium

lacking leucine and tryptophan (CSM -Leu -Trp) to maintain plasmid selection, and then 10-fold serial dilutions were spotted onto CSM -Leu -Trp control medium and CSM -Leu -Trp -His selective medium to assay for two-hybrid interactions.

2.3.3 *Mutation Rate and Mutation Spectra Analysis*

S. cerevisiae strains were grown in YPD (1% yeast extract, 2% Bacto Peptone, and 2% dextrose) or the appropriate synthetic dropout media (0.67% yeast nitrogen base without amino acids, 2% dextrose, and amino acid dropout mix at the concentration recommended by the manufacturer (US Biological) at 30°C. All *S. cerevisiae* strains in this study were derived in the S288C strain background using standard gene deletion and pop-in, pop-out methods.

Mutator phenotypes were evaluated using the *hom3–10* frameshift reversion assay. Mutation rates were determined by fluctuation analysis using a minimum of 2 independently derived strains and 14 or more independent cultures; comparisons of mutation rates were evaluated using 95% confidence intervals.

One independent Thr$^+$ revertant was isolated per culture from fluctuation tests. Chromosomal DNA was isolated from each revertant using a Qiagen Puregene Yeast/Bact. Kit B and the *hom3-10* region were amplified by PCR using the Primer: 5'-AGTTGTTTGTTGATGACTGC and Primer: 5'-TTCAGAAGCTTCTTCTGGAG and sequenced with the Primer: 5'-CTTTCCTGGTTCAAGCATTG using a commercial sequencing facility [27].

2.3.4 *Bioinformatic Analyses*

Bioinformatic analysis of potential MIP and SHIP motifs with good peptide matching scores in regions predicted to be unstructured was carried out as described

previously [26]. Briefly, we determined the count of each amino acid at each position in the alignment of the SHIP boxes 1 and 2 or the MIP box from fungal Exo1 homologs. A pseudo count of 1 was added to all positions that were zero, and then the counts were converted to a fraction, $F_{k,j}$, for each amino acid k at position j. $F_{k,j}$, values were then converted to log probabilities ($M_{k,j}$) scaled by a background model: $M_{k,j} = log(\ F_{k,j}\ /\ b_k\ )$. The background model was calculated using the frequency of the different amino acids in the proteins encoded by the *S. cerevisiae* genome. Raw scores (S_{raw}) for peptides were calculated by adding all $M_{k,j}$ values from the PSSM for each amino acid k at position j within the peptide sequence. We scaled the raw scores to be in the range 0 to 1 using the equation: $S_{scale} = (S_{raw} − S_{min}\ )\ /\ (S_{max} − S_{min}\ )$, where S_{min} and S_{max} are the minimum and maximum scores possible for any peptide scored by the PSSM. The long-term disorder prediction score for each position in the proteins was generated using IUPRED [118], and the disorder prediction score for each peptide was calculated by averaging the scores for each of the residues in the peptide.

Identification of Rad5 homologs for the analysis of the conservation of the candidate MIP and SHIP motifs was performed by categorizing BLAST hits from each species by building a phylogenetic tree with MAFFT version 7.305 [119] and PHYLIP version 3.696 [120] that contained all of the BLAST hits from that species with all of the *S. cerevisiae* Rad5 homologs (Chd1, Fun30, Ino80, Irc20, Irc5, Isw1, Isw2, Mot1, Rad16, Rad26, Rad5, Rad54, Rdh54, Snf2, Sth1, Swr1, and Uls1). Homologs were then assigned if the BLAST hit was on the same branch as the phylogram as only one of the *S. cerevisiae* reference sequences using the program idwtree [26]. Alignments of assigned fungal Rad5

homologs were then performed with MAFFT for analyzing conservation and building sequence logos with Seq2Logo [121].

2.3.5   *Cell Culture*

All cell lines were cultured at 5% CO_2 and 37ºC. HEK293 cells were cultured in DMEM supplemented with 10% FBS (Gibco Life Technologies Corporation) and 1% Penicillin/Streptomycin (Gibco, Life Technologies). HeLa S3 cells were cultured in RPMI supplemented with 10% FBS and 1% Penicillin/Streptomycin.

2.3.6   *Generation of Knockout Lines*

HeLa MLH1, MSH2, HLTF, and SHPRH single knockout cell lines and the HLTF and SHPRH double knockout cell line were generated by CRISPR-Cas9 technologies, using single guide RNA (sgRNA) sequences (Table 3) for each of the genes listed. The LentiCRISPRv2 was a gift from Feng Zhang (Addgene plasmid #52961). The plasmid was digested with BsmBI and gel purified using the QIAquick PCR purification kit according to the manufacturer's instructions. Complementary oligonucleotides (synthesized by Integrated DNA Technologies) encoding the sgRNA were then annealed and cloned into LentiCRISPRv2. Cells were then transfected with Lipofectamine 3000 (Thermo Scientific L3000008), and the cells were selected with puromycin (Promega). Single-cell clones were grown up under puromycin selection and expanded. Loss of protein expression was confirmed for each clone using SDS-PAGE and Western blot analysis.

2.3.7   *Short-Term Cytotoxicity Assay*

Twenty-four hours before transfection, HEK293 cells were plated at 750,000 cells/well in a 6-well plate. Cells were transfected with siHLTF (Origene) or siSHPRH (Origene) alone or in combination utilizing the Lipofectamine RNAiMAX Transfection Reagent (Invitrogen). After transfection for 24 hours, the cells were seeded at 10,000 cells/well in 96-well plates, and the remaining cells were collected for protein analysis. Media was removed 24 hours after seeding, and cells were treated with the indicated doses of MNNG for 1 hour. The media was then replaced and allowed to grow for 72 hours, at which time cell viability was measured using the CellTiter 96 Aqueous One Solution Cell Proliferation Assay (MTS) kit (Promega) according to the manufacturer's instructions.

2.3.8   *Long-Term Clonogenic Cytotoxicity Assay*

Twenty-four hours prior to treatment, HEK293 or HeLa S3 cells were plated in a 6-well plate. Cells were pre-treated with 10μM O^6-benzylguanine (6-(benzyloxy-7H-purin-2-amine, Thermo Scientific, H60274-MD) for 2 hours and then pulsed with MNNG or DMSO vehicle control for 1 hour. Cells were then trypsinized and plated in a 6-well plate at a density of 300 cells/well for HeLa or 3,000 cells/well for HEK293 with normal media and were allowed to grow for ten days or until colonies of approximately 50 cells could be seen. The cells were then stained with crystal violet and the number of colonies was counted.

2.3.9   *Nuclear Protein Extraction*

Cells were washed with PBS, resuspended in cytoplasm extract buffer (20 mM Hepes, 10 mM KCl, 0.1 mM EDTA, 1 mM DTT, and protease inhibitor), and then chilled on ice for 10 minutes. 0.75% Nonidet P-40 (NP-40) lysis buffer was added, and the solution was pipetted to mix, followed by vortex mixing for 10 seconds. The cells were centrifuged at 800 x g for 3 minutes at 4ºC to separate the nuclei pellet from the cytoplasm (supernatant). The cytoplasm extract was placed in a separate tube and the nuclei pellet was resuspended in 25% sucrose/cytoplasm extraction buffer and pipetted to disperse. The cells in 25% sucrose/cytoplasm extraction buffer were underlaid with half the volume of 50% sucrose/cytoplasm extraction buffer and centrifuged at 10,000 x g for 15 minutes at 4ºC. The supernatant was removed, and the nuclei pellet was lysed in PBE150Na (50mM Tris-HCl at pH 7.5, 1mM ethylenediaminetetraacetic acid (EDTA) at pH 8.0, 150mM NaCl, 0.5% sodium deoxycholate and 1% NP-40, containing 1x Complete protease inhibitor cocktail (Roche Diagnostics GmbH, Germany)). The pellet was then sonicated and centrifuged at 10,000 x g for 15 minutes at 4ºC. The supernatant was collected as the nuclear extract.

2.3.10 *Immunoprecipitation*

Co-immunoprecipitations of endogenous or tagged proteins were performed using magnetic protein A/protein G beads (Thermo Scientific) followed by a conjugation step to either the IgG control or antibody of interest with BSA for 2 hours, followed by washes. Conjugated beads were incubated with whole cell lysate or nuclear extracts (described above) with rotation overnight at 4°C, followed by increasing salt

washes. Beads were boiled with 6x loading buffer and samples were run on SDS-PAGE gels followed by Western blot.

2.3.11 *HPRT Mutagenesis Assay*

The HPRT forward mutagenesis assay was performed in HeLa S3 wild-type and knockout cells as described previously [72]. Cell lines were first cultured in hypoxanthine, aminopterin, and thymidine (HAT) supplemented media (ThermoFisher Scientific, supplied as 50x supplement) for at least five passages to clear background HPRT mutations. HAT passaged cells were seeded at 5×10^5 cells per 100mm dish in triplicate, allowed to adhere overnight, then treated with 5 µM 6-thioguanine (6-TG). The plating efficiency of the cells was determined by culturing 5×10^2 HAT passaged cells per 100 mm dish plated in triplicate in the absence of 6-TG. The media was replaced every two to three days. After ten days of culturing, cell colonies were stained with 0.5% crystal violet in 25% methanol and colonies containing more than 50 cells were counted. Mutation frequency was determined by calculating the median for mutant cells (number 6-TG selected colonies/ 5×10^5 cells plated) and the median for plating efficiency (number untreated colonies/ 5×10^2 cells plated) and dividing mutation by plating efficiency for each cell line.

2.3.12 *Cell Synchronization*

Cell synchronization was conducted by performing a double thymidine block in HeLa cells. The protocol for double thymidine block was adapted from a previous publication [122]. HeLa cells were plated and after twenty-four hours, washed once with warmed PBS and cultured in complete medium containing 2 µM thymidine (Sigma T9250) for 18 hours. The HeLa cells were washed twice with warmed PBS and released in media

without thymidine for 9 hours. The cells were then cultured with 2 µM thymidine for 16 hours, washed once with warmed PBS, and replaced with fresh media for collection at each of the times indicated for each figure. For treated cells, cells were released into complete media containing 0.2 µM MNNG or DMSO containing O^6-benzylguanine.

2.3.13 *Cell Cycle Analysis*

After cell synchronization using double thymidine block, cells were trypsinized and quenched with media then centrifuged at 2,000 xrpm for 5 minutes. Th e cells were then resuspended in 75% ethanol for at least 1 hour at -20ºC for fixation. The cells were centrifuged at 4,000 x rpm for 2 minutes and then resuspended in PBS containing 0.25% Triton X-100 for 15 minutes. Cells were centrifuged at 4,000 rpm for 2 minutes and resuspended in PBS containing 10 µg/mL RNase A (Qiagen) and Propidium Iodide Ready Flow Reagent (ThermoFisher Scientific). Subsequent detection of the cell cycle phase distribution was accomplished by using propidium iodide for nuclear staining and detection using the BD FACSymphony A3 flow cytometer and collecting FSC, SSC, PE for propidium iodide, and BB515 for compensation with gating for single cells. The resulting data was analyzed by FlowJo software.

2.3.14 *Statistical Analysis*

Calculations of the mean, standard error, statistical analysis, and comparison of each set of experimental means were performed with Graphpad Prism 9.0 (Graphpad Software Inc., La Jolla, CA, USA).

2.4 Results

2.4.1 *Rad5 Physically Interacts with Yeast Mlh1 and Msh2*

To identify candidate MMR-interacting proteins, we computationally screened the *S. cerevisiae* for proteins containing sequences resembling MIP and SHIP box motifs following our previous strategy that identified the Msh2-interacting and SHIP box-containing proteins Fun30 and Dpb3 [26]. First, the MIP motif match score and the SHIP motif match score were calculated for every seven amino acid peptides computationally generated from the *S. cerevisiae* S288c proteome using a position-specific scoring matrix (PSSM, [123]) derived from an alignment of 301 fungal Exo1 MIP box sequences and a PSSM from an alignment of 566 fungal Exo1 SHIP box sequences. Second, high-scoring hits were filtered for proteins known to be in the nucleus or with an unknown cellular localization. Third, the average disorder score for each peptide was determined by averaging the long-range disorder score for the seven amino acids of the peptides after analysis of the relevant proteins for long-range disorder with IUPRED [118]. The motif match scores were then plotted against the average disorder scores (Fig. 2.1A) to identify candidate peptides that matched the MIP box consensus or the SHIP box consensus and that were in disordered protein regions. These analyses identified proteins containing known functional MIP boxes (Exo1, Ntg2, Sgs1) and known functional SHIP boxes (Exo1, Fun30, Dpb3) in unstructured protein regions as well as high-scoring SHIP box-like peptides in proteins previously demonstrated as not interacting with Msh2 (Utp18, Bir1) (Fig. 2.1B; [26]).

Because this analysis suggested that Rad5 resembled Exo1, which also has MIP and SHIP box motifs and uses both motifs for recruitment to MMR [26], we sought to

confirm the predicted Rad5 interactions using yeast two-hybrid analysis. We generated a bait plasmid containing *S. cerevisiae* Rad5 fused to the LexA DNA-binding domain. This plasmid, a positive control bait plasmid encoding the Exo1 C-terminus fused to LexA, or a negative control empty bait plasmid encoding only the LexA DNA-binding domain were then co-transformed into the *S. cerevisiae* tester strain L40 with prey plasmids that encoded *S. cerevisiae* Mlh1 or Msh2 fused to the Gal4 transcriptional activation domain. In the L40 tester strain, physical interaction between the bait and prey proteins drives expression of the HIS3 gene and hence supports growth on a medium lacking histidine. As expected, the yeast two-hybrid analysis revealed an interaction between the Exo1 C-terminus and both the Mlh1 and Msh2 prey vectors. The Rad5 bait plasmid also supported growth on -His medium in combination with both the Mlh1 and Msh2 prey vectors, but not the empty prey vector (Fig. 2.1B), indicating that Rad5 can interact with both Mlh1 and Msh2.

2.4.2   *Rad5 Binds to Mlh1 through the MIP Box Motif*

To gain insight into the Rad5 interactions with Mlh1 and Msh2, we sought to determine if these interactions were mediated through the predicted MIP box (peptide 7-EERKRFF-13) and the predicted SHIP box (peptide 30-NKESFLF-36), which are in the unstructured N-terminus of Rad5 (Fig. 2.2A and 2.2C). Analysis of the conservation of these predicted motifs revealed that the predicted MIP box is extensively conserved in all fungi, whereas the predicted SHIP box is restricted to fungi in the order Saccharomycetales, which includes *S. cerevisiae* (Fig. 2.2B). We and others have previously shown that mutating the conserved phenylalanine and tyrosine amino acids in these motifs to alanine disrupts the ability of these motifs to mediate interactions [24,26]. We therefore mutated the predicted Rad5 MIP motif 7-EERKRFF-13 to 7-EERKRAA-13

(Rad5-MIPΔ) and the predicted SHIP motif 30-NKES<u>F</u>L<u>F</u>-36 to 30-NKES<u>A</u>L<u>A</u>-36 (Rad5-

SHIPΔ) in our Rad5 yeast two-hybrid bait plasmid. Yeast two-hybrid analysis

demonstrated that the Rad5-MIPΔ mutant binds to Msh2 but not to Mlh1, indicating the

Rad5-Mlh1 interaction, but not the Rad5-Msh2 interaction, is mediated by the predicted

MIP box motif (Fig 2.2B). In contrast, the Rad5-SHIPΔ mutant bound to both Mlh1 and

Msh2 (Fig 2.2D), indicating that the Rad5-Msh2 interaction involves another region of

Rad5, an extended SHIP box that requires additional mutations to disrupt, or redundant

interactions with either the putative SHIP box or another region of Rad5.

2.4.3 *Loss of* RAD5 *Causes a Minor Increase in Mutation Rate and a Mutation Spectrum That is Not Representative of That Caused by an MMR Defect*

Given that Rad5 binds to Msh2 and Mlh1, we investigated if loss of RAD5

gave rise to an MMR defect in the absence of DNA damage by determining the mutation

rate of a RAD5 deletion strain with the hom3-10 frameshift reversion assay. In the hom3-

10 assay, -1 frameshift mutations restore growth on a medium lacking threonine. An

MSH2 deletion strain, which is completely deficient for MMR, had a 336-fold increase in

mutation rate over the wild-type strain. However, the rad5Δ strain only had a 2.5-fold

increase in mutation rate (Table 2.1). To determine whether this modest rate increase was

representative of a defect in the canonical mutation avoidance MMR pathway, the HOM3

gene was sequenced for 14-37 reversion isolates from each genotype (Fig 2.3A). MMR

deficient strains result in almost entirely T7 → T6 frameshifts ([27,124,125]), and consistent

with this, 100% of the revertants from the msh2Δ strain were T7 → T6 frameshifts (Fig

2.3B). The wild-type revertants had a wider variety of frameshift reversion mutations (only

65% T7 → T6 frameshifts), although at a much lower rate of occurrence (Fig 2.3B). The

RAD5 deletion strain had a mutation spectrum more like the wild-type strain with even

more kinds of frameshifts observed (only 39% T7 → T6 frameshifts), which may reflect the roles of RAD5 in PRR and not MMR. Together, these data suggest that loss of RAD5 does not strongly influence MMR's canonical mutation avoidance pathway during unperturbed growth, consistent with previous results [126].

2.4.4 *Human Homologs of Rad5, HLTF and SHPRH, Have Split Binding between MSH2 and MLH1*

To test whether the interactions identified between Rad5 and the MMR proteins are conserved in humans, we used co-immunoprecipitation of nuclear fraction lysates from HeLa cells to detect interactions between MMR proteins and the Rad5 human homologs, HLTF and SHPRH. HeLa cells have proficient MMR and undergo MMR-mediated apoptosis after alkylating agents [46,72]. MSH2 directly interacted with HLTF (Fig 2.4A). This interaction was stable even after DNase treatment, indicating that the co-immunoprecipitation was not simply through simultaneous association with DNA (Fig 2.4B). MSH2 and HLTF interacted constitutively in basal conditions and the interaction did not change when the DNA alkylating agent MNNG was added (Fig 2.4A). No co-immunoprecipitation of HLTF with MLH1 was observed under basal or DNA-damaging conditions (Fig 2.4A). In contrast, we found that SHPRH co-immunoprecipitated with MLH1 under basal conditions and the presence of MNNG-induced DNA damage enhanced the interaction (Fig 2.4A). Unlike HLTF, SHPRH did not co-immunoprecipitated with MSH2 under either basal or DNA damaging conditions (Fig 2.4A). Together, this shows that the binding between Rad5 and MMR proteins is conserved to human cells, and interestingly, the interactions with the core MMR proteins seem to be split between the two human Rad5 homologs.

2.4.5 *HLTF Interacts Differently with MSH2 than Other SHIP Box-Containing Proteins*

Given that Rad5's interaction with Msh2 could not be disrupted by mutation of the predicted SHIP box (Fig 2.2), we further investigated the human HLTF-MSH2 interaction. During the *S. cerevisiae* studies that identified the SHIP box motif, we also identified that the *msh2-M470I* mutation, which affects an amino acid in the hinge linker, disrupted the ability of Msh2 to bind to the SHIP box peptide [26]. To determine if HLTF interacted with MSH2 in a manner similar to Rad5, we generated the equivalent human mutation M453I in our GFP-tagged MSH2 construct. We confirmed that the human mutation also disrupted SHIP box interactions by testing the co-immunoprecipitation of MSH2 and MSH2-M453I with SMARCAD1 (Fig 2.5A). SMARCAD1 is the human homolog of *S. cerevisiae* Fun30; both SMARCAD1 and Fun30 contain a conserved N-terminal SHIP box. SMARCAD1 interacts with MSH2 in humans and Xenopus, and the Fun30-Msh2 interaction in yeast is eliminated by the *msh2-M470I* mutation [26,40,46]. We found that SMARCAD1 interacts with wild-type MSH2 but has markedly reduced binding to the MSH2-M453I mutant (Fig 2.5A). In contrast, HLTF co-immunoprecipitated with both wild-type MSH2 and the MSH2-M453I mutant (Fig 2.5B). Evidence from both the *S. cerevisiae* Rad5-Msh2 interaction and the human HLTF-MSH2 interaction studies suggests that this interaction is mediated through a mode of binding distinct from SHIP box motif-mediated interactions. Investigations into this mode of binding are ongoing.

2.4.6 *SHPRH Interacts with MLH1 Only During S-Phase*

To further investigate the interaction between MLH1 and SHPRH, we looked at whether there was a cell-cycle dependency to the interaction, based on the data that the interaction is enhanced with MNNG-induced DNA damage. We first synchronized

HeLa cells with a double thymidine block and followed cell cycle progression through DNA distribution by propidium iodide staining and fluorescence-activated cell sorting (FACS) analysis. We carried out this experiment in the presence or absence of MNNG. After release from the double thymidine block, we observed that the untreated and MNNG-treated cells began moving from the G1 phase to the S phase at 4 hours and primarily in the S phase by 6 hours (Fig 2.6A). At the 10-hour time point, cells were in the G2/M phase and completed a cell cycle by 12 hours (Fig 2.6A). Consistent with the literature, we observed that MNNG induced a prolonged G2/M arrest in the second cell cycle after treatment (24- and 36-hour timepoints, Fig 2.6A) that is not observed in DMSO treated cells.

We then synchronized HeLa cells with a double thymidine block and collected nuclear lysates at the indicated time points corresponding with the cell cycle analysis above. The interaction between MLH1 and SHPRH is only observed by co-immunoprecipitation in the S phase (6-hour time point, Fig 2.6B) and is not detectable during G1 or G2/M.

2.4.7   *Loss of SHPRH Leads to DNA Damage Resistance but Not Increase Mutation Rate*

Treatment of mammalian cells with alkylating agents is known to cause MMR-mediated apoptosis in which loss of MMR activity causes increased alkylating agent resistance [12,13]. Given the interactions of HLTF and SHPRH with MMR proteins, we tested whether the loss of HLTF and SHPRH individually or together would increase resistance to alkylation damage. To test this, we generated HeLa S3 cells in which either MSH2, MLH1, SHPRH, or HLTF was knocked out by CRISPR-Cas9. We also generated a double knockout cell line with both SHPRH and HLTF knocked out. Expression of the

target proteins was eliminated in each cell line respectively and remained stably lost after more than six passages (Supplemental Fig 2.1). MSH2 and MLH1 knockout cells show resistance to MNNG as previously reported for MMR deficient cells [12,127] (Fig 2.7A). The HLTF and SHPRH double knockout cells showed a mild resistance to MNNG compared to the parental cells, although this did not reach the level of resistance equivalent to that of a total loss of MMR (Fig 2.7B). We compared the MNNG sensitivity of the single knockout cell lines to the double knockout to determine if this phenotype was associated with a single Rad5 homolog or if it required the loss of both proteins. HLTF knockout cells remained sensitive to MNNG in the clonogenic survival assay (Fig 2.7C); however, the SHPRH single knockout cell line showed moderate resistance to MNNG similar to the double knockout cell line (Fig 2.7D). While the resistance to MNNG was observed consistently with SHPRH loss, the cells were still markedly more sensitive to alkylating agents than cells that had lost critical MMR proteins. Similar patterns of sensitivity to MNNG were observed for SHPRH and HLTF in a separate cell line that also has proficient MMR (HEK293) utilizing siRNA knockdown of SHPRH, HLTF, or both as measured in a short-term survival MTS assay (Supplemental Fig. 2.2) or long-term clonogenic assay (Supplemental Fig. 2.3). This suggests that SHPRH may play a role in the promotion of apoptosis in a subset of alkylation-induced mispairs. This also demonstrates a functional difference between the two human Rad5 homologs regarding MMR responses to alkylating damage, potentially mediated by the evolutionary split of binding partners between the two homologs (Fig. 2.10).

To determine the mechanisms of SHPRH involvement with the DNA MMR apoptotic response after alkylating damage, we also investigated the G2/M arrest occurring

during the second cell cycle after exposure. A prolonged G2/M arrest in the second cell cycle after alkylation damage is a well-established phenotype for MMR-mediated apoptosis [12]. Cells without MMR do not arrest or undergo apoptosis. We synchronized parental HeLa S3 wild-type and knockout cell lines using a double thymidine block and released after MNNG treatment. The parental cells showed the typical G2/M arrest starting at 24 hours after treatment and maintained it through 48 hours (Fig. 2.8). The MLH1 knockout cells progressed through two regular cell cycles as reported in the literature (Fig. 2.8). The HLTF knockout cells retained the G2/M arrest, consistent with their normal sensitivity to MNNG. Intriguingly, the SHPRH knockout cells also had a typical G2/M arrest despite a decreased sensitivity to MNNG (Fig. 2.9). This suggests that SHPRH may play a role in the steps between G2/M arrest and the lack of resolution of the arrest that then leads to apoptosis. We also observed that untreated SHPRH knockout cells progressed through the cell cycle at a slower rate after synchronization and that, without damage, they had a level of G2/M arrest (between 8 and 10 hours, Fig. 2.9). This was not observed in the HLTF knockout or MSH2 or MLH1 knockout cell lines (Fig. 2.9). This change in cell cycle may be indicative of trouble resolving endogenous damage occurring in culture, potentially related to SHPRH's role in translesion synthesis or template switching pathways.

Given the role of SHPRH in MMR-dependent apoptosis after alkylation damage, we wanted to determine if SHPRH, unlike Rad5 in *S. cerevisiae*, acted in the canonical MMR mutation avoidance pathway. To test this in our HeLa S3 knockout cells, we used the hypoxanthine phosphoribosyl transferase (HPRT) forward mutagenesis assay, as reported by Li et. al [72]. The parental HeLa S3 cells had a mutation frequency of less

than 4.78 x 10^{-6} and the MLH1 and MSH2 knockout cells had increased mutation frequency of about 2.45 x 10^{-4}, similar to the reported frequency for other MMR deficient cell lines (Table 2.2, [72]). The SHPRH knockout cells had an estimated rate approximately equal to the parental cell lines, without any significant colony formation observed at even higher plating densities (Table 2.2). Together, this data suggests that SHPRH influences the MMR-mediated response to alkylation-induced mispairs but not the repair of replication errors through canonical MMR.

2.5   Discussion

The identification of the MIP box motif [24] and, more recently, the SHIP box motif [26] have revealed how many proteins are recruited to sites of MMR. These proteins include those directly involved in MMR (e.g. Exo1) and have identified several other proteins whose roles in MMR and MMR-mediated processes are less well understood, including *S. cerevisiae* Ntg2, Sgs1, Fun30, and Dpb3 [24,26,95] and human FAN1, SMARCAD1, WDHD1, and MCM9 [25,28,40,46,89]. Here, we analyzed candidate MIP and SHIP box sequences to identify *S. cerevisiae* Rad5 as a MIP box-mediated Mlh1 interactor and a SHIP box-independent Msh2 interactor. These interactions found in Rad5 are conserved through evolution to the human homologs HLTF and SHPRH; however, the interaction seems to have split during evolution between the two homologs, with HLTF retaining MSH2 binding and SHPRH retaining MLH1 binding.

Why Rad5 homologs can bind to MMR proteins remains an open question. Numerous screens for mutations that cause MMR defects in *S. cerevisiae* have not identified *rad5* mutations [128,129]. Unlike forward mutation assays like the Can1^{R} and HPRT assays, *hom3-10* and similar frameshift reversion assays measure mutation events

primarily specific to MMR defects [130,131]. Sequence analysis of the mutation spectra in MMR-deficient strains has shown that the primary *hom3-10*-reverting mutation is T7 →T6 (100%, 73 of 73 in MMR-defective genotypes; and 93%,162 of 181 in partial MMR-defective genotypes) [27,124,125]. The *rad5Δ* mutation caused only a minimal increase in the *hom3-10* frameshift reversion rate, and this rate increase is attributable to a different spectrum of mutations than those expected due to an MMR defect (39% T7 →T6 frameshifts). These results suggest that Rad5 either does not play a significant role in mutation avoidance by MMR, consistent with prior results [126], or it is redundant with other MMR sub-pathways, similar to other MMR components such as Exo1 [11].

To model the MMR-mediated response to SN1-type alkylating agents in budding yeast, studies must be carried out in strains that have a *Δrad52Δmgt1* double mutation background to overcome immediate repair by either direct reversal or homologous recombination pathways that are highly efficient in yeast [132]. The sensitivity of Δr*ad5* strains to replication-blocking lesions specific to SN2-type alkylating agents, such as MMS, has been heavily studied in the context of PRR [103]. However, to our knowledge, few studies have looked at Δr*ad5* mutation-containing strains in the context of SN1-type agents in the appropriate background to determine their impact on non-canonical MMR. Cjeka et. al. did conduct a genome-wide screen using the yeast deletion library in the *Δrad52Δmgt1* genetic background and did not identify any factors beyond MMR as having a significant loss of sensitivity to MNNG [133]. However, in the same manuscript, they did a second screen only in the presence of *Δmgt1* to identify factors that may help resolve MMR-mediated toxic intermediates. In this second screen, *RAD5* was identified and, interestingly, was far more sensitive than other members of the PRR pathway [133],

suggesting that *RAD5* may be playing a unique role that we hypothesize is due to its physical interactions with MMR.

Based on these results, we focused our efforts on understanding the role of Rad5 human homologs, HLTF and SHPRH, in non-canonical functions of MMR. Since our report that Msh2 interacts with the Fun30 helicase (SMARCAD1 in humans), another group has confirmed the human MSH2-SMARCAD1 interaction and demonstrated that SMARCAD1 knockout cell lines are moderately resistant to alkylating agent-induced apoptosis likely through changes in the chromatin association of MMR proteins [46]. Similarly, we found that depletion or knockout of SHPRH results in moderate resistance to alkylation-induced cell death consistent with the Rad5-Mlh1 MIP box interaction and the SHPRH-MLH1 interaction. Interestingly, the SHPRH knockout lines retain the MNNG-mediated G2/M arrest but have reduced cell death. SHPRH has several functional domains, including a helicase and an E3 ligase domain [134]. Complementation studies are ongoing to determine which SHPRH domains are critical to mediating sensitivity to alkylation damage. Intriguingly, SHPRH and SMARCAD1 are SNF2-family DNA helicases with very different functions: fork reversal and nucleosome remodeling, respectively. It is currently unclear if there is any redundancy or additive effect between SHPRH and SMARCAD1 roles in influencing this pathway.

We find it especially interesting that while the interactions of both Msh2 and Mlh1 with Rad5 are conserved through evolution to the human homologs, the binding sites seem to have been split between the two homologs (Fig. 2.10). Given the differences of HLTF and SHPRH in alkylation sensitivity, it seems possible that the Msh2-Rad5 and Mlh1-Rad5 interactions have different functional roles that are retained in different Rad5

homologs after gene duplication and specialization [135]. An intriguing possibility, since Rad5 does not appear to act in the canonical MMR mutation avoidance pathway, is that the HLTF-MSH2 interaction works in a separate non-canonical role of MMR, such as heteroduplex rejection [136] or that MSH2 influences the function of HLTF in PRR. Several groups have shown an interaction between nuclease FAN1 and MLH1, mediated by an MIP box and an additional MLH1-interaction domain [25,28]. This binding seems to influence apoptotic response to MNU and control FAN1's role in trinucleotide repeat stabilization and interstrand cross-link repair [25,57]. HLTF and SHPRH may be similarly impacted by MMR interactions that affect their previously identified cellular roles. Porro et al. also demonstrate that the MIP box's phosphorylation status changes the association between FAN1 and MLH1, raising questions on whether post-translational events may also regulate the interactions between MMR proteins and Rad5 homologs.

Table 2.1 hom3-10 Reversion Rates.
Reported rates are the median rates with a 95% confidence interval in square brackets. The
fold increase in mutation rate is listed in parenthesis as compared to the wild-type strain.
n=14-57 independent cultures from two independently derived isolates.

Genotype	Strain	hom3-10 reversion rate
Wild type	RDKY6677	7.50 [4.61-8.95] x 10^{-9} (1)
Δmsh2	RDKY6696	2.52 [1.72-3.04] x 10^{-6} (336)
Δrad5	RDKY6898	1.84 [1.27-3.06] x10^{-8} (2.5)

Table 2.2. HPRT Mutation Frequency.
Reported frequency is the median frequency with a 95% confidence interval in square brackets calculated as described in materials and methods. n=6 per cell line.

Cell Line	HPRT Mutation Frequency
HeLa S3	$< 4.78 \times 10^{-6}$
SHPRH KO	$< 9.31 \times 10^{-6}$
MLH1 KO	2.44 [2.29-2.70] $\times 10^{-4}$
MSH2 KO	2.47 [1.82-3.08] $\times 10^{-4}$

Table 2.3 sgRNA Sequences for Knockout Cell Line Generation.

Name	Forward primer	Reverse Primer
sgHLTF+2	5'-CACCGGTTGGACTACGCTATTACAC-3'	5'-AAACGTGTAATAGCGTAGTCCAACC-3'
sgSHPRH +1	5'-CACCGCTGGAGGAGCACGTTTCCGT-3'	5'-AAACACGGAAACGTGCTCCTCCAGC-3'
sgSHPRH -2	5'-CACCGTTGTGACAAGGGTATTCTGG-3'	5'-AAACCCAGAATACCCTTGTCACAAC-3'
sgMLH1 -1	5'-CACCGTGATAGCATTAGCTGGCCGC-3'	5'-AAACGCGGCCAGCTAATGCTATCAC-3'
sgMSH2 +4	5'-CACCGCTTCTATACGGCGCACGGCG-3'	5'-AAACCGCCGTGCGCCGTATAGAAGC-3'
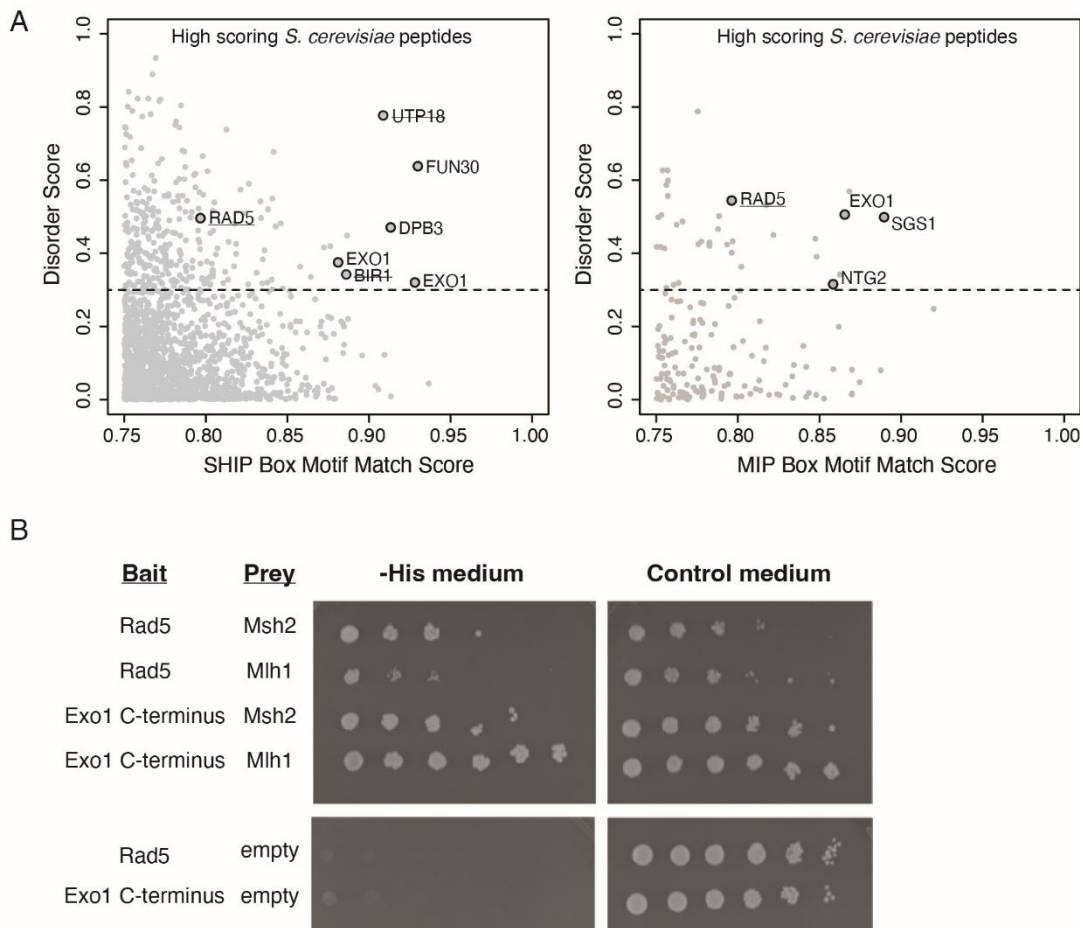
Figure 2.1 Rad5 has a predicted MIP and SHIP box and interacts with Mlh1 and Msh2
A. The match score of 1,745 peptides from the nuclear S. cerevisiae proteome with a moderate or good motif matching to either the MIP or SHIP box motif as determined from bioinformatic analysis using a position-specific scoring matrix (PSSM) are plotted against their long-range disorder predicted by IUPRED [118]. Rad5 was identified in the analysis for both MIP and SHIP motifs. B. Yeast two-hybrid analysis shows that Msh2 and Mlh1 prey constructs interact with Rad5 bait (growth on –Leu –Trp –His selective medium and growth on the control –Leu –Trp medium). Exo1-C terminus bait positively interacts with Msh2 and Mlh1 prey as a positive control. Neither Rad5 nor Exo1-C terminus bait constructs autoactivate in the presence of an empty prey vector.
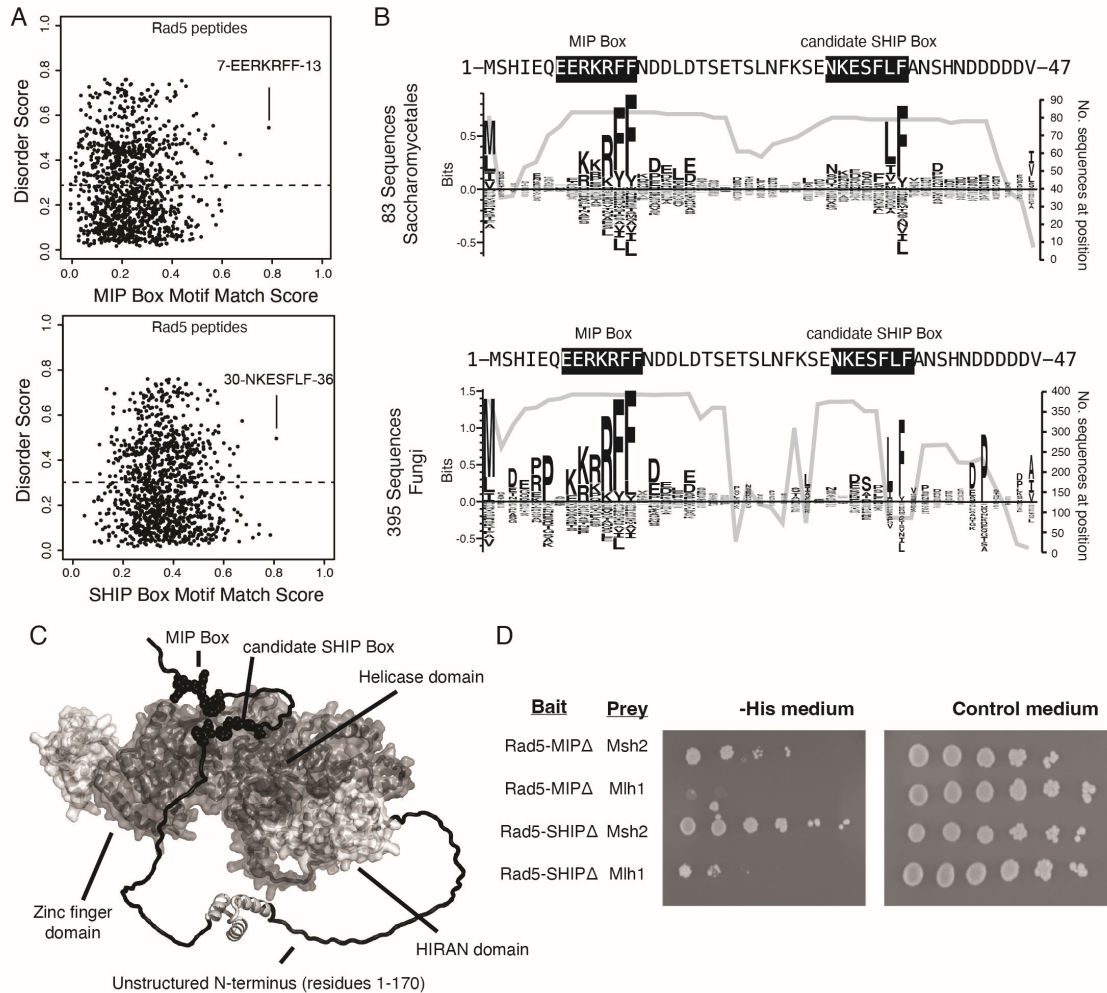
Figure 2.2 Rad5 interacts with Mlh1 through a MIP box motif but does not interact with Msh2 through a SHIP box motif.

The MIP box and SHIP box motif matching scores for every 7mer peptide in S. cerevisiae Rad5 are plotted against the predicted disorder score, showing that the predicted MIP and SHIP boxes have the best peptide scores and are predicted to be disordered by IUPRED [118]. B. Sequence logos of the first 47 amino acids of S. cerevisiae Rad5 generated by Seq2Logo [121] were calculated from an alignment of 83 Saccharomycetales Rad5 sequences (top) or 395 fungal Rad5 sequences (bottom). Large letters above the zero line correspond to highly conserved residues in the alignment. The number of sequences with residues at this location is plotted underneath the sequence logo; note that the MIP box is present in almost all fungal Rad5 sequences aligned, whereas the candidate SHIP box is present only in a small subset of the fungal Rad5 sequences corresponding to the Saccharomycetales (bottom). C. Mapping the predicted MIP and SHIP motifs (black spheres) onto the Alphafold2-predicted structure of S. cerevisiae Rad5 [137,138] reveals that these predicted motifs are in the unstructured N-terminus (black). D. Yeast two-hybrid analysis shows that mutation of the predicted MIP box in the Rad5 bait vector retained the interaction with the Msh2 prey but resulted in a loss of interaction (indicated by no growth on selective -Leu -

Trip -His medium) with the Mlh1 prey vector. In contrast, mutation of the predicted SHIP box in the Rad5 bait vector retained interaction with both the Msh2 and Mlh1 prey vectors.

A

| 0 | 0 | 5 | 0 | | 3 | | 24 | 4 | 0 | 1 | | 0 | | wild type |

```
  0    0   50       3        24  4    0  1      0        wild type

  0    0   00       0        14  0    0  0      0        msh2Δ

  0    0   22       0        11  8    1  3      1        rad5Δ

CCAGTCTTTACAGGGTTTTTTTGGTTTAGTTCCAA
ΔA  ΔC ΔTΔA   ΔG      ΔT ΔG ΔTΔG   ΔC
```

B

hom3-10 reversion rate

T7->T6 rate

Other frameshift rate
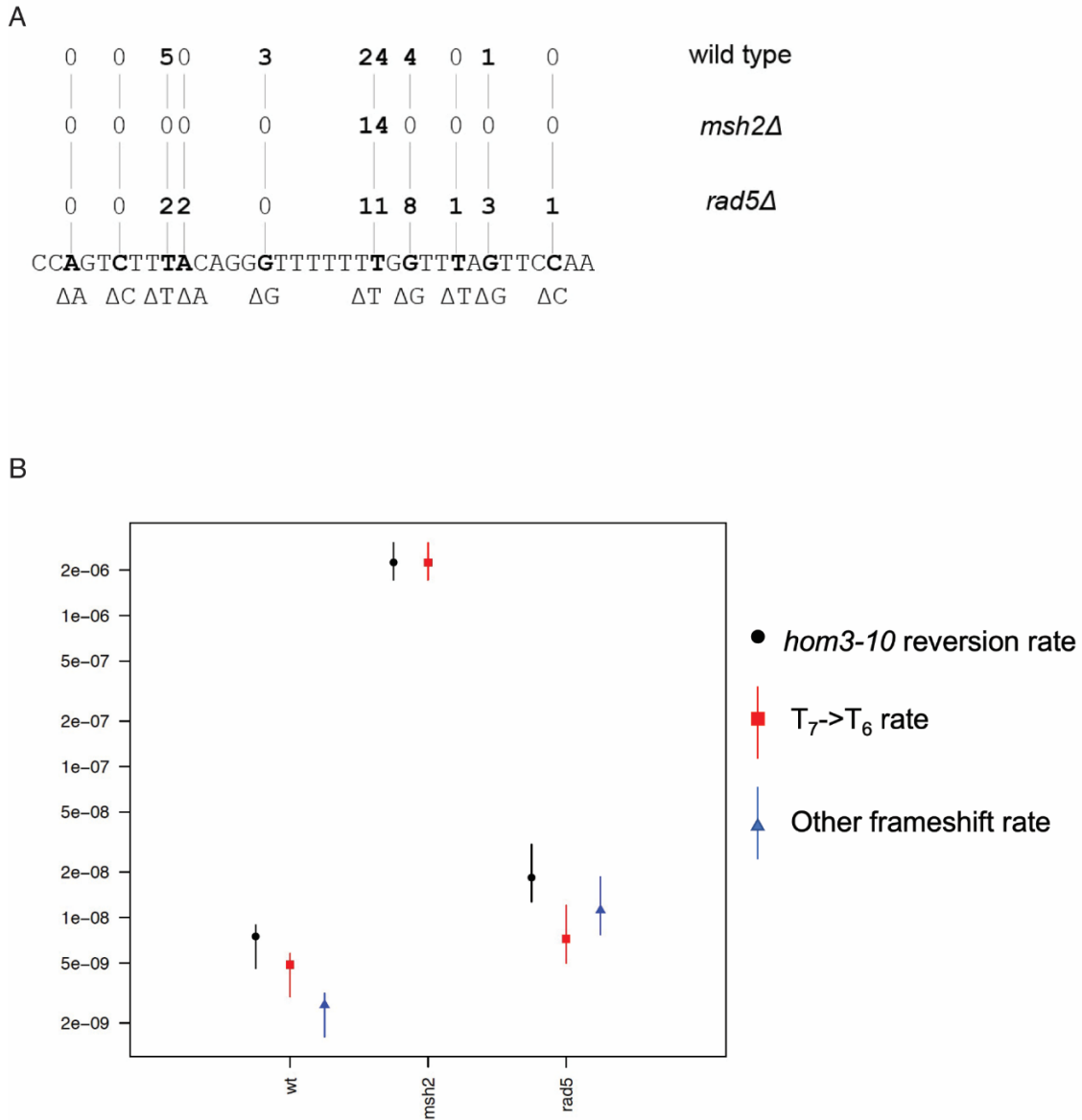
Figure 2.3 Rad5 deletion strain has an altered mutation spectrum from MMR deficient strains

A. Spectrum of mutations selected in the hom3-10 frameshift reversion assay that measures 1 base pair frameshift in the modified HOM3 gene that is required for the synthesis of threonine. Thirty-seven isolates were analyzed for the wild-type strain, 14 isolates were analyzed for the msh2Δ strain, and 28 isolates were analyzed for the rad5Δ strain. MMR deficient strains primarily have T7→ T6 frameshifts. MMR proficient strains have more non T7 → T6 reversion isolates. Δrad5 mutation spectra resembles a wild-type strain more than an MMR-deficient strain. B. Graph of portion of overall hom3-10 mutation rate made up of T7 → T6 reversions or non T7 → T6 reversions. The overall mutation rate for each strain is in black. The proportion of the rate represented by the T7 → T6 reversion rate is in red.
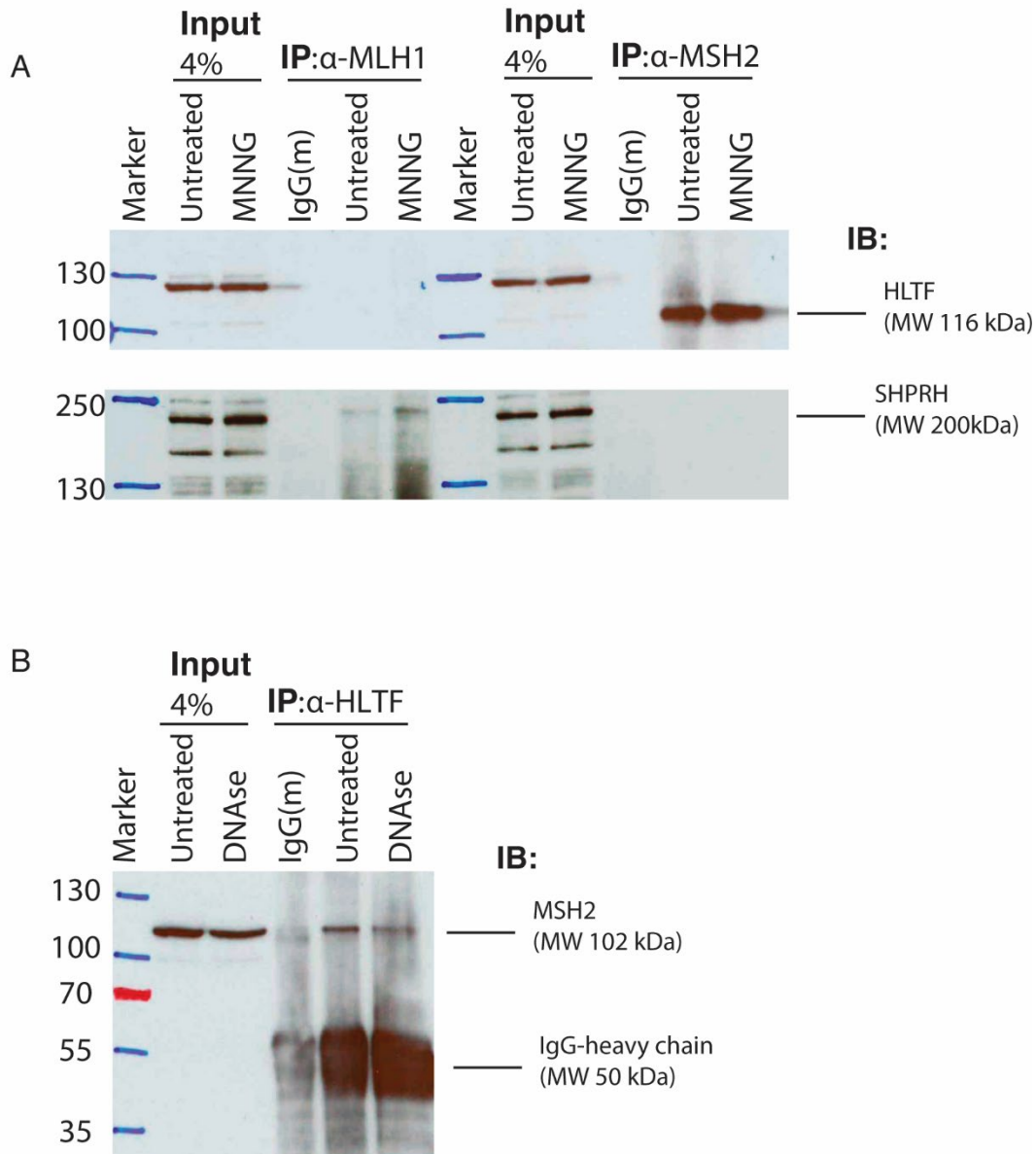
Figure 2.4 Human homologs of Rad5 HLTF and SHPRH interact with MSH2 and MLH1
A. HeLa cells were treated with DMSO or 30μM MNNG and lysates were fractionated to obtain the nuclear fraction. Nuclear fractions were immunoprecipitated with either anti-MLH1 or anti-MSH2 beads and immunoblotted for HLTF and SHPRH. HLTF co-immunoprecipitated with MSH2. Immunoprecipitated HLTF runs at the predicted molecular weight of 116 kDa; however, the non-immunoprecipitated HLTF in the input lanes runs at a slightly higher MW and has several additional bands consistent with the product sheet for the ThermoFisher HLTF antibody. SHPRH co-immunoprecipitated with MLH1 and the interaction is increased after MNNG treatment. B. HeLa cell nuclear lysates were treated with or without DNAse. Nuclear fractions were obtained and immunoprecipitated with anti-HLTF beads and immunoblotted for MSH2. MSH2 interacts with HLTF regardless of DNAse treatment.
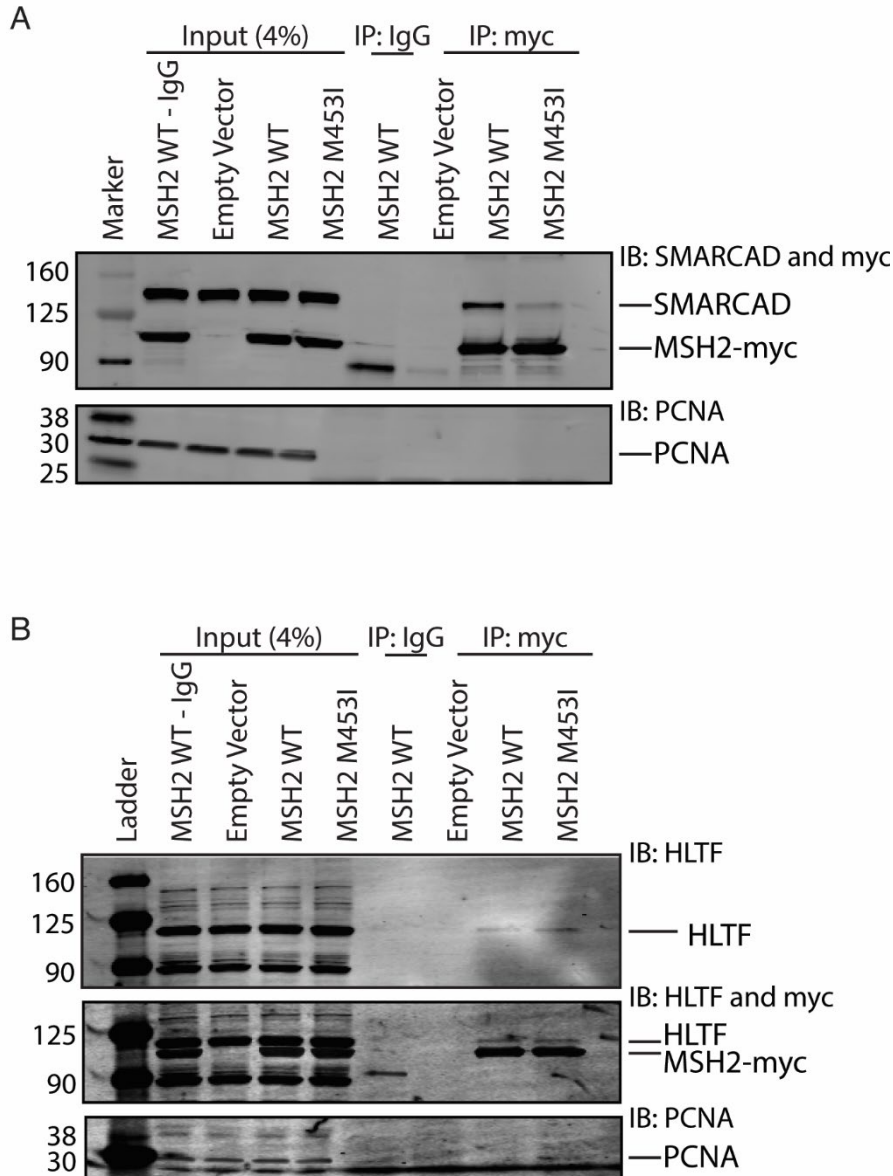
Figure 2.5 HLTF retains binding with the MSH2 M453I mutation

A. HEK293 cells were transfected with c-terminal Myc-FLAG tagged MSH2 WT or MSH2-M453I mutant constructs. Myc-tagged MSH2 was immunoprecipitated with anti-Myc beads and immunoblotted for SMARCAD1. SMARCAD1 co-immunoprecipitated with MSH2 WT but not the MSH2 M453I hinge region mutation. B. HEK293 cells were transfected with c-terminal Myc-FLAG tagged MSH2 WT or MSH2 M453I mutant constructs and Myc-tagged MSH2 was immunoprecipitated with anti-Myc beads and immunoblotted for HLTF. HLTF co-immunoprecipitated with MSH2 WT as we observed with endogenous protein co-IPs. HLTF is also co-immunoprecipitated with MSH2 M453I, unlike SMARCAD1.
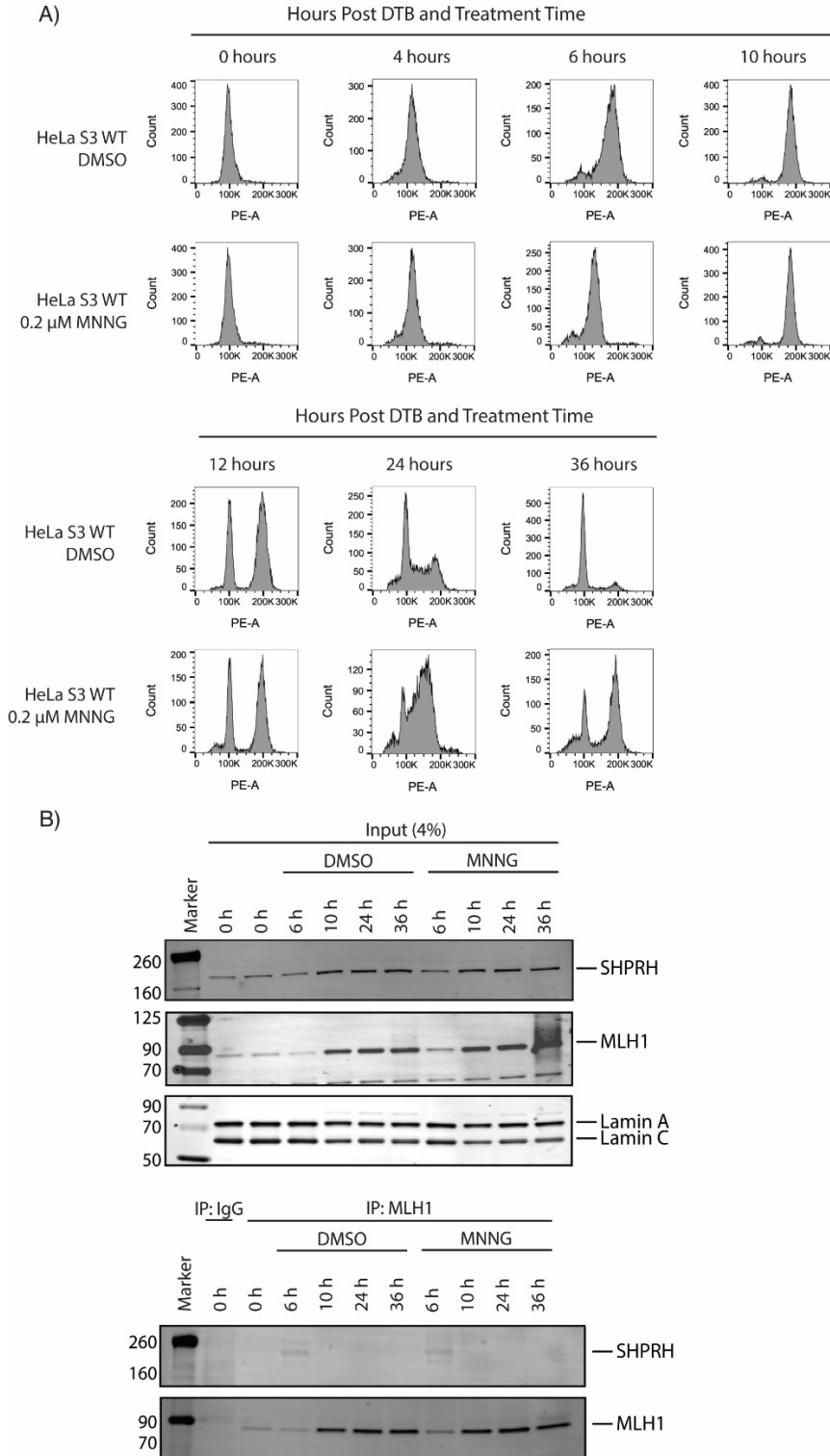
Figure 2.6 SHPRH interaction with MLH1 occurs within S phase of the cell cycle.
A. Cell cycle progression of HeLa WT cells treated with DMSO or 0.2 μM MNNG after
release from double thymidine block (DTB) synchronization. HeLa WT cells have a G2/M
arrest after the second cell cycle (24 hours) following treatment with MNNG. The G2/M

arrest does not occur in HeLa S3 WT cells treated with DMSO. B. HeLa S3 WT cells were synchronized in the G0/G1 cell cycle utilizing DTB synchronization. After synchronization, cells were treated with DMSO or 0.2 µM MNNG and nuclear extracts were collected at indicated time points. Endogenous MLH1 was immunoprecipitated with anti-MLH1 beads and immunoblotted for endogenous SHPRH and MLH1. The input was probed for SHPRH, MLH1, and Lamin A/C as the loading control. SHPRH-MLH1 interaction was seen at the 6-hour timepoint, correlating with the S phase in part A.
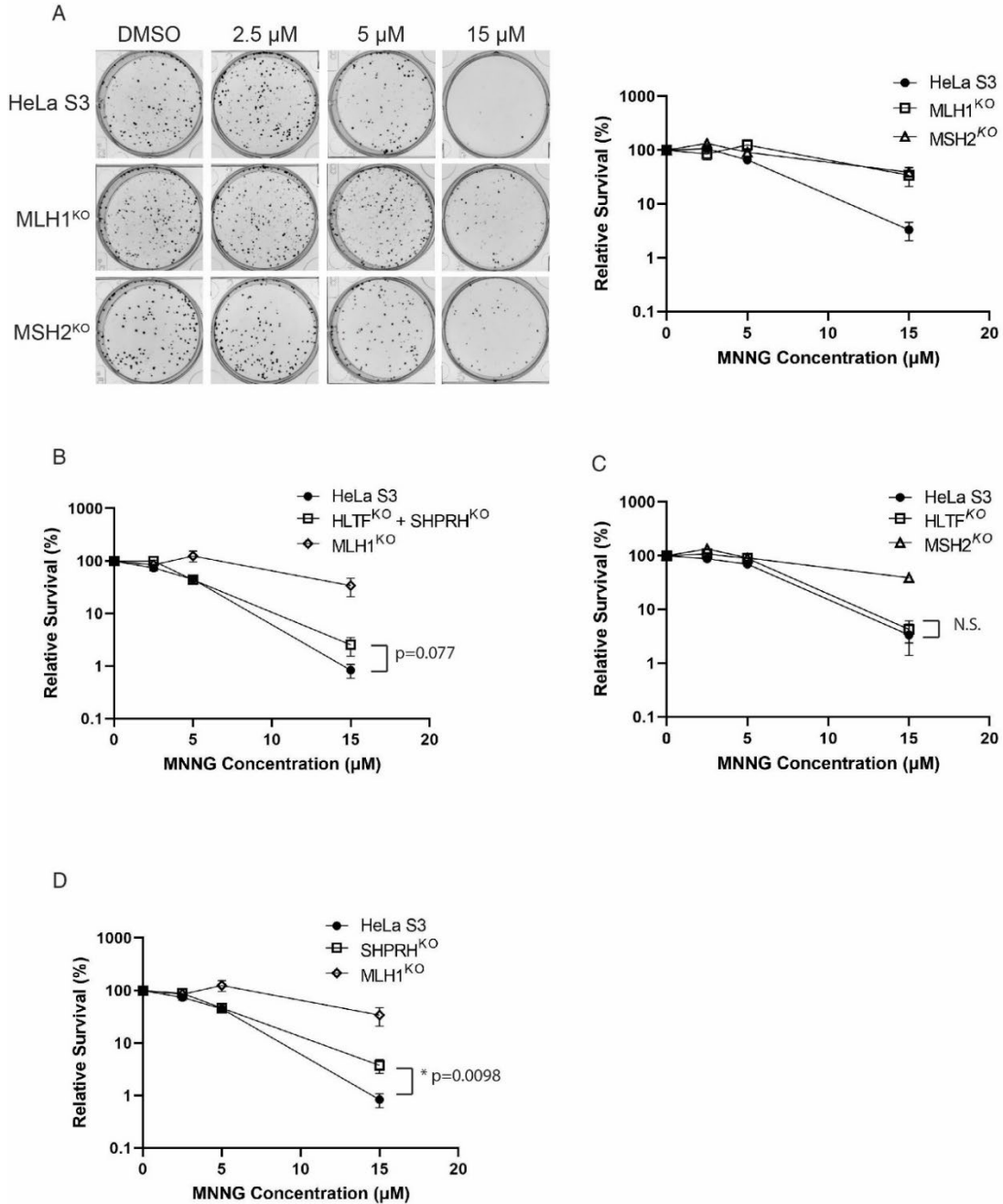
Figure 2.7 Loss of SHPRH results in resistance to alkylating agents.

A. HeLa S3 and CRISPR MLH1 and MSH2 knockout cells were seeded into 6-well plates for 24 hours, followed by a 2-hour pre-treatment with O^6-benzylguanine and a 1-hour treatment of MNNG with O^6-benzylguanine and seeded at a low density into a 6-well plate for a clonogenic survival assay. The left panel is a representative of stained colonies. The right panel is cell viability with colony counting. Data is shown as the mean of n=3 with 4 replicate wells each +/- SEM. B. HeLa S3 and CRISPR HLTF+SHPRH double knockout cells were treated the same as part A for the clonogenic survival assay. Data is shown as the mean of n=3 with 4 replicate wells +/- SEM. Survival is compared to HeLa MLH1 KO

survival from part A. C. HeLa S3 and CRISPR HLTF knockout cells were treated the same as part A for the clonogenic survival assay. Data is shown as the mean of n=3 with 4 replicate wells +/- SEM. Survival is compared to HeLa MSH2 KO survival from part A. D. HeLa S3 and CRISPR SHPRH knockout cells were treated the same as part A for the clonogenic survival assay. Data is shown as the mean of n=3 with 4 replicate wells +/- SEM. Survival is compared to HeLa MLH1 KO survival from part A. Statistical significance was determined by unpaired t-test * p< 0.05.
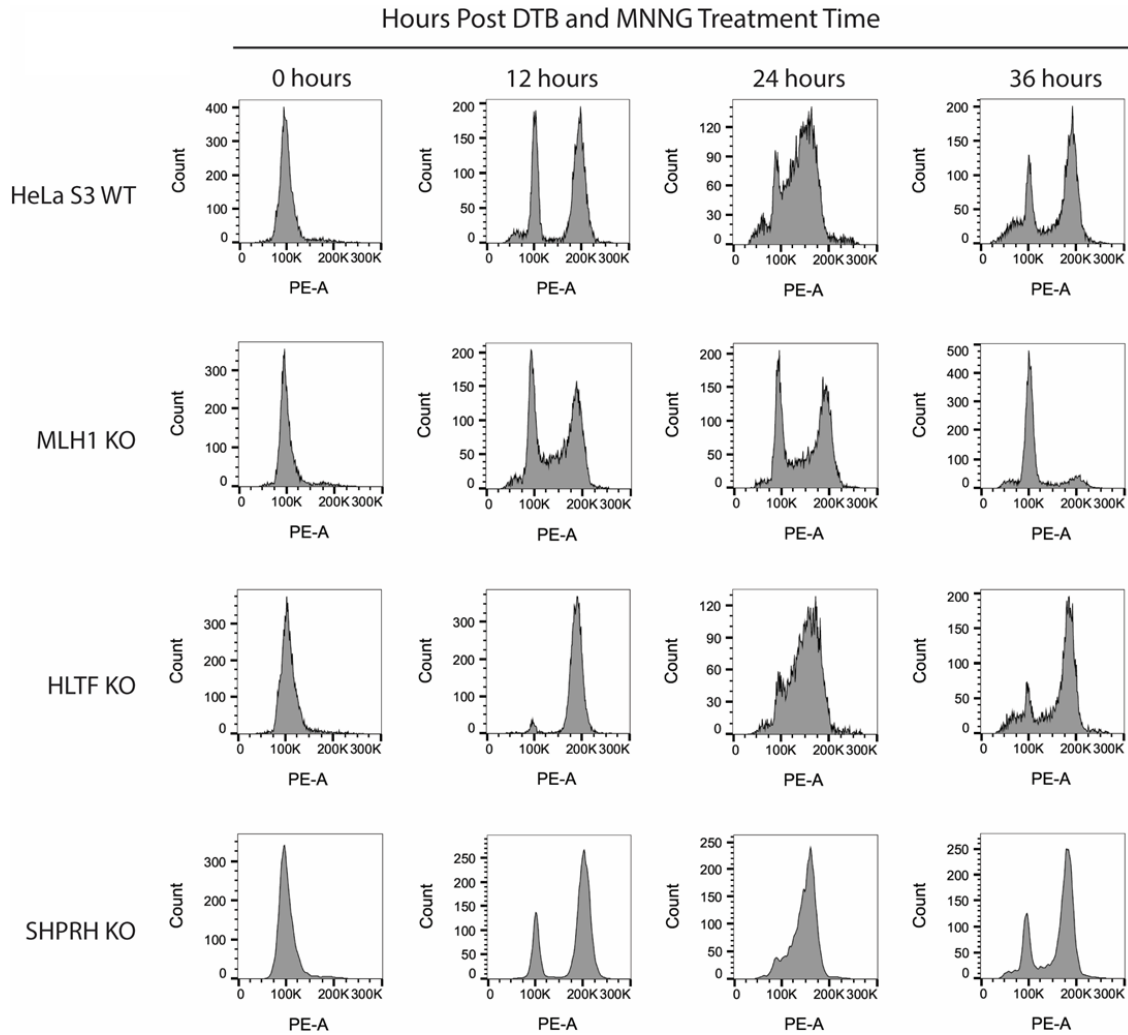
Figure 2.8 HLTF and SHPRH knockout cells retain MNNG-induced G2/M arrest in the second cell cycle after damage.

Cell cycle FACS analysis of HeLa WT, MLH1 KO, HLTF KO, and SHPRH KO cells treated with 0.2 µM MNNG for the times indicated after DTB synchronization. HeLa WT cells have G2/M arrest after the second cell cycle (24 hours). HeLa MLH1 KO cells do not have the G2/M arrest that HeLa WT cells showed. HeLa HLTF KO and SHPRH KO have G2/M arrests comparable to the HeLa WT cells.
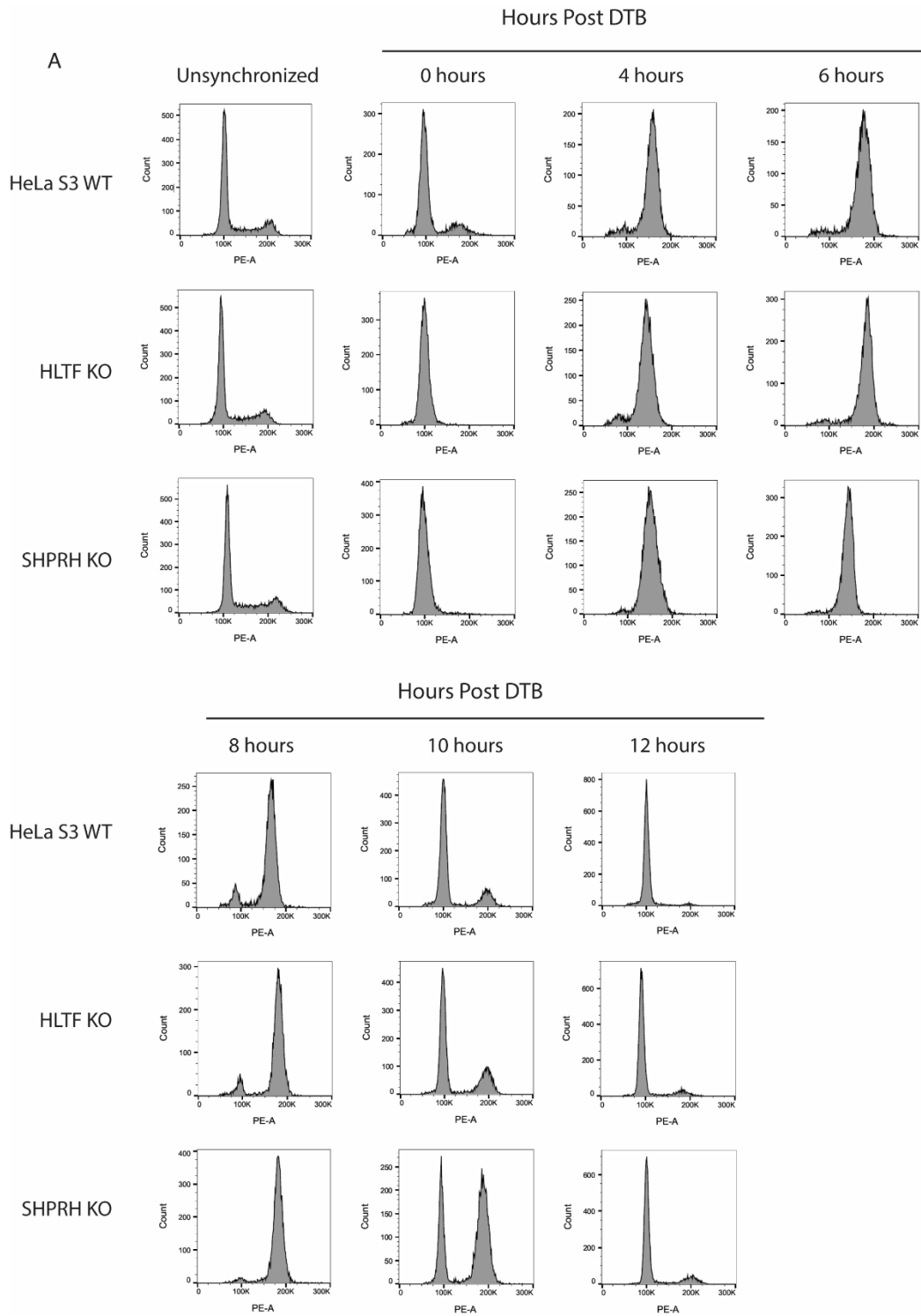
Figure 2.9 SHPRH knock out cells demonstrate delayed cell cycle without exogenous damage.

Cell cycle FACS analysis of HeLa WT, HLTF KO, and SHPRH KO cells after release from DTB synchronization. HeLa HLTF KO cells follow the same cell cycle progression

as the HeLa S3 WT cells. HeLa SHPRH KO cells have a slower cell cycle progression and G2/M arrest compared to the HeLa S3 WT cells.
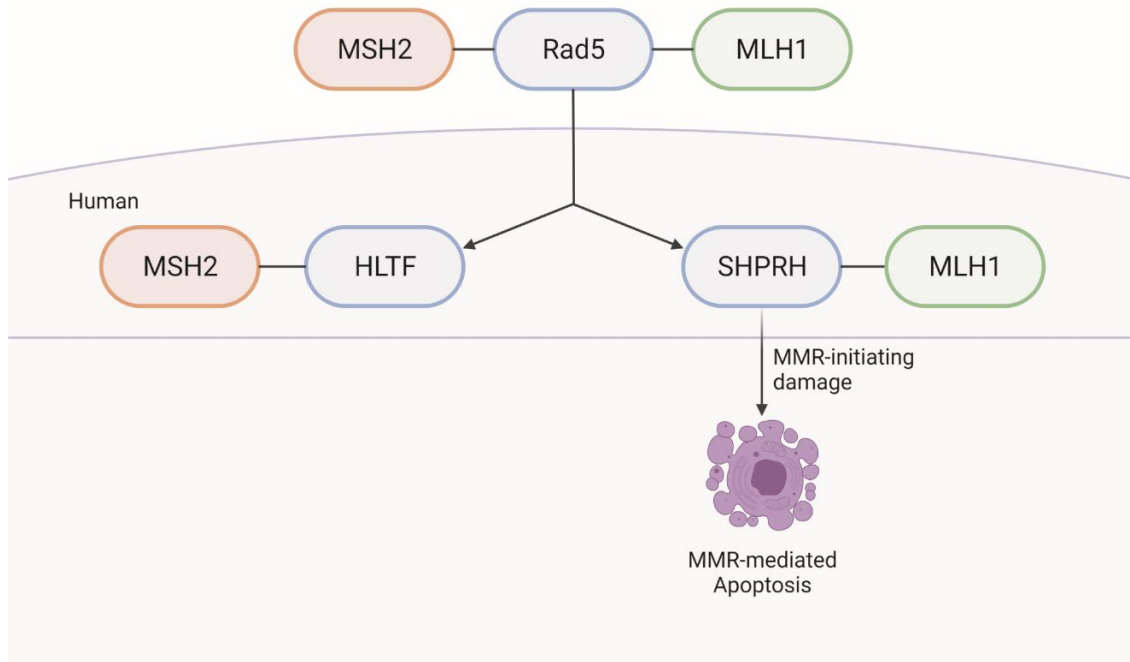
Figure 2.10 Rad5 and human homologs interact with the MMR pathway.
Saccharomyces cerevisiae helicase/E3 ligase Rad5 interacts with both key players in eukaryotic MMR, Msh2 and Mlh1. Rad5 has two human homologs, HLTF and SHPRH. Binding to the MMR pathway is conserved throughout evolution but split between the human homologs with HLTF binding MSH2 and SHPRH binding MLH1. SHPRH plays a role in apoptosis after alkylation damage, as depletion of SHPRH results in resistance to MNNG, similar to the loss of MMR proteins.
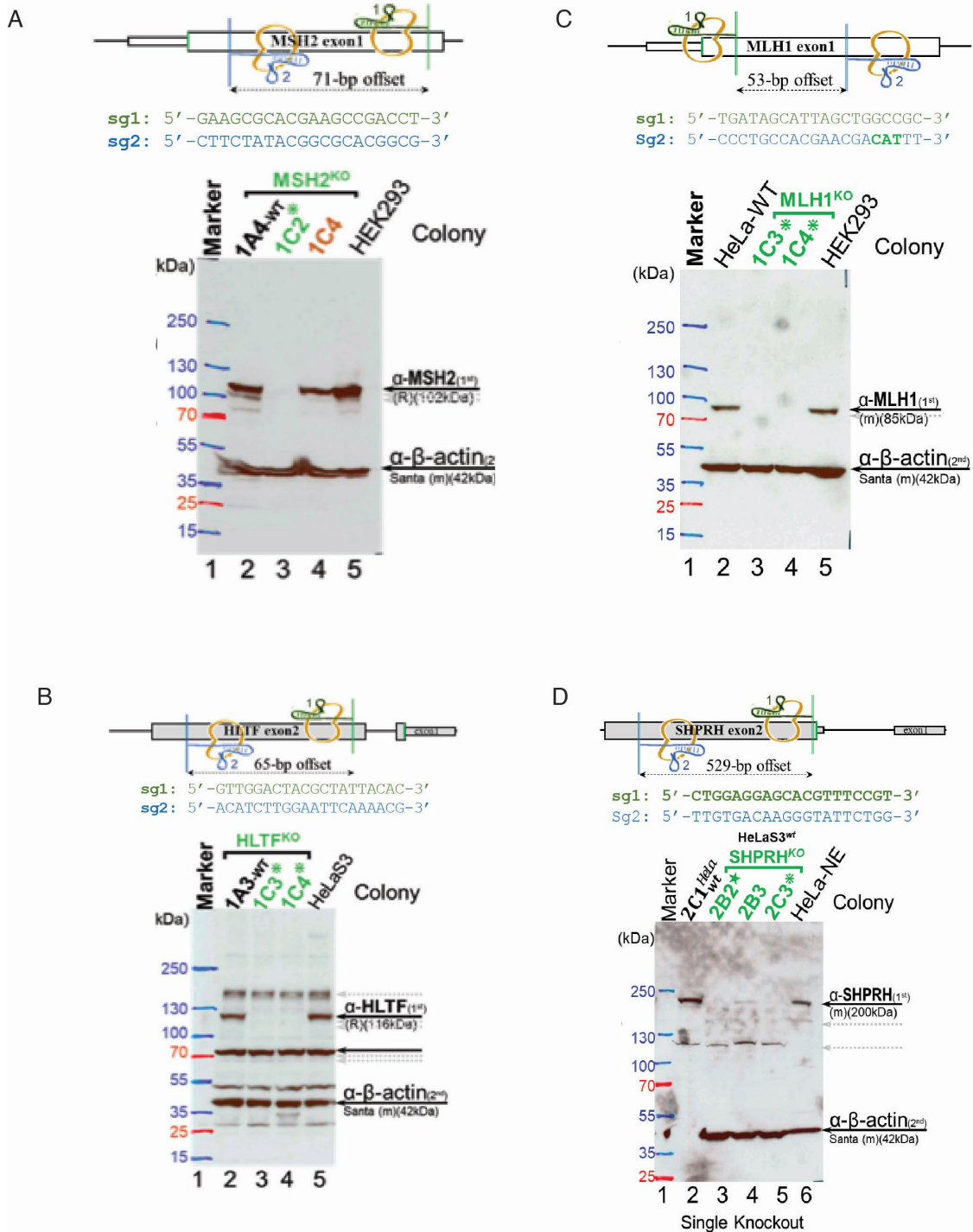
Supplemental Figure 2.1 Generation of Knockout Cells by CRISPR-Cas9.

A. Schematic of sgRNA sequence and target for generating Msh2 knockout Hela S3 cells (top). Immunoblot of Msh2 protein levels in parental cells and selected clones after six continuous passages. Msh2 knockout was retained in clone 2 but re-expressed in clone 4.

B. Schematic of sgRNA sequence and target for generation of HLTF knockout Hela S3 cells (top). Immunoblot of HLTF protein levels in parental cells and selected clones after

six continuous passages. HLTF knockout was retained in clone 3 and clone 4. The double knockout cell line was made by knockout of SHPRH in the HLTF knockout background C. Schematic of sgRNA sequence and target for generation of MLH1 knockout Hela S3 cells (top). Immunoblot of MLH1 protein levels in parental cells and selected clones after six continuous passages. MLH1 knockout was retained in clone 3 and clone 4. D. Schematic of sgRNA sequence and target for generation of SHPRH knockout Hela S3 cells (top). Immunoblot of SHPRH protein levels in parental cells and selected clones after six continuous passages. SHPRH knockout was retained in clone B2 and clone C3.
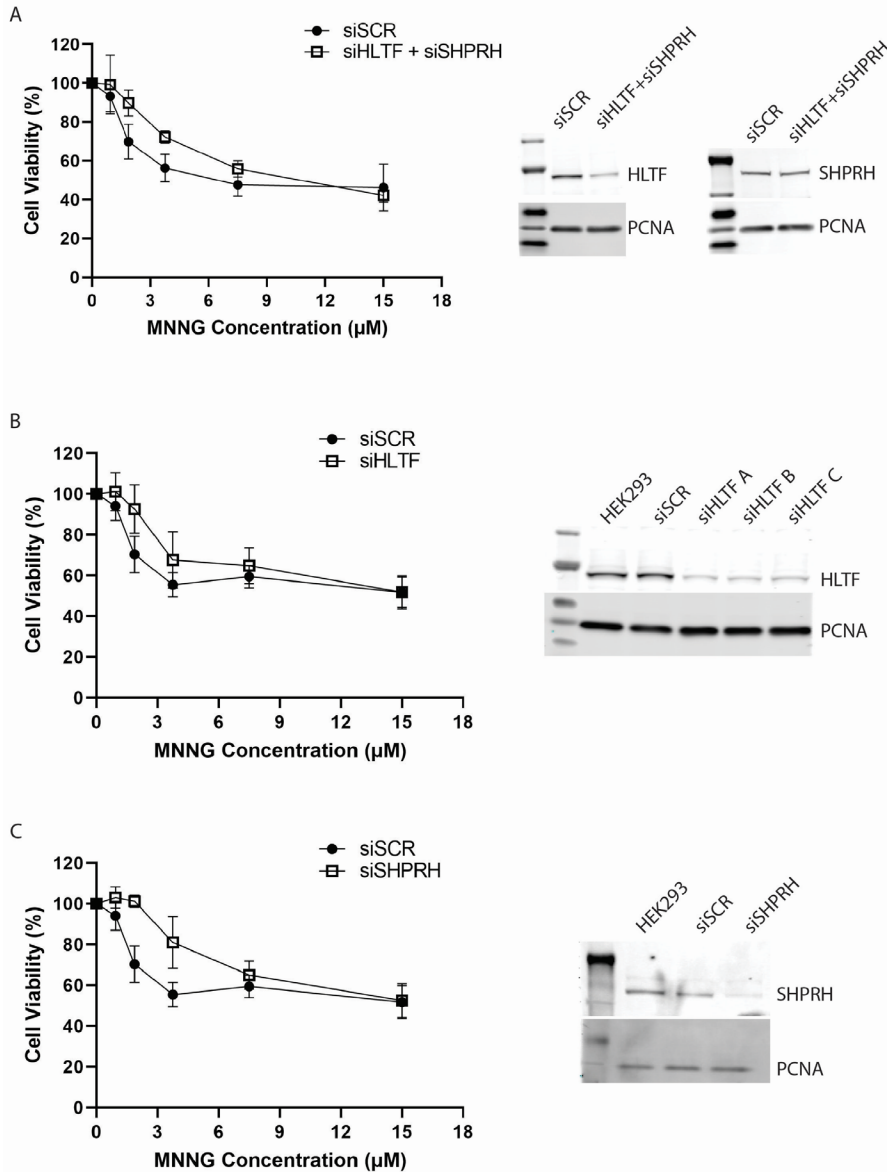
Supplemental Figure 2.2 Loss of SHPRH results in resistance to alkylating agents.
A. HEK293 cells were co-transfected with siRNA to both HLTF and SHPRH. Cells were seeded into 96-well plates for 24 hours, followed by a 1-hour treatment of MNNG and assayed for survival after 72 hours by MTS assay. Data is shown as the mean of n=3 +/- SEM. The efficiency of knockdown for the used siRNA duplex is shown in the right panel. B. HEK293 cells were transfected with siRNA to HLTF. Cells were seeded into 96-well plates for 24 hours followed by a 1-hour treatment of MNNG and assayed for survival after 72 hours by MTS assay. Data is shown as the mean of n=3 +/- SEM. The efficiency of knockdown for the used siRNA duplex is shown in the right panel. C. HEK293 cells were transfected with siRNA to SHPRH. Cells were seeded into 96-well plates for 24 hours followed by a 1-hour treatment of MNNG and assayed for survival after 72 hours by MTS assay. Data is shown as the mean of n=3 +/- SEM. The efficiency of knockdown for the used siRNA duplex is shown in the right panel.
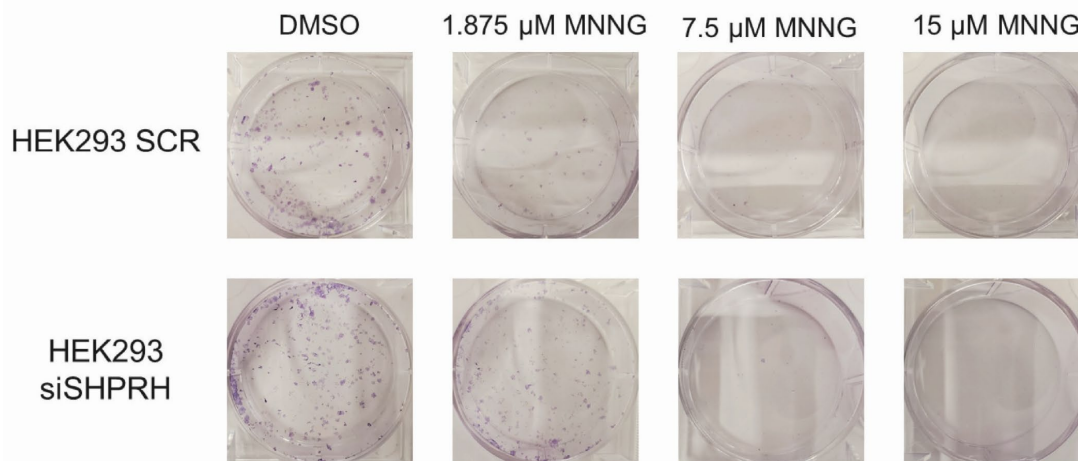
Supplemental Figure 2.3 Clonogenic survival assay of HEK293 cells transfected with siSHPRH.

HEK293 cells with SHPRH knocked down with siRNA were treated with indicated doses of alkylating agents in a long-term clonogenic survival assay. HEK293 cells do not form countable colonies. Visually, siSHPRH cells have greater survival than siSCR cells.

CHAPTER 3. Understanding the Interaction Between HLTF, SHPRH, and Mismatch Repair Proteins and the Interplay Between the Repair Pathways

3.1 <u>Introduction</u>

Throughout the years, many proteins have been found to interact with mismatch repair (MMR) in both yeast and human model systems. MMR has two main roles: the canonical role of correcting mismatches left after replication and the non-canonical role of initiating apoptosis in the presence of particular exogenous damage resulting in damage-dependent mismatches. Many MMR interacting proteins have been found to have a role in canonical MMR, influencing MMR mutation rate either alone or in tandem with critical MMR proteins [26,27,31,71,72,74,79,89,92,94]. Some other proteins identified as accessory factors play some part in MMR-mediated apoptosis, although the exact mechanism is not entirely understood [40,46,57,79,92,95]. Some interacting proteins identified were not studied for a role in MMR but show that MMR proteins play a role in different repair pathways [24,25,28,41,43,87].

Some of the previously identified interacting partners have been identified in yeast and human models through an MIP or SHIP box [26,34]. These conserved motifs are the reason yeast Rad5 was identified as a MMR interactor in Chapter 2 (Figure 2.1A). Rad5 is primarily involved in the template switching (TS) portion of post-replicative repair (PRR) due to its complex with Mms2-Ubc13 and their polyubiquitination of PCNA [27,139,140]. PRR bypasses DNA lesions that can cause fork stalling and collapse [102–104]. The two main branches of PRR are error-prone translesion synthesis (TLS) and error-free TS, with the main distinction being mono- or poly-ubiquitination of PCNA, respectively [102–104]. Rad5 has two human homologs, HLTF and SHPRH, which conserved the polyubiquitination of PCNA and Rad5's role in TS [105,109,110,141]. Rad5 was also found to be

a potential player in TLS, and this potential role was also found in SHPRH and HLTF, with a split between the two proteins [103,112,142,143]. HLTF was found to play a role in PCNA monoubiquitination and associated with a TLS polymerase following UV damage; SHPRH interacted with Rad18 in the presence of MMS treatment [112]. Rad5's interactions with Msh2 and Mlh1 extended to HLTF and SHPRH, splitting the interactions with the critical MMR proteins. Furthermore, SHPRH was found to have some functional significance in the MMR apoptotic response to alkylating agents, although the specific role in this process is not yet known.

Understanding how proteins interact through specific sequences or domains can give more information about the function of the interaction. For example, the S2 site on Mlh1 and the hinge region of Msh2 can facilitate the interaction of proteins that have a partial role in MMR [24,26]. We identified that the N-terminal region of HLTF is important for HLTF's interaction with MSH2. This is significant due to the presence of the HIRAN domain in this region. HLTF's HIRAN domain is vital in HLTF's role in PRR, specifically by binding the 3' end of DNA and facilitating fork reversal and remodeling [144–148]. In addition to understanding the HLTF-MSH2 interaction, knowing that HLTF does not play a role in MMR lends itself to the idea that MSH2 plays a role in PRR.

Additionally, it has been found that loss of proteins in the MutSα complex results in a decreased sensitivity to MMS in a yeast *rad5Δ* strain [149]. We also found that MSH2 likely plays a role in post-replicative repair, with MSH2 having decreased sensitivity to different PRR agents. MMS and UVB were used as PRR damaging substrates, which have been previously used to study PRR [111,112]. MMS is an alkylating agent with low doses used to identify PRR mutants and look at the mechanism of the PRR

branches [111,112,150]. UV damage has also been used to study post-replicative repair, primarily TLS, which has a DNA polymerase that can bypass the UV-induced lesions with fewer errors than other TLS polymerases [111,112,151]. Effects seen with UV and MMS damage can give further insight into PRR, both TLS and TS. We found that loss of MSH2, but not MMR, has been found to decrease sensitivity to both MMS and PRR, which indicated a role of MSH2 in PRR.

This study confirms that HLTF and SHPRH interact with their respective MMR proteins, MSH2 and MLH1, within the cellular environment. We previously found that SHPRH plays a functional role in MMR-mediated apoptosis. We have now identified that SHPRH localization changes when expression of the critical MMR proteins MLH1 and MSH2 are lost. Protein localization can change in response to damage or interaction with other proteins, and similar localization between proteins may indicate a functional relationship [152]. The difference in SHPRH localization with defective MMR further supports the idea that SHPRH has an active role in MMR.

We also identified that HLTF interacts with MSH2 via its N-terminal region, containing the DNA-binding HIRAN domain. Interestingly, MSH2 but not MLH1 had significant resistance to UV radiation and the alkylating agent MMS, leading to the hypothesis that MSH2 plays a role in post-replicative repair. Together, these data confirm that the interactions between HLTF and MSH2 and SHPRH and MLH1 are direct and occur within the cellular environment, there is a functional difference between the interactions, and there is likely an interplay between MMR and PRR.

3.2   Materials and Methods

3.2.1   *Chemicals and Reagents*

Antibodies used in this study include: anti-SHPRH (Origene TA501443), MLH1 (Abcam ab92312, CST 4256S), HLTF (Santa Cruz sc-298357; Invitrogen DA5-83525; Invitrogen PA5-30173), MSH2 (CST 2017S; Invitrogen 337900), DDK (FLAG; Origene TA50011-100), SMARCAD1 (Invitrogen PA553482), PCNA (CST 2586S), Lamin A/C (Santa Cruz sc-376248), Rabbit IgG AlexaFluor 594 (CST-8889S), and Mouse IgG AlexaFluor 488(CST 4408S). The drugs and other chemicals used are as described in Chapter 2. Methyl methanesulfonate (MMS) was purchased from Millipore Sigma (Catalog #129925). UVB radiation was used for UV treatment.

3.2.2   *Immunofluorescence Microscopy*

The immunofluorescence protocol was performed according to the Cell Signaling Technologies protocol. Cells were grown on chamber slides (ThermoFisher 154453) for 24 hours before treatment or fixation. After seeding, cells were treated with DMSO or MNNG for 24 hours before fixation and staining. Cells were fixed with 4% formaldehyde (diluted to 4% from 16% formaldehyde – CST 12606S) for 15 minutes. After washing three times for 5 minutes in 1X PBS (diluted from CST 9808S), slides were blocked in blocking buffer (CST12411S) for 1 hour at room temperature. After blocking, primary antibodies were diluted in dilution buffer (CST 12378S) and incubated overnight at 4°C. The following dilutions were used for each antibody: 1:50 (Santa Cruz HLTF mouse), 1:100 (CST MSH2 rabbit, Origene SHPRH mouse, Invitrogen HLTF DA5-82525 Rabbit), 1:150 (Invitrogen MSH2 mouse), and 1:250 (Abcam MLH1 rabbit). After incubation, the slides were washed three times for 5 minutes in 1X PBS. After washing,

secondary antibodies were diluted in dilution buffer and incubated in the dark at room temperature for 1-2 hours. Secondary antibodies were diluted 1:500 (Rabbit AlexaFluor 594 and Mouse AlexaFluor 488). After incubation in the secondary antibody, the slides were washed three more times for 5 minutes in 1X PBS, protected from light, and the coverslip was mounted with Prolong Gold Antifade Reagent with DAPI (CST 8961S). Confocal microscopy was performed at 100X magnification on a Nikon A1R Confocal Microscope. Super resolution microscopy was performed using the Nikon Super Resolution Inverted Microscope. Image acquisition was performed using Nikon Elements, and analysis was performed using ImageJ software. Measurement of nuclear/cytoplasmic ratio was determined using methods previously described, where a ratio of 1 denotes equal distribution in the cell and an increasing ratio denotes a greater nuclear localization [153].

3.2.3   *Proximity Ligation Assay (PLA)*

Cells were mounted on chamber slides and 24 hours after seeding, were treated with DMSO or MNNG for 24 hours. After treatment, cells were fixed with 4% formaldehyde, washed three times for 5 minutes with 1X PBS, and *in situ* PLA was performed using Duolink PLA technologies (Sigma Aldrich) according to the manufacturer's instructions. Slides were blocked at 37°C for 1 hour and the primary antibodies were diluted in the Duolink antibody diluent overnight at 4°C. The following dilutions were used for each antibody: 1:100 (Origene SHPRH mouse, Invitrogen DA5-82525 HLTF rabbit), 1:150 (Invitrogen MSH2 mouse), and 1:250 (Abcam MLH1 rabbit). Cells were washed twice for 5 minutes at room temperature with Wash buffer A and the PLA Anti-Rabbit PLUS and Anti-Mouse MINUS probes (Sigma-Aldrich; each diluted 1:5) were incubated with the slides for 1 hour at 37°C in a humidity chamber. The slides

were washed twice for 5 minutes in Wash buffer A and the PLA probes were ligated for 30 minutes at 37°C in a humidity chamber. Slides were washed two times for 5 minutes in the dark with Wash buffer A and the slides were amplified using the Duolink In Situ Detection Reagents Green for 100 minutes at 37°C in a humidity chamber. The slides were washed twice for 10 minutes in Wash buffer B and once in 0.01X Wash buffer B for 1 minute. The slides were mounted with Duolink In Situ Mounting Medium with DAPI and imaged on a Nikon A1R Confocal microscope at 40X magnification. Image acquisition was performed using Nikon Elements and foci quantification was performed using ImageJ software.

3.2.4   *Site-Directed Mutagenesis*

Site-directed mutagenesis was used to create the point mutations and the internal deletions discussed in this chapter. Primers for the mutations and deletions were created using Agilent's QuikChange Primer Design Program (primers listed in Table 3.1). The parental DNA was amplified with the designed primers using the QuikChange II or QuikChange II XL Site-Directed Mutagenesis kits. The QuikChange II kit was used for a majority of the mutations and internal deletions; however, QuikChange II XL kit was used for SHPRH internal deletions and hard-to-create mutations and deletions. The PCR products were transformed and selected on plates with necessary antibiotics. Colonies were then grown and sequenced to confirm mutation or deletion and rule out additional gene mutations.

3.2.5   *Short-Term Cytotoxicity Assay*

For UVB treatment, HeLa S3 wild-type or knockout cells were plated at 500,000 cells/well in a 6-well plate prior to UVB treatment. Twenty-four hours after

plating, the cells were treated with the indicated doses of UVB and allowed to recover for three hours. After recovery, the cells were seeded at 10,000 cells/well in 96-well plates and allowed to grow for 48 hours, at which time cell viability was measured using the CellTiter 96 Aqueous One Solution Cell Proliferation Assay (MTS) kit (Promega) according to the manufacturer's instructions.

For MMS treatment, HeLa S3 wild-type and knockout cells were split into a 96-well plate at 10,000 cells per well. Twenty-four hours after plating, cells were treated with indicated doses of MMS, with the treatment left on the cells for 48 hours. After treatment, cell viability was measured using the CellTiter 96 Aqueous One Solution Cell Proliferation Assay (MTS) kit according to the manufacturer's instructions.

3.2.6 *Statistical Analysis*

Calculations of the mean, standard error, statistical analysis, and comparison of each set of experimental means were performed with Graphpad Prism 9.0 (Graphpad Software Inc., La Jolla, CA, USA).

3.3 Results

3.3.1 *HLTF Interacts with Mismatch Repair Partner MSH2 in the Cellular Environment*

We previously showed via co-immunoprecipitation that HLTF interacts with MSH2 constitutively and SHPRH interacts with MLH1 in a damage-dependent manner (Fig. 2.4A); however, this method does not provide detailed information about their interaction within the cellular environment. To test whether the interactions in Chapter Two were also seen within the cellular environment, we first performed basic immunofluorescence confocal microscopy to determine whether there was an overlap between the interacting proteins. We used HeLa cells due to the presence of proficient

MMR and MMR-mediated apoptosis [46,72]; additionally, we could use our knockout cell lines developed in Chapter Two. We began with studying HLTF and MSH2 since they had the strongest interaction via co-immunoprecipitation (Fig. 2.4A). We utilized basic immunofluorescent confocal microscopy to find that HLTF seemed to have overlapping cellular localization with MSH2 (Fig. 3.1A). The interaction occurred constitutively and did not change with the treatment of DNA alkylating agent MNNG, similar to what was seen in chapter two (Fig. 3.1A and 2.4A).

Confocal microscopy has a resolution limit of approximately 250 nm [154]; however, many protein complexes occur below the diffraction limit. Therefore, a higher resolution would be necessary to confirm that the co-localization of proteins is occurring. Structured illumination microscopy (SIM) super-resolution resolution microscopy is an approach that can achieve resolution beyond the diffraction limit, up to approximately 100 nm [154]. We utilized SIM super-resolution microscopy to increase our resolution to 125 nm and found that there was still an overlap between HLTF and MSH2 signals within the cellular environment (Fig. 3.1B). Increasing the resolution of the images further supports the hypothesis that HLTF and MSH2 co-localize within the cellular environment.

To strengthen the argument that HLTF and MSH2 constitutively interact within the cellular environment, we employed the proximity ligation assay (PLA). *In situ* PLA allows the detection of protein-protein interactions at a close proximity – the proteins have to be within 40 nm of each other in the cellular environment [155]. When the proteins are in close proximity, the DNA primers linked to the antibodies can be amplified and foci can be visualized and quantified [155]. The presence of foci within control samples of the experiment are almost non-existent, ruling out the possibility of non-specific binding of

the antibodies used (Fig. 3.1C). Foci were present in the HLTF-MSH2 PLA regardless of treatment with MNNG, confirming the constitutive co-localization of HLTF and MSH2 within the cellular environment (Fig. 3.2C). The overlap of expression occurring at increasing resolutions, the presence of foci from *in situ* PLA, and the immunoprecipitation data seen in Chapter Two allows us to conclude that HLTF and MSH2 constitutively interact within the cell.

3.3.2 *SHPRH Interacts with Mismatch Repair Partner MLH1 in the Cellular Environment*

The other human interaction shown in Chapter Two was between SHPRH and MLH1. With immunofluorescent confocal microscopy, there is a slight overlap between SHPRH and MLH1 independent of MNNG treatment, but this overlap increases with MNNG treatment, like what was seen in the co-immunoprecipitation (Fig. 3.2A and 2.4A). We also employed SIM super-resolution microscopy for SHPRH and MLH1 – DMSO cells were unable to be imaged, therefore, we show a lower concentration of MNNG for comparison. Overlap between SHPRH and MLH1 increases with increasing doses of MNNG, and the localization begins to appear in the cytoplasm as well (Fig. 3.2B). The cytoplasmic localization of MLH1 is not unexpected since MLH1 has both a nuclear localization signal and nuclear export sequence [156].

To strengthen the argument that SHPRH and MLH1 interact in a damage-dependent manner, we used *in situ* PLA to examine the interaction. The presence of foci was seen in control cells (mean of approximately 2 foci/cell) and the number of foci per cell was tripled when treated with MNNG (mean of approximately 6 foci/cell) (Fig. 3.2C). This data supports what is seen in both the confocal and super-resolution microscopy as well as the co-immunoprecipitation in Chapter Two. The number of foci for SHPRH and

MLH1 is fewer than HLTF and MSH2, which parallels what is seen in Fig. 2.4A, indicating that HLTF and MSH2 interact more strongly (Fig. 3.1C and 3.2C). The fact that the interactions seen in the cellular environment occur in a manner and at an intensity similar to the co-immunoprecipitation further supports a functional relevance for the interactions between these post-replicative repair and mismatch repair proteins.

3.3.3   *N-Terminal Region of HLTF Important for MSH2 Interaction*

To define the HLTF-MSH2 interaction, we performed a series of internal deletions to test for loss of interaction with MSH2 (Fig. 3.3A). Although there was a decrease in pulldown in a few internal deletions, only the HLTF Δ2-243 internal deletion completely abolished binding with MSH2 (Fig. 3.3B). The 2-243 region of HLTF contains the HIRAN domain, which binds the 3' hydroxyl end of ssDNA. The HIRAN domain is thought to bind to damaged DNA and stalled replication forks [144,148]. The HIRAN domain is also crucial in PRR due to its role in fork remodeling and reversal, which is one of the mechanisms of template switching – a pathway of PRR [145–147]. If the HLTF 2-243 region is essential for MSH2 binding and contains the HIRAN domain, then it indicates that the HLTF-MSH2 interaction may have a role in PRR.

We also mutated a potential SHIP box on HLTF to determine if this region is important for HLTF-MSH2 interaction. The SHIP motif is in the 243-722 region of HLTF, which retained interaction with MSH2 (Fig. 3.3B). Although mutation of the SHIP region decreased MSH2 binding, the interaction remained, indicating that the SHIP region is not essential for binding to MSH2 (Fig. 3.3B). This matches the co-immunoprecipitation in Fig. 2.5B, where mutation of MSH2 M453 did not disrupt binding with HLTF. The MSH2 M453 region is important for proteins that bind to MSH2 via the SHIP box motif,

such as SMARCAD1 (Fig. 2.5B). SMARCAD1 and its yeast counterpart Fun30 have SHIP boxes and a role in MMR [26,29]. The HLTF SHIP mutant failing to disrupt MSH2 binding and the MSH2 M453I mutant not affecting HLTF binding confirms that HLTF interacts differently from other MSH2 interactors.

MSH2 also has a Walker A ATPase domain that is important for ATP-dependent conformational changes of MSH2 during MMR. Therefore, we tested whether a Walker A motif mutation affected interaction with HLTF. We created MSH2 G674 and K675 mutants, which are Walker type A motif MSH2 mutants that can bind to DNA mismatches but are defective in ATP processing [157–161]. These mutants are deficient in their repair efficiency but still able to initiate apoptosis, and these mutations have effects on trinucleotide repeat instability, class switch recombination, somatic hypermutation, and genomic instability [157,162–164]. MSH2 G674 mutations have also been associated with microsatellite instability (MSI) and found in Lynch syndrome families [165,166]. We found that the MSH2 ATPase mutants decreased binding with SMARCAD1, a protein known to interact with MSH2 and have a role in MMR (Fig. 3.3C). Conversely, mutations in the Walker A motif of MSH2 do not affect interaction with HLTF (Fig. 3.3C). This is in line with our other data indicating that MSH2 and HLTF interact in a different manner than MSH2 and SHIP box-containing proteins (Fig. 2.5).

Since the loss of HLTF was not found to affect canonical or non-canonical MMR and MSH2 mutants that disrupt the interaction of other MMR accessory factors do not affect HLTF binding, we can assume that the HLTF-MSH2 interaction does not play a part in MMR; however, HLTF is involved in post-replicative repair and their interaction may play a role in PRR since deletion of HLTF's 2-243 region abolishes MSH2 binding

and the HIRAN domain, which is within this region, is essential for HLTF's function in PRR.

3.3.4 *SHPRH Likely Has Two Sites Important for MLH1 Interaction*

To narrow down the region of SHPRH important for interaction with MLH1, we tested internal deletions of SHPRH for loss of interaction with MLH1 in a manner similar to our studying of the HLTF-MSH2 interaction (Fig. 3.4A). We began with the N-terminal deletions since a possible MIP box was identified in the N-terminal region of SHPRH (Fig. 3.4A). Internal deletions of the N-terminal region did not affect the interaction between SHPRH and MLH1 (Fig. 3.5B). Additionally, deleting the putative MIP box did not disrupt the interaction between SHPRH and MLH1 (Fig. 3.5B).

We then tested internal deletions of SHPRH's C-terminal region and, comparable to what was seen with the N-terminal internal deletions, there was no change in the SHPRH-MLH1 interaction (Fig. 3.5C). This suggests that two regions of SHPRH likely are important for interaction with MLH1, and the presence of one region can compensate for the loss of another region. Multiple interaction sites have been found on numerous MMR interacting proteins, such as yeast Exo1 and human FAN1. Exo1 has two SHIP boxes and loss of both is required for loss of interaction with MSH2 [26]. FAN1 is an MMR accessory factor that interacts with MLH1 by two regions, a MIP box and an MLH1-interacting motif (MIM) region, with the mutation of both regions required to abolish interaction with MLH1 [25]. This supports the hypothesis that SHPRH likely has two sites for MLH1 interaction, with the potential of multiple MIP or MIM regions being the required sites.

We also created a mutation on MLH1 that could be responsible for the interaction with SHPRH. Yeast Mlh1 has an S2 site involved in the interaction with Exo1, Ntg2, and Sgs1 – each of these interacting proteins has an MIP box important for MLH1 interaction [24,34]. It was found that yeast Mlh1 L511, which was identified as a hypermutator with *pms1-A99V*, plays a role in the interaction of Mlh1's S2 site with MIP-box containing proteins, specifically Exo1 [34,167]. We created an MLH1 L503F mutant, the human equivalent to the yeast Mlh1 L511F mutant previously studied. Mutation of the S2 site of MLH1 did not affect interaction with SHPRH, even in the presence of MNNG damage (Fig. 3.4D). This data supports the hypothesis that SHPRH likely has a MIM site, or a different site on SHPRH, in addition to a putative MIP box that is important for the SHPRH-MLH1 interaction.

3.3.5 *Loss of HLTF Alters MSH2 Cellular Localization*

Protein localization can be altered due to changes in the chemical or genetic environment. We therefore wanted to determine whether the localization of the post-replicative repair proteins and their mismatch repair partners changed with the loss of the interacting protein utilizing SIM super-resolution microscopy. We began with HLTF and MSH2 subcellular localization with the loss of their interacting partners since HLTF and MSH2 had the strongest interaction. Treatment of HeLa wild-type cells with MNNG did not affect the nuclear/cytoplasmic ratio of MSH2, which remained primarily nuclear (Fig. 3.5A; wild-type DMSO mean = 8.5; wild-type MNNG mean = 5.685). This is expected since MSH2 mainly localizes to the nucleus and chromatin association increases in the presence of MNNG, indicating that MSH2 would remain in the nucleus [168]. However, loss of HLTF increases MSH2 nuclear localization, regardless of damage (Fig. 3.5A; HLTF[KO]

DMSO mean = 15.7; HLTF^{KO} MNNG mean = 11.5). This data supports the hypothesis that the HLTF-MSH2 interaction could be significant for PRR.

We then performed the inverse of the previous experiment and found no effect on HLTF localization with the loss of MSH2. Treatment of HeLa wild-type cells with MNNG did not affect the nuclear/cytoplasmic ratio of HLTF, which had a broader distribution throughout the cell when compared to MSH2 subcellular localization (Fig. 3.5B; wild-type DMSO mean = 3.9; wild-type MNNG mean = 2.9). This is expected since MNNG treatment is not primarily associated with PRR, and HLTF was not found to have a role in MMR canonically or non-canonically. Loss of MSH2 had a minimal effect on HLTF subcellular distribution, with a slight decrease in nuclear localization regardless of treatment (Fig. 3.5B; MSH2^{KO} DMSO mean = 2.7; MSH2^{KO} MNNG mean = 2.0). This work indicates that HLTF may be an essential factor in MSH2's role in PRR, but MSH2 is likely not a leading part in HLTF's role in PRR.

3.3.6 *Loss of MMR Proteins Alters SHPRH Cellular Localization*

To understand whether there are subcellular localization changes between SHPRH and MLH1, we continued to use super-resolution microscopy with HeLa wild-type and SHPRH or MLH1 knockout cells. We first looked at MLH1 localization and found that treatment of HeLa wild-type cells with the alkylating agent MNNG did not affect MLH1's subcellular localization, which remained primarily nuclear (Fig. 3.6A; wild-type DMSO mean = 7.6; wild-type MNNG mean = 6.6). There is a slight decrease in nuclear localization after MNNG treatment, possibly due to SHPRH interaction, which we saw began to occur in the cytoplasm in Figure 3.2B. The loss of SHPRH also did not have a large effect on MLH1, although there was a slight decrease in nuclear localization of

MLH1 when SHPRH was lost (Fig. 3.6A; SHPRH^{KO} mean = 4.6; SHPRH^{KO} mean = 5.8). The subtle changes in MLH1 localization could play a part in MMR efficiency and partially explain how the loss of SHPRH has a moderate effect on MMR-mediated apoptosis [156].

Since SHPRH was found to have a slight role in MMR-mediated apoptosis, we expected that SHPRH localization may change due to MNNG treatment. SHPRH also has a nuclear localization sequence, and localization of SHPRH has been found to change when SHPRH is mutated [169,170]. Previous work also suggests that loss of interaction with other proteins affect SHPRH localization [170]. We discovered that SHPRH localization changes in HeLa wild-type cells that are treated with MNNG, with SHPRH nuclear localization increasing in the presence of MMR-initiating damage (Fig. 3.6B; wild-type DMSO mean = 2.7; wild-type MNNG mean = 4.1). This would support our previous finding that the SHPRH-MLH1 interaction increases in the presence of MNNG, where SHPRH localization starts to mirror MLH1 localization, which is primarily nuclear. SHPRH nuclear localization significantly increases, similar to wild-type MNNG treatment levels, without treatment when MLH1 is lost (Fig. 3.6B; MLH1^{KO} DMSO mean = 5.3). However, when we treated MLH1 knockout cells with MNNG, SHPRH nuclear localization significantly decreased, like wild-type untreated cells (Fig. 3.6B; MLH1^{KO} MNNG mean = 2.6). Loss of MLH1 could be changing SHPRH interaction with other proteins, such as PCNA, which could play a role in altering SHPRH's subcellular localization.

Since SHPRH localization changed with the loss of MLH1, we also wanted to determine whether this change was due to the loss of SHPRH's interacting partner or

defective MMR. Treatment of HeLa wild-type cells with MNNG had similar ratios of SHPRH localization changes when performed in the MLH1 knockout experiments, with SHPRH nuclear localization increasing with MNNG treatment (Fig. 3.6C; wild-type DMSO mean = 2.8; wild-type MNNG mean = 5.6). Comparable to MLH1 knockout cells, SHPRH nuclear localization significantly increases without treatment with loss of MSH2 (Fig. 3.6C; MSH2^{KO} DMSO mean = 4.7). Additionally, SHPRH nuclear localization returns to wild-type untreated levels when MSH2 knockout cells are treated with MNNG (Fig. 3.6C MSH2^{KO} MNNG mean = 2.3). Taken together, the fact that SHPRH localization changes with the presence of MMR-initiating damage MNNG and SHPRH localization also changes following the loss of critical MMR proteins demonstrate that SHPRH plays a role in MMR and loss of MMR changes SHPRH's function within the cell. This is further supported by the data showing similar SHPRH localization changes within MSH2 knockout cells, and not solely with SHPRH's interacting partner, MLH1.

3.3.7 *MSH2, Not MMR, Has Potential Role in Post-Replicative Repair*

We then wanted to test whether the MMR proteins had a role in sensitivity to agents associated with post-replicative repair. We utilized UVB and MMS treatments as different damaging agents to study PRR, which have been previously used to examine PRR activity [111,112]. There was no substantial change in UVB sensitivity with the loss of SHPRH or HLTF alone; however, double knockout of HLTF and SHPRH resulted in decreased sensitivity to UVB (Fig. 3.7A and 3.7B). The reduced sensitivity with double knockout could be due to forcing other DNA damage tolerance pathways to repair the damage, such as NER or BER to compensate. Loss of MSH2 also decreased UVB sensitivity at a level similar to the HLTF^{KO}SHPRH^{KO} cell line, which could indicate a role

in the PRR pathway (Fig. 3.7A). This sensitivity is only found in MSH2 knockout cells, with MLH1 knockout sensitivity being comparable to wild-type sensitivity, indicating that MSH2, not MMR, plays a role in PRR's response to UV damage (Fig. 3.7A and 3.7B).

We also utilized MMS, which was also studied for PRR response, and found that loss of HLTF did not have a significant difference in MMS sensitivity at multiple MMS concentrations; however, loss of SHPRH has a significantly increased sensitivity to MMS at higher concentrations. (Fig. 3.7C and 3.7D). This difference emphasizes that there is a separation between SHPRH and HLTF in PRR, where SHPRH was found to have increased interactions with PRR proteins following MMS treatment [112]. Loss of both HLTF and SHPRH again had a decreased sensitivity to MMS treatment (Fig. 3.7D). This further supports the idea that the loss of both Rad5 homologs forces cells to repair the DNA in a mechanism external to PRR by utilizing other DDT pathways.

Loss of MSH2 also decreased MMS sensitivity at a level similar to the HLTF^{KO}SHPRH^{KO} cell line, which indicates a role in the PRR pathway (Fig. 3.7C). This sensitivity is only found in MSH2 knockout cells, with loss of MLH1 being comparable to wild-type sensitivity, indicating that MSH2, and not MMR, plays a role in PRR's response to MMS (Fig. 3.7C and 3.7D). Taken together, the data showing HLTF interacts with MSH2 via a region containing its HIRAN domain, MSH2 interactions that disrupted other MMR accessory factors not affecting HLTF, and loss of MSH2 and not both critical MMR proteins leading to decreased sensitivity to PRR-associated damaging agents support the hypothesis that MSH2 plays a role in PRR.

3.4   Discussion

Mismatch repair is one of the five main DNA repair mechanisms, with the canonical purpose of MMR being to repair mismatches from replication [2]. MMR increases the fidelity of replication to one error every billion base pairs, which maintains genomic stability [1]. MMR also has the non-canonical role of responding to certain types of exogenous damage, such as alkylating agents [12,13]. The core mechanism of MMR is well known; however, accessory factors that interact with the critical MMR proteins and have a role in MMR continue to be identified [26–28,40,57,58,69,72,74,89,94,95]. Understanding the role of accessory factors in MMR can give more details about the differences between canonical and non-canonical MMR. Identifying novel accessory factors also gives a greater insight into the nuances of MMR, its role in other repair pathways, and how defects in the proteins or their interactions can lead to disease formation and progression.

When MMR is defective, it leads to genomic instability and the formation of diseases such as cancer [8,12,14]. Faulty MMR results in microsatellite instability (MSI), identified by expansions and contractions in regions of repeated sequences known as microsatellites [15,16]. MSI-high cancers have been identified in approximately 15% of sporadic colorectal cancers; defective MMR is also found in Lynch syndrome, a familial condition resulting in a predisposition to multiple cancer types [20–23]. MSI-high cancers have also been found in various cancer types, in addition to colorectal cancer and cancer types associated with Lynch syndrome [171]. MSI status is now being identified as a positive predictor of clinical response to immunotherapy in multiple cancer types, likely due to the increased mutational burden and potential neoantigen production, which may be a target for immunotherapy [19,172–174].

Mutations and defects in MMR and post-replicative repair both lead to genomic instability. HLTF and SHPRH have been associated with different cancer types, some of which are associated with MSI. Loss of HLTF expression by hypermethylation has been associated with colorectal cancer [113]. Loss of SHPRH has also been connected to various cancers by the accumulation of point mutations in SHPRH in cancer, circular SHPRH levels being decreased in glioblastoma compared to regular brain tissue, and the fact that SHPRH is located on a chromosome region thought to contain a tumor suppressor region [114–116]. Methylation of SHPRH was recently found to be associated with elevated MSI [175]. SHPRH and MLH1 methylation were found in mutational signature 6, which is related to MMR defects and is most common in colorectal and uterine cancers [175]. A subset of sporadic colorectal cancers with MSI do not have alterations in the core MMR proteins [176]. This gives credence to our hypothesis that SHPRH is an accessory factor in MMR, although SHPRH's role in MMR had not been previously studied.

We previously speculated that since HLTF and SHPRH had different sensitivity to the alkylating agent MNNG, there may be a split between the functional role of Rad5's interaction with Mlh1 and Msh2. Therefore, understanding subcellular localization, regions required for interaction, and the effect on PRR is necessary to understand the function of HLTF with MSH2 and SHPRH with MLH1 in DNA damage response. It has been shown that HLTF and SHPRH interact with MMR proteins via co-immunoprecipitation (Fig. 2.4A); however, localization within the cellular environment had not been previously studied. In this study, we show that HLTF and MSH2, as well as SHPRH and MLH1, localize and interact within the cell. This evidence, and the evidence

that SHPRH plays a role in MMR-mediated apoptosis, strengthens the argument that SHPRH has a role in the noncanonical MMR pathway.

To further understand the interaction between HLTF and MSH2, and SHPRH and MLH1, we performed internal deletions of HLTF and SHPRH and mutagenesis of MSH2 and MLH1 to understand the domains necessary for the interaction. We could not find the location on SHPRH essential for MLH1 binding, even with mutation of a potential MIP box. This suggests the possibility of two sites on SHPRH important for MLH1 binding, which could include the presence of multiple MIP boxes. Mutation in the S2 site of MLH1, which was found to be important for MIP box containing proteins[24], did not wholly abolish SHPRH interaction. This could indicate that an MIP box may not be the only way that SHPRH interacts with MLH1, especially with the identification of an MLH1-interacting motif (MIM) being identified in other MLH1 accessory factors [25]. Potential MIP and multiple MIM sequences have been identified on SHPRH and require further investigation.

We found that the N-terminal region of HLTF, containing the HIRAN domain, was responsible for MSH2 binding. The HIRAN domain has a functional role in fork remodeling and reversal, which is essential in PRR. The HIRAN domain has the function of binding to the 3' hydroxyl end of DNA – other DNA binding proteins were found to interact with MutS, which supports the possibility of MSH2's interaction with another DNA binding protein, such as HLTF, that may be important in another repair pathway [92,94,95,145]. We previously showed that disruption of the MSH2 site important for SHIP-mediated interactions did not affect HLTF-MSH2 binding (Fig. 2.5). We also found that an MSH2 mutation affecting the ATPase domain does not affect HLTF-MSH2

interaction like it does with the MMR accessory factor SMARCAD1 (Fig. 3.3C). The ATPase domain is essential for repair efficiency, with MSH2's loss of ATP processing inhibiting its repair ability [157–161]. This suggests that interaction between HLTF and MSH2 occurs in a different mechanism than MSH2-interacting proteins with a role in MMR, indicating a potential role in another repair pathway.

More evidence suggesting that MSH2 has a role in PRR comes from the change in MSH2 subcellular localization with loss of HLTF (Fig. 3.5A). This change is not dependent on treatment with the alkylating agent MNNG. Still, it would be interesting to see whether MSH2 localization changes in the presence of PRR-damaging agents such as UV or MMS. HLTF may be the player involved in recruiting MSH2 to PRR since the loss of MSH2 did not greatly affect HLTF subcellular localization. Since protein subcellular localization is important in determining protein functions and protein-protein interactions, losing HLTF's interaction could prevent MSH2 from being recruited for PRR.

We also looked to understand how the loss of expression in the PRR or MMR proteins affects the subcellular localization of their interacting partner. Loss of SHPRH did not alter MLH1 subcellular localization regardless of treatment with the MMR-initiating agent MNNG (Fig. 3.6A). Conversely, loss of MLH1 altered SHPRH subcellular localization by increasing nuclear localization without damage and distributing SHPRH to wild-type untreated levels when treated with MNNG. The same results were observed with loss of MSH2, pointing to a localization change due to defective MMR and not solely the loss of interacting partner MLH1 (Fig. 3.6B and 3.6C). The difference in SHPRH localization is plausible since SHPRH has a nuclear localization signal and has been found to change localization subsequent to the loss of an interacting partner [169,170].

84

Other nucleosome assembly and remodeling proteins contain an NLS and participate in nucleocytoplasmic shuttling [177]. The change in localization due to defective MMR and the lack of change in MLH1 localization with loss of SHPRH strengthens the hypothesis that SHPRH is an accessory factor to MMR and alterations in MMR affect SHPRH function within the cellular environment. SHPRH may be recruited to the nucleus for DNA damage repair at a higher rate when MMR is defective, and other repair pathways might be utilized in response to exogenous damage when MMR is defective.

The next step was determining whether the MMR proteins played a role in post-replicative repair (PRR). Msh2 was shown to alter sensitivity to MMS treatment in Rad5-deficient cells in yeast, indicating a potential role in PRR[149]. Our study shows that loss of MSH2 does confer an apoptotic resistance to both MMS and UV treatment, demonstrating its potential role in the PRR pathway (Fig. 3.7). Loss of MLH1 does not have a large effect on survival from MMS or UV, suggesting that MSH2, and not all of MMR, plays a role in PRR (Fig. 3.7). Understanding the downstream signal responses in the PRR pathway is essential in verifying this. Looking at PCNA mono- and poly-ubiquitination and replication fork stability and progression would be a crucial step in understanding the role of MSH2 in PRR.

Table 3.1 Primer Sequences Designed for Mutations and Internal Deletions.

Name	Primer #1	Primer #2
HLTF Δ2-243	CGCCGCGATCGCCATGCAAAAACAAGCTCTAGC	GCTAGAGCTTGTTTTTGCATGGCGATCGCGGCG
HLTF Δ243-722	CATTGGAAGACACTGCATTTGGAAGCAGTGGTGTTTCA	TGAAACACCACTGCTTCCAAATGCAGTGTCTTCCAATG
HLTF Δ722-831	AAATTTGTTGCCATACTTACCTTCTTTCAAAGATTAATGCGCTAATGC	GCATTAGCGCATTAATCTTTGAAAGAAGGTAAGTATGGCAACAAATTT
HLTF Δ831-1008	CGCGTACGCGTACTGGATGTCCATTCCATATC	GATATGGAATGGACATCCAGTACGCGTACGCG
HLTF SHIP	GCCATGGAACCATCCAAACGAGTAGCCACAGCTCCAGAGGCTTTAAGTGGTATTTC	GAAATACCACTTAAAGCCTCTGGAGCTGTGGCTACTCGTTTGGATGGTTCCATGGC
MSH2 G674A	TCGAATATATGTTGATTTAGCTCCCATATTGGGGCCAG	CTGGCCCCAATATGGGAGCTAAATCAACATATATTCGA
MSH2 K675R	TGTCGAATATATGTTGATCTACCTCCCATATTGGGGCC	GGCCCCAATATGGGAGGTAGATCAACATATATTCGACA
MSH2 K675M	GTTTGTCGAATATATGTTGACATACCTCCCATATTGGGGCCAGTA	TACTGGCCCCAATATGGGAGGTATGTCAACATATATTCGACAAAC
MSH2 K675A	GTTTGTCGAATATATGTTGATGCACCTCCCATATTGGGGCCAGT	ACTGGCCCCAATATGGGAGGTGCATCAACATATATTCGACAAAC
SHPRH Δ2-439	CCGCGATCGCCATGCCTCCTACACGTGT	ACACGTGTAGGAGGCATGGCGATCGCGG
SHPRH Δ439-987	GCAAGAACTCTCCACGTTGAACTTTTTCTTTTGGTTCAAATTCG	CGAATTTGAACCAAAAGAAAAAGTTCAACGTGGAGAGTTCTTGC
SHPRH Δ987-1510	CTGTCACCCACAGGCTAAAGTGGAAGCTGTGG	CCACAGCTTCCACTTTAGCCTGTGGGTGACAG
SHPRH Δ1510-1683	CCTGTGAAGGGCAGCCATTCTACGCGTACGCG	CGCGTACGCGTAGAATGGCTGCCCTTCACAGG
SHPRH ΔMIP	ACCTTGTGAATCGGGATTTTTTGTGGATGGAACAAGCTTTTTC	GAAAAAGCTTGTTCCATCCACAAAAAATCCCGATTCACAAGGT
MLH1 L503F	AGACTCAAAACACTAGTGAAGTTAATGATCCTTCTCCGG	CCGGAGAAGGATCATTAACTTCACTAGTGTTTTGAGTCT
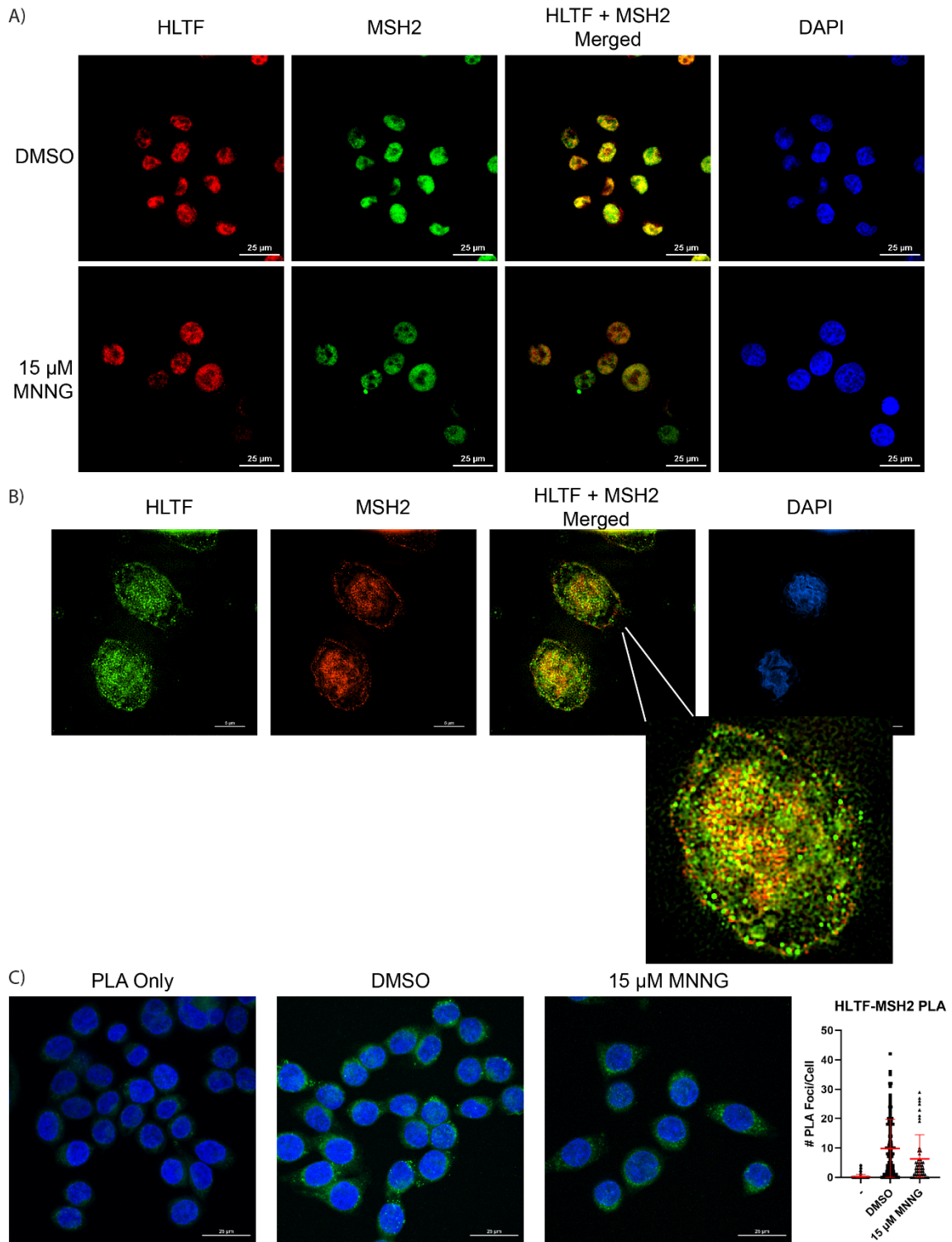
Figure 3.1 HLTF interacts with MSH2 within the cellular environment.
A. Confocal microscopy of HeLa S3 cells treated with DMSO or 15 μM MNNG for 24 hours before fixation and staining. Images show HLTF (Invitrogen DA5-82525; Rabbit) or MSH2 (Invitrogen; Mouse) individually and merged, indicating potential overlap between HLTF and MSH2 cellular localization. Cells were stained with DAPI to show the nucleus,

scale bar, 25 µm. B. Super-resolution microscopy of HeLa S3 cells treated with the same conditions as A before fixation and staining. Images show HLTF (Santa Cruz; mouse) or MSH2 (CST; Rabbit) individually and merged, indicating potential overlap between HLTF and MSH2 cellular localization. Cells were stained with DAPI to show the nucleus; scale bar, 5 µm. C. HeLa cells were treated with the same conditions as A before fixation and immunofluorescent confocal microscopy with *in situ* PLA was performed. Nuclei were stained with DAPI, and green dots in the images indicate physical interaction between HLTF and MSH2 (same antibodies as A).Far-right panel: quantification of the PLA signal showing foci in each quantified cell from one independent experiment; red line showing mean $\pm$ SEM; scale bar, 25 µm (Control, n =56; DMSO, n=110; 15 µM MNNG, n=50)
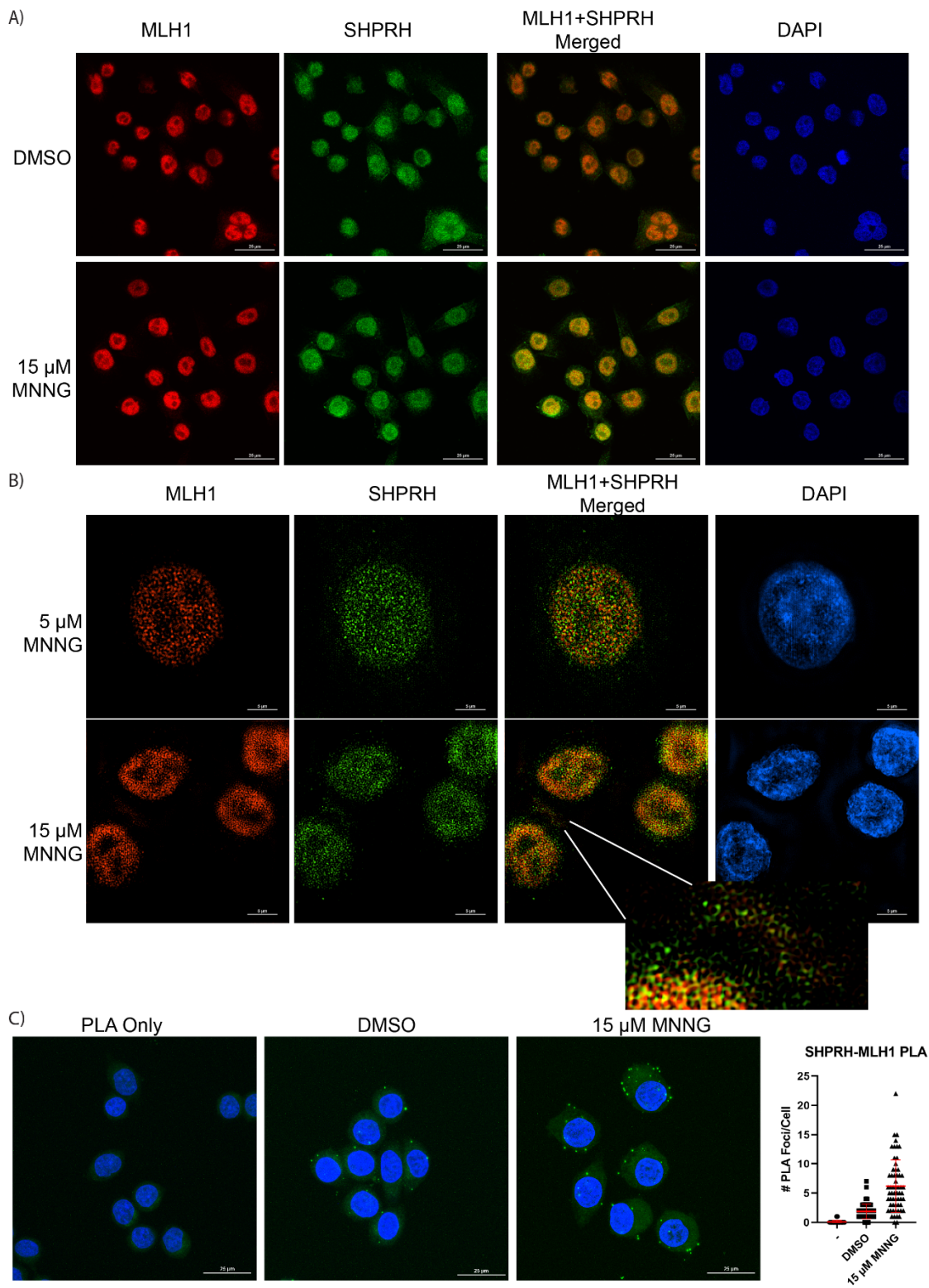
Figure 3.2 SHPRH interacts with MLH1 within the cellular environment.
A. Confocal microscopy of HeLa S3 cells treated with DMSO or 15 µM MNNG for 24
hours before fixation and staining. Images show SHPRH (Mouse) or MLH1 (Rabbit)

individually and merged, indicating potential overlap between SHPRH and MLH1 cellular localization, with increased overlap after damage. Cells were stained with DAPI to show the nucleus, scale bar, 25 µm. B. Super-resolution microscopy of HeLa S3 cells treated with the same conditions as A before fixation and staining. Images show SHPRH and MLH1 individually and merged, indicating potential overlap between SHPRH and MLH1 cellular localization, increasing with damage and overlapping outside the nucleus. Cells were stained with DAPI to show the nucleus; scale bar, 5 µm. C. HeLa cells were treated with the same conditions as A before fixation and immunofluorescent confocal microscopy with *in situ* PLA was performed. Nuclei were stained with DAPI, and green dots in the images indicate physical interaction between SHPRH and MLH1, which increased after damage. Far-right panel: quantification of the PLA signal showing foci in each quantified cell from one independent experiment; red line showing mean $\pm$ SEM; scale bar, 25 µm (Control, n =35; DMSO, n=76; 15 µM MNNG, n=59).
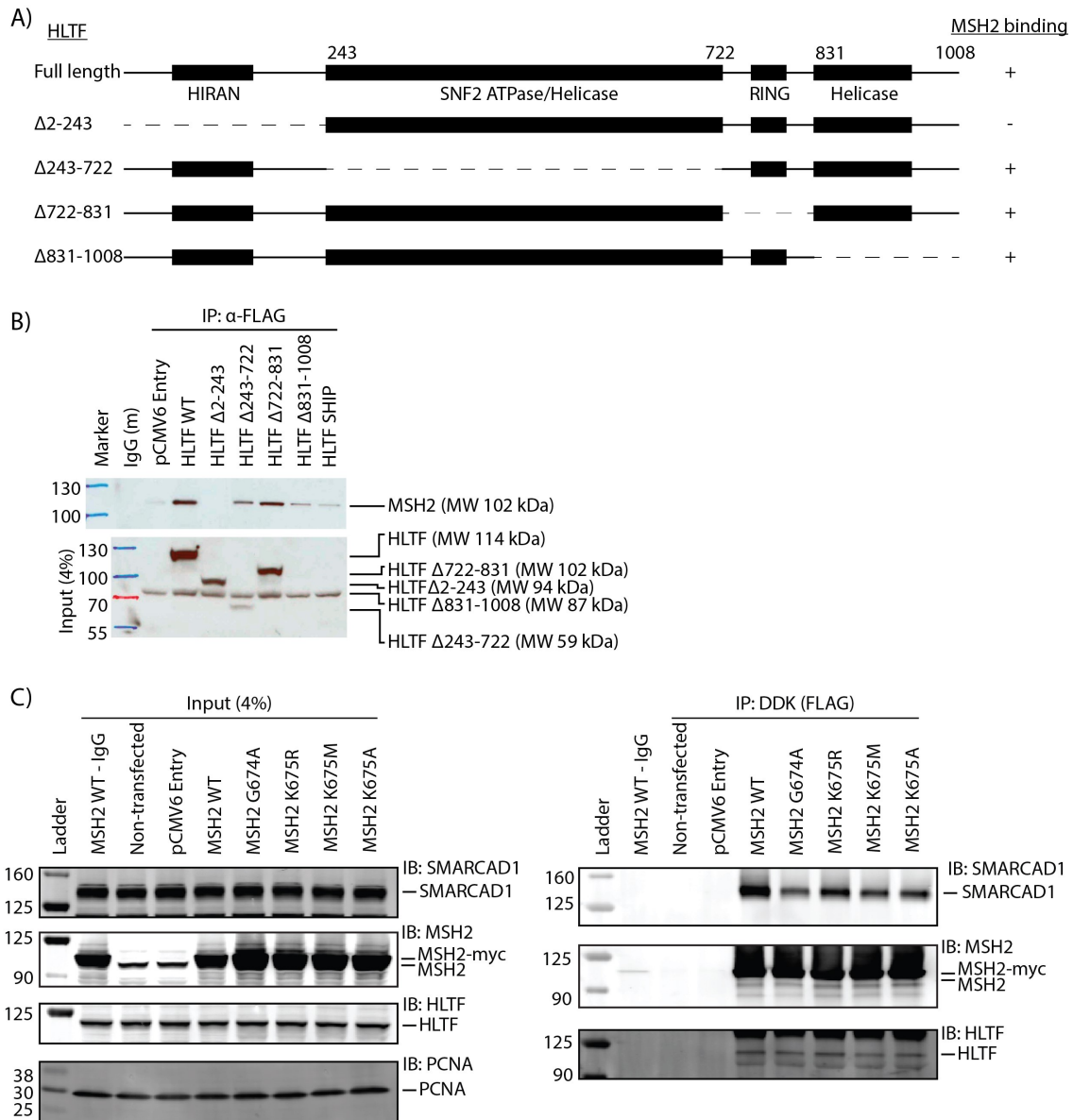
Figure 3.3 N-terminal region of HLTF is important for MSH2 interaction.
A. Summary of immunoprecipitation interactions of MSH2 with HLTF internal deletion plasmids. The HLTF Δ2-243 plasmid results in a complete loss of interaction with MSH2. B. HEK293T cells were transfected with HLTF internal deletion plasmids with MYC/DDK(FLAG) tag. HLTF WT and internal deletion exogenous protein was pulled down using anti-FLAG antibody and only the Δ2-243 plasmid abolishes interaction with MSH2. C. HEK293T cells were transfected with C-terminal MYC-FLAG tagged MSH2 WT or MSH2-ATPase mutant constructs. MSH2 was immunoprecipitated with anti-DDK(FLAG) beads and immunoblotted for SMARCAD1 and HLTF. SMARCAD1 loses interaction with MSH2 ATPase mutants. HLTF interacts with MSH2 WT and ATPase mutants at comparable levels.
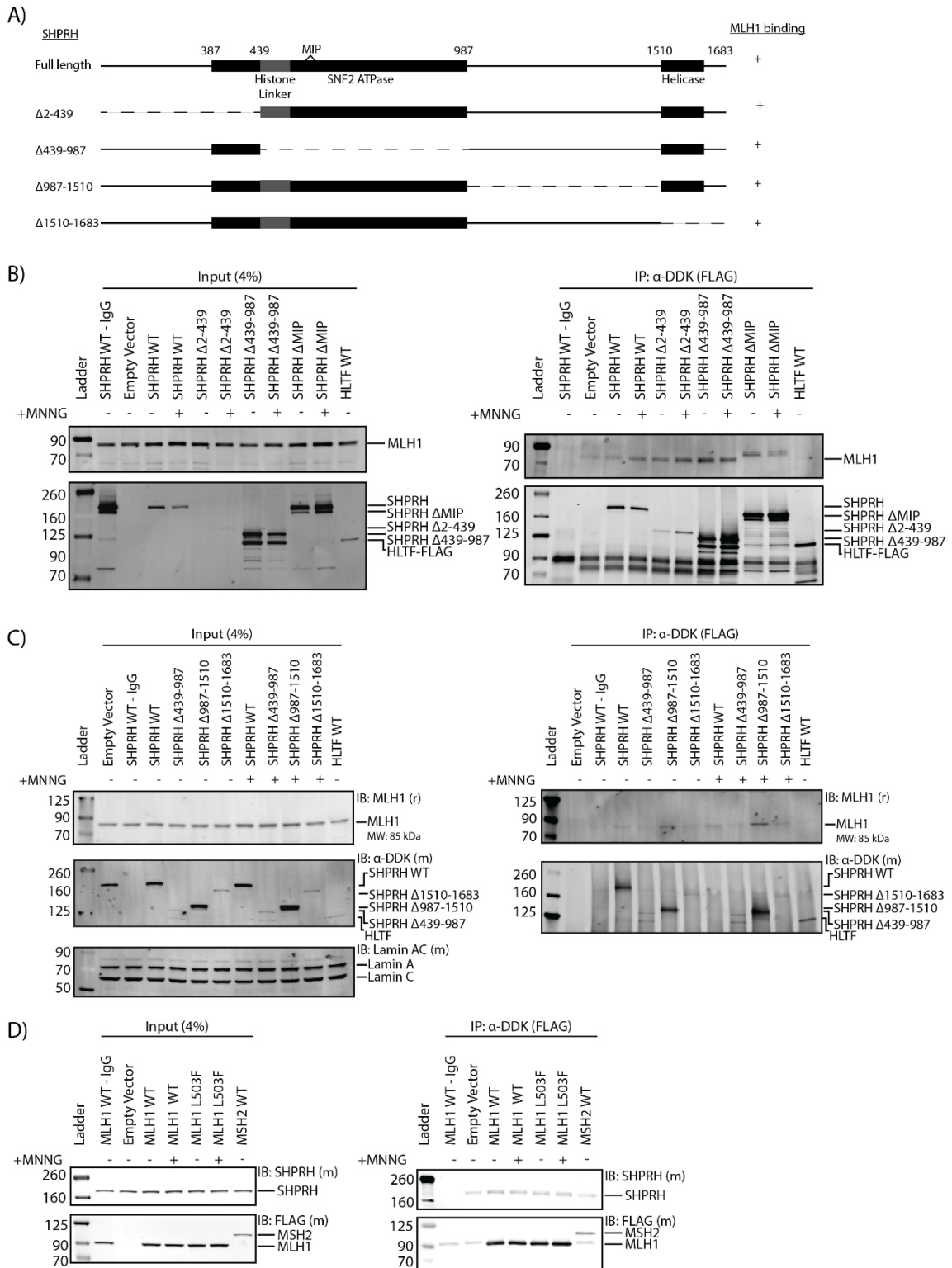
Figure 3.4 SHPRH likely has two sites for interaction with MLH1.
A. Summary of immunoprecipitation interactions of MLH1 with SHPRH internal deletion
plasmids. MLH1 maintains interaction with the SHPRH internal deletions and the MIP
deletion. B. HEK293T cells were transfected with SHPRH N-terminal internal deletion

plasmids with MYC/DDK(FLAG) tag and treated with DMSO or 15 µM MNNG 24 hours after collection. Twenty-four hours after treatment with DMSO or MNNG, SHPRH WT and internal deletion exogenous protein were pulled down using an anti-FLAG antibody and each of the SHPRH internal deletions still interacted with MLH1. C. The same experiment was performed as in part B but with SHPRH C-terminal internal deletions. MLH1 maintains interactions with all the internal deletions of SHPRH. D. HEK293T cells were transfected with C-terminal MYC-FLAG tagged MLH1 WT or MLH1 L503F S2 site mutant constructs. MLH1 was immunoprecipitated with anti-DDK(FLAG) beads and immunoblotted for SHPRH. SHPRH maintains interaction with MLH1 S2 mutant, indicating potential interaction in addition to MIP binding.
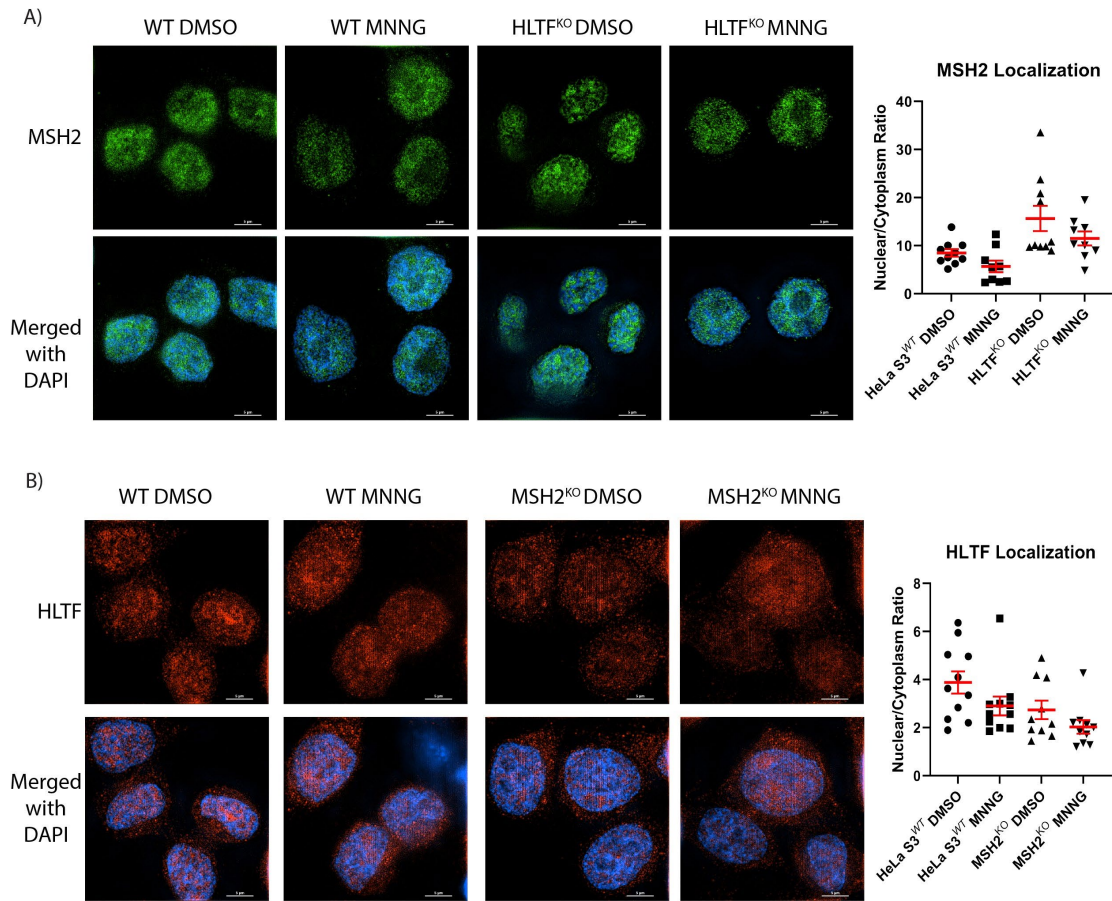
Figure 3.5 Loss of HLTF affects cellular localization of MSH2.

A. Super-resolution microscopy of HeLa S3 wild-type or HLTF knockout cells treated with DMSO or 15 µM MNNG for 24 hours before fixation and staining. Images show MSH2 (Invitrogen; Mouse) individually and merged with DAPI. Cells were stained with DAPI to show the nucleus; scale bar, 5 µm. Far-right panel: quantification of MSH2 expression in nuclear/cytoplasmic ratio from one independent experiment; red line showing mean $\pm$ SEM; scale bar, 25 µm (Wild-type DMSO, n =10; Wild-type MNNG, n=9; HLTF^{KO} DMSO, n=10; HLTF^{KO} MNNG, n=9). B. Super-resolution microscopy of HeLa S3 wild-type or MSH2 knockout cells treated with DMSO or 15 µM MNNG for 24 hours before fixation and staining. Images show HLTF (Invitrogen DA5-82525; Rabbit) individually and merged with DAPI. Cells were stained with DAPI to show the nucleus; scale bar, 5 µm. Far-right panel: quantification of HLTF expression in nuclear/cytoplasmic ratio from one independent experiment; red line showing mean $\pm$ SEM; scale bar, 25 µm (Wild-type DMSO, n =11; Wild-type MNNG, n=11; MSH2^{KO} DMSO, n=10; MSH2^{KO} MNNG, n=10).
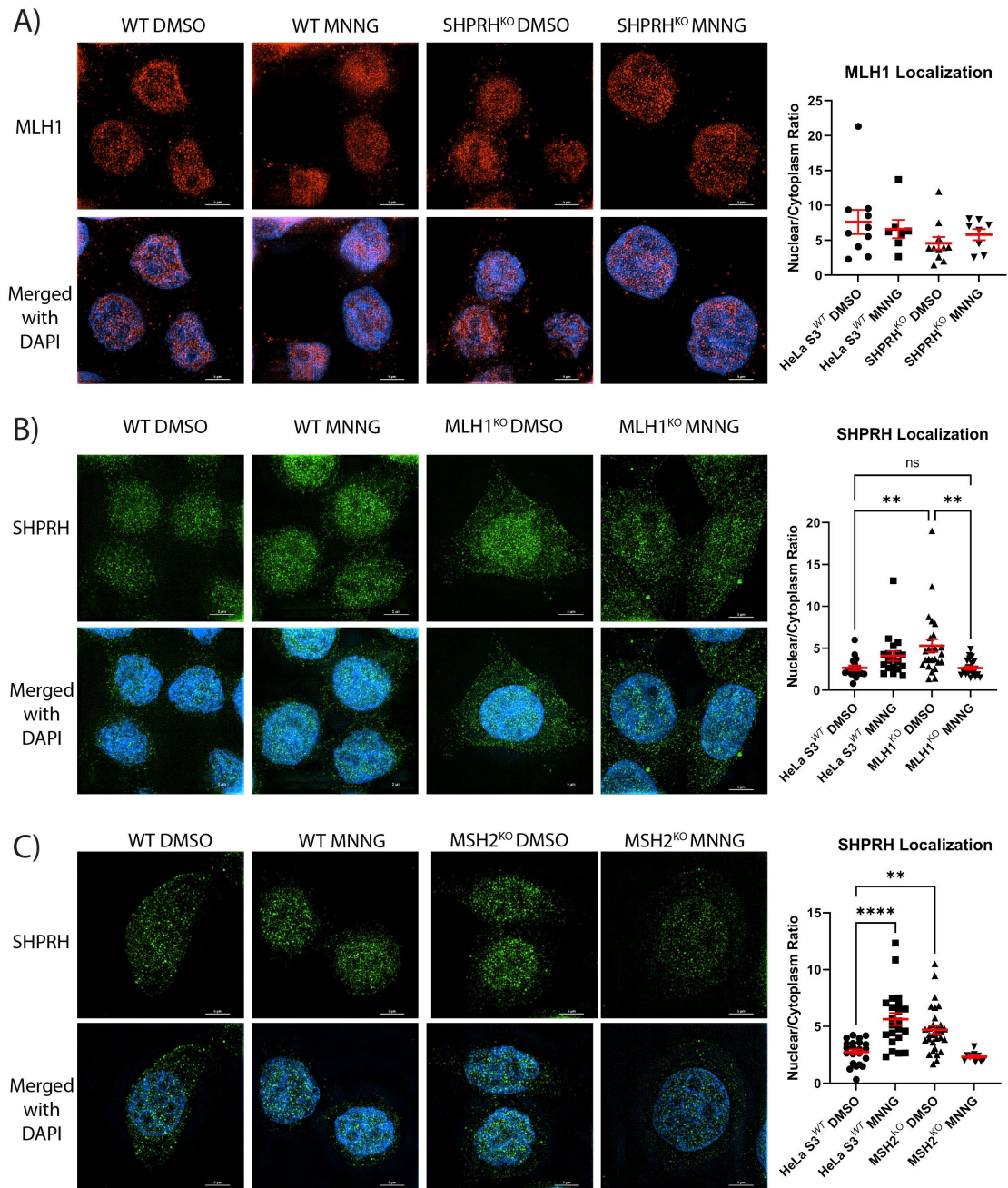
Figure 3.6 Loss of MMR proteins affect SHPRH cellular localization.

A. Super-resolution microscopy of HeLa S3 wild-type or SHPRH knockout cells treated with DMSO or 15 µM MNNG for 24 hours before fixation and staining. Images show MLH1 individually and merged with DAPI. Cells were stained with DAPI to show the nucleus; scale bar, 5 µm. Far-right panel: quantification of MLH1 expression in nuclear/cytoplasmic ratio from one independent experiment; red line showing mean $\pm$ SEM; scale bar, 25 µm (Wild-type DMSO, n=10; Wild-type MNNG, n=7; SHPRH^{KO} DMSO, n=11; SHPRH^{KO} MNNG, n=8). B. Super-resolution microscopy of HeLa S3 wild-type or MLH1 knockout cells treated with DMSO or 15 µM MNNG for 24 hours before fixation and staining. Images show SHPRH individually and merged with DAPI. Cells

95

were stained with DAPI to show the nucleus; scale bar, 5 μm. Far-right panel: quantification of SHPRH expression in nuclear/cytoplasmic ratio from two independent experiments; red line showing mean $\pm$ SEM; scale bar, 25 μm; (Wild-type DMSO, n =16; Wild-type MNNG, n=19; MLH1^{KO} DMSO, n=25; MLH1^{KO} MNNG, n=21); Statistical significance was determined using one-way ANOVA with multiple comparisons; **$p\leq0.01$. C. Super-resolution microscopy of HeLa S3 wild-type or MSH2 knockout cells treated with DMSO or 15 μM MNNG for 24 hours before fixation and staining. Images show SHPRH individually and merged with DAPI. Cells were stained with DAPI to show the nucleus; scale bar, 5 μm. Far-right panel: quantification of SHPRH expression in nuclear/cytoplasmic ratio from two independent experiments (MSH2^{KO} MNNG only imaged in one independent experiment – not included in analysis); red line showing mean $\pm$ SEM; scale bar, 25 μm (Wild-type DMSO, n =22; Wild-type MNNG, n=22; MSH2^{KO} DMSO, n=30; MSH2^{KO} MNNG, n=10). Statistical significance was determined using one-way ANOVA with multiple comparisons; **$p\leq0.01$; ****$p\leq0.0001$.
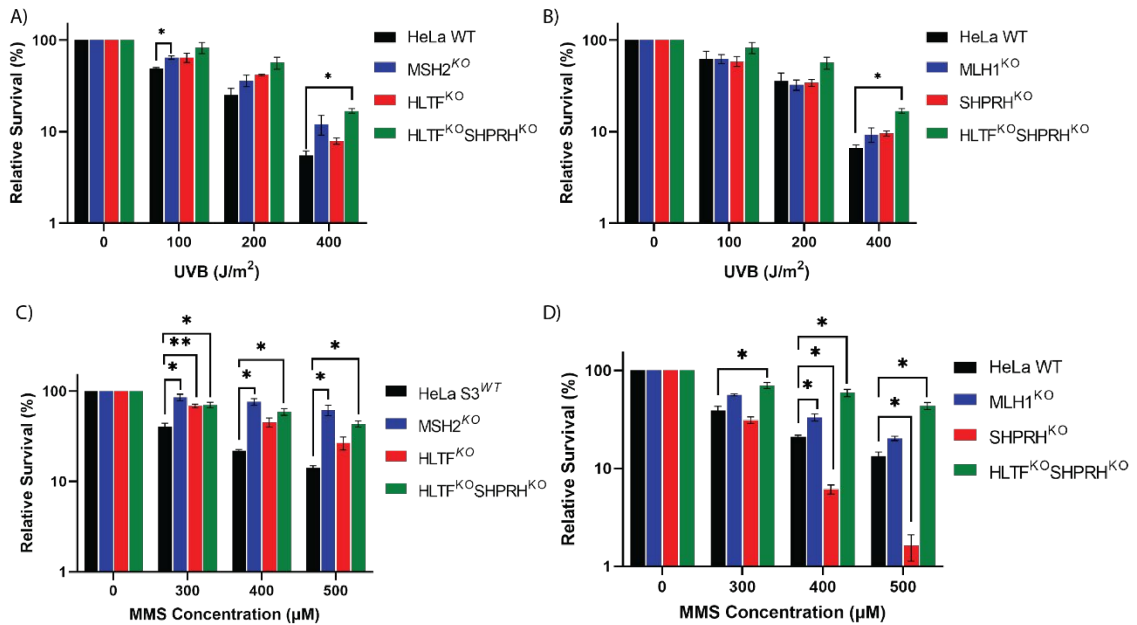
Figure 3.7 MSH2, but not MMR, likely has a role in post-replicative repair.
A. HeLa S3 wild-type, MSH2 or HLTF knockout cells developed in Chapter 2 were seeded into 6-well plates for 24 hours followed by treatment with indicated doses of UVB and allowed to recover for 3 hours before plating into a 96-well plate and assayed for survival after 48 hours by MTS assay. Data is shown as the mean of n=3 $\pm$ SEM. Statistical significance was determined using two-way ANOVA with multiple comparisons; $*p \leq 0.05$.
B. HeLa S3 wild-type, MLH1, SHPRH, or HLTF and SHPRH double knockout cells were treated with the same conditions as A and assayed for survival by MTS assay. Data is shown as the mean of n=3 $\pm$ SEM. Statistical significance was determined using two-way ANOVA with multiple comparisons; $*p \leq 0.05$. C. HeLa S3 wild-type, MSH2 or HLTF knockout cells were seeded into 96-well plates for 24 hours followed by treatment with indicated doses of MMS for 48 and assayed for survival by MTS assay. Data is shown as the mean of n=3 $\pm$ SEM. Statistical significance was determined using two-way ANOVA with multiple comparisons; $*p \leq 0.05$. D. HeLa S3 wild-type, MLH1, SHPRH, or HLTF and SHPRH double knockout cells were treated with the same conditions as C and assayed for survival by MTS assay. Data is shown as the mean of n=3 $\pm$ SEM. Statistical significance was determined using two-way ANOVA with multiple comparisons; $*p \leq 0.05$; $**p \pm 0.01$.

4.1   Conclusions

Mismatch repair (MMR) is one of the primary DNA repair mechanisms and defects in this pathway have been associated with cancer development and progression. The results presented in this dissertation demonstrate that MMR interacting proteins continue to be identified and have a role as MMR accessory factors. Accessory factors identified in yeast often have a conserved role in MMR with their human homologs, as seen in previous studies with *S. cerevisiae*'s Fun30 and its human homolog SMARCAD1 having a conserved MMR role; additionally, in this dissertation with *S. cerevisiae*'s Rad5 having conserved interactions in its human homologs, HLTF and SHPRH. Furthermore, the conservation of Rad5's interaction demonstrated a role in MMR-mediated apoptosis, with SHPRH interacting with MLH1 in an MMR-specific, damage-dependent manner and having a role in MMR-mediated apoptosis. Rad5's conserved interaction between HLTF and MSH2 exemplifies the interplay between MMR and other repair pathways, with the loss of HLTF disrupting MSH2's localization and the loss of MSH2 having increased resistance to post-replicative repair (PRR) damaging agents. Overall, the results of this study highlight the identification of new MMR accessory factors and the importance of these interactions in MMR and other DNA repair pathways.

4.1.1   *Rad5 is a Yeast MMR Interacting Protein*

Many of the initial MMR accessory factors were identified in *Saccharomyces cerevisiae* since the MMR mechanism was primarily established in *E. coli* and *S. cerevisiae* model systems. The Mlh1-interacting peptide (MIP) and Msh2-interacting peptide (SHIP) motifs were discovered in yeast [24,26,34]. MIP and SHIP motifs

have already been employed in detecting new MMR accessory factors in both yeast and humans, with proteins containing an MIP or SHIP motif found to affect the MMR response [24–26,28,29,34,41].

Our study detected an MMR interacting protein that had not been previously identified or studied relating to MMR – *S. cerevisiae*'s Rad5. Rad5 is a helicase and E3 ubiquitin ligase involved in post-replicative repair (PRR), which allows the bypass of DNA lesions in an error-free or error-prone manner to avoid replication fork stalling and collapse [102,103]. Rad5 has been known as a player in the error-free template switching (TS) branch of PRR but is now being implicated as a potential player in the error-prone translesion synthesis (TLS) branch of PRR [102,103]. In a computational screen for yeast proteins containing putative MIP and SHIP boxes, Rad5 was found to potentially have both motifs. A follow-up of the screen confirmed that Rad5 did interact with both yeast Mlh1 and Msh2, with Mlh1 interaction occurring via the MIP box.

Since many proteins identified by the MIP and SHIP boxes have a role in MMR, we studied whether a *rad5Δ* strain had characteristics like the defective MMR phenotype. Utilizing a frameshift reversion assay to understand the MMR efficiency and mutation phenotype, we found that although *rad5Δ* slightly increased mutation frequency, the mutation spectrum was not representative of an MMR defect. This increased mutation frequency is likely due to its role in the PRR pathway. Therefore, although Rad5 interacts with Mlh1 and Msh2, it was not found to have a role in canonical MMR.

4.1.2 *Yeast Rad5-MMR Interactions Conserved in Human HLTF and SHPRH*

Rad5 has two known human homologs identified based on the conservation of domains and functions – Helicase Like Transcription Factor (HLTF) and SNF2 Histone

Linker PHD Ring Helicase (SHPRH). HLTF had previously been found to be methylated in colorectal cancers, a cancer with high rates of MMR defects, and SHPRH methylation was recently found to be positively correlated with the presence of MSI [113,175]; however, neither of the proteins had been studied for a role in MMR. We discovered that Rad5's interaction with Mlh1 and Msh2 was split between its human homologs, with SHPRH interacting with MLH1 in a damage-dependent manner and HLTF interacting with MSH2 constitutively. The interaction was seen via co-immunoprecipitation and in the cellular environment. The split between the two human homologs showed a functional difference between the Rad5's interaction with Mlh1 and Msh2.

4.1.3 *MMR Interactions with HLTF and SHPRH Demonstrate Functional Repair Differences*

We were also able to better understand the interactions between SHPRH, HLTF, and their interacting partner, MLH1 and MSH2, respectively. We showed that interaction between SHPRH and MLH1 occurred in a damage-dependent manner. We also found that the interaction between SHPRH and MLH1 is the strongest in the S phase of the cell cycle. This strengthens the hypothesis that SHPRH plays a role in MMR since MMR is coupled to replication and MMR activity is found to be highest during S phase [64–67]. We also found that SHPRH nuclear localization increases in the presence of MNNG, an MMR-initiating alkylating agent, which further confirms that SHPRH plays a role in MMR's response to exogenous damage. Additionally, we discovered that the loss of critical MMR proteins MLH1 and MSH2 alters the subcellular localization of SHPRH, potentially increasing recruitment to the nucleus to respond to DNA damage. When MMR defective cells are treated with MNNG, SHPRH nuclear localization decreases, which could indicate the recruitment of other DNA repair pathways to the site of damage.

We found that interaction between MSH2 and HLTF occurs in a different manner than MSH2 accessory factors that play a role in MMR. MSH2 mutations that disrupt SHIP-box interactors or cause a loss of MMR efficiency decrease MSH2 interaction with the known accessory factor SMARCAD1 but do not affect HLTF's interaction [157–160]. The interaction also potentially occurs within the HIRAN domain of HLTF, which is vital for fork reversal and remodeling in PRR [144–147]. We also found that loss of MSH2, but not MLH1, increased resistance to multiple PRR damaging agents. Similar resistance was seen when a double knockout of HLTF and SHPRH was treated with PRR-damaging agents. The resistance seen by the HLTF-SHPRH double knockout could point to increased recruitment of another DNA repair pathway to respond to the damage. The fact that MSH2 had a similar resistance to the PRR agents could indicate that there may be a sub-pathway of PRR that is MSH2-dependent.

4.1.4   *Final Conclusions*

Previous MMR interacting proteins and accessory factors have been found to be important for MMR. Some of these interactions have also affected the interacting protein's original repair pathway. Identification and understanding of novel interacting proteins and accessory factors of MMR can help to better understand the DNA repair mechanisms and potentially their role in disease development and progression. We identified a new MMR interacting protein, Rad5, which has a primary role in PRR, and the novel interactions are conserved in its human homologs, HLTF and SHPRH, with a split in the interaction pointing to a functional difference between the interactions. Neither Rad5 nor its human homologs were found to have a role in canonical MMR; however, SHPRH was found to have a functional implication in the MMR apoptotic response. The

HLTF-MSH2 interaction occurs independent of MSH2 regions important for MMR and occurs by the N-terminal region of HLTF containing the HIRAN domain, which is important for PRR, and MSH2 likely has a role in PRR. The interactions identified in this study have given further insight into a distinction between the MMR canonical and non-canonical response and show the interplay between multiple DNA repair mechanisms.

4.2   Future Directions

The findings from this study have identified new interactions between two pathways, MMR and PRR, whose interplay has yet to be studied in depth. While the results have given us more insight into the interactions between these pathways, the findings in this dissertation warrant future investigations, including the following:

4.2.1   *How do SHPRH and MLH1 Interact?*

Our study identified when SHPRH and MLH1 interact within the cell; however, we could not determine where the interaction occurred on each protein. SHPRH interaction with MLH1 likely depends on at least one MIP site on SHPRH; this hypothesis is because Rad5 interacts with Mlh1 via its MIP box. Since the loss of one MIP box site did not abolish interaction with MLH1, there are likely two sites for interaction with MLH1, and the presence of one site accounts for the loss of another. Other accessory factors have also been found to have two sites for interaction, with the presence of an MIP and MIM box [25]. There are additional putative MIP boxes and numerous putative MIM sites throughout the protein, so identifying different sites that may contribute to SHPRH's interaction would be a likely next step.

Additionally, identifying the domain of MLH1 that is important for the SHPRH-MLH1 interaction would give further insight into the role of SHPRH in MMR

and the distinction between canonical and non-canonical MMR. The S2 site on MLH1 did not abolish binding with SHPRH, which indicates a potential SHPRH region alternative/in addition to the MIP box. Other domains important in MLH1's role in MMR, such as the ATPase or endonuclease region, have not been studied yet and could lead to understanding how the interaction between SHPRH and MLH1 plays a role in MMR-mediated apoptosis.

4.2.2 *What SHPRH Domains are Important for MMR-Mediated Apoptosis?*

SHPRH is part of the SWI/SNF family of ATPases/helicases and is also a ubiquitin ligase known to polyubiquitinate PCNA for error-free PRR [110,141,178]. Understanding the domain within SHPRH that is important for MMR-mediated apoptosis could also be identified by the SHPRH region important for interaction with MLH1. We established that loss of SHPRH does not influence canonical MMR but has a functional role in the non-canonical MMR-mediated apoptosis. If the domain of SHPRH is important in MMR-mediated apoptosis can be identified, it will define in greater detail the MMR-mediated apoptotic response, whose complete mechanism is still unknown.

4.2.3 *What MSH2 Domain/Region is Important for its Interaction with HLTF?*

We determined that the N-terminal region of HLTF containing the HIRAN domain is essential for interaction with MSH2; however, we were unable to determine the region of MSH2 important for interaction with HLTF. Mutation of the ATPase or SHIP-box mediated domain did not affect interaction with HLTF; however, MSH2 has five domains – mismatch binding, connector, lever, clamp, and ATPase domains [166]. Only mutation of the ATPase domain has been studied for interaction with HLTF, although the MSH2 M453I region is contained within the lever domain of MSH2. Identifying the region

of MSH2 that is important for interaction with HLTF can give insight into how MSH2 is involved in PRR.

4.2.4 *What Role Does MSH2 Play in Post-Replicative Repair?*

MSH2 has been found to have a role in additional DNA repair pathways, with a role in oxidative damage associated with BER and also being involved in HR [4,5,7]. Based on this evidence, the involvement of MSH2 in another repair pathway would not be unheard of. Evidence from this study indicates that MSH2 likely plays a role in PRR, with the loss of MSH2, but not MMR, leading to resistance to PRR damaging agents. The role of MSH2 in PRR could provide further insight into how PRR distinguishes between error-prone TLS and error-free TS. One distinction between these branches is known to be due to the mono- or poly-ubiquitination of PCNA; however, additional details in the selection between these branches still need to be uncovered. If we can determine the domain of MSH2 necessary for interaction with HLTF, it would likely lead to understanding the role of MSH2 in PRR. This is hypothesized because the loss of HLTF changes the subcellular localization of MSH2 regardless of MMR-initiating damage.

4.2.5 *Final Thoughts*

Our study has identified novel accessory factors of MMR that have been conserved between yeast and human model systems, with Rad5's MMR interactions conserved to human HLTF and SHPRH. HLTF and SHPRH have been correlated with cancers commonly associated with defective MMR, although their role in MMR remained unstudied [113–116,175]. We found that the interaction split between HLTF and SHPRH leads to a functional difference in the DNA repair pathways, with SHPRH playing a role in MMR-mediated apoptosis and MSH2 likely having a role in PRR. If we can understand

104

how these proteins interact, we can understand more about the distinction between canonical and non-canonical MMR and the interplay of MMR proteins in additional DNA repair pathways, specifically PRR.

APPENDIX: ACRONYMS

MMR	Mismatch Repair
PRR	Post-Replicative Repair
HLTF	Helicase Like Transcription Factor
SHPRH	SNF2 Histone Linker PHD Ring Helicase
MNNG	N-Methyl-N'-Nitro-N-Nitrosoguanidine
O^6-BG	O6-Benzylguanine
MMS	Methyl Methanesulfonate
BER	Base Excision Repair
NER	Nucleotide Excision Repair
HR	Homologous Recombination
NHEJ	Non-Homologous End Joining
MSI	Microsatellite Instability
HNPCC	Hereditary Non-Polyposis Colorectal Cancer
MIP	Mlh1-Interacting Peptide
MIM	Mlh1-Interacting Motif
SHIP	Msh2-Interacting Peptide
SSA	Single Strand Annealing
ICL	Interstrand Crosslink
TLS	Translesion Synthesis
TS	Template Switching
PCNA	Proliferating Cell Nuclear Antigen

REFERENCES

1.   McCulloch SD, Kunkel TA. The fidelity of DNA synthesis by eukaryotic replicative and translesion synthesis polymerases. *Cell Res*. 2008;18(1):148-161. doi:10.1038/cr.2008.4

2.   Chaterjee N, Walker GC. Mehcanisms of DNA Damage, Repair and Mutagenesis. *Environ Mol Mutagen*. 2017;58(April):235-263. doi:10.1002/em

3.   Dexheimer T. DNA Repair Pathways and Mechanisms. In: *DNA Repair of Cancer Stem Cells*. ; 2014:19-32. doi:10.1007/978-94-007-4590-2

4.   Slupphaug G, Kavli B, Krokan HE. The interacting pathways for prevention and repair of oxidative DNA damage. *Mutat Res - Fundam Mol Mech Mutagen*. 2003;531(1-2):231-251. doi:10.1016/j.mrfmmm.2003.06.002

5.   Gu Y, Parker A, Wilson TM, Bai H, Chang DY, Lu AL. Human MutY homolog, a DNA glycosylase involved in base excision repair, physically and functionally interacts with mismatch repair proteins human MutS homolog 2/human MutS homolog 6. *J Biol Chem*. 2002;277(13):11135-11142. doi:10.1074/jbc.M108618200

6.   Kumar N, Moreno NC, Feltes BC, Menck CFM, Van Houten B. Cooperation and interplay between base and nucleotide excision repair pathways: From DNA lesions to proteins. *Genet Mol Biol*. 2020;43(1):1-14. doi:10.1590/1678-4685-GMB-2019-0104

7.   Oh J, Myung K. Crosstalk between different DNA repair pathways for DNA double strand break repairs. *Mutat Res - Genet Toxicol Environ Mutagen*. 2022;873:503438.

8.   Li GM. Mechanisms and functions of DNA mismatch repair. *Cell Res*. 2008;18(1):85-98. doi:10.1038/cr.2007.115

9.   Fishel R. Mismatch repair. *J Biol Chem*. 2015;290(44):26395-26403. doi:10.1074/jbc.R115.660142

10.   Kolodner RD, Marsischky GT. Eukaryotic DNA mismatch repair. *Curr Opin Genet Dev*. 1999;9(1):89-96.

11.   Goellner EM, Putnam CD, Kolodner RD. Exonuclease 1-dependent and independent mismatch repair. *DNA Repair (Amst)*. 2015;32:24-32. doi:10.1016/j.dnarep.2015.04.010

12.   Fu D, Calvo JA, Samson LD. Balancing repair and tolerance of DNA damage caused by alkylating agents. *Nat Rev Cancer*. 2012;12(2):104-120. doi:10.1038/nrc3185

13.   Li Z, Pearlman AH, Hsieh P. DNA mismatch repair and the DNA damage response. *DNA Repair (Amst)*. 2016;38:94-101. doi:10.1016/j.dnarep.2015.11.019

14.   Peña-Diaz J, Bregenhorn S, Ghodgaonkar M, et al. Noncanonical Mismatch Repair

as a Source of Genomic Instability in Human Cells. *Mol Cell*. 2012;47(5):669-680. doi:10.1016/j.molcel.2012.07.006

15. Peltomäki P. Role of DNA mismatch repair defects in the pathogenesis of human cancer. *J Clin Oncol*. 2003;21(6):1174-1179. doi:10.1200/JCO.2003.04.060

16. Loeb LA. Microsatellite Instability: Marker of a Mutator Phenotype in Cancer. *Cancer Res*. 1986;54(19):5059-5063.

17. Grady WM, Carethers JM. Genomic and Epigenetic Instability in Colorectal Cancer Pathogenesis. *Gastroenterology*. 2008;135(4):1079-1099. doi:10.1053/j.gastro.2008.07.076

18. Sinicrope FA, Sargent DJ. Clinical implications of microsatellite instability in sporadic colon cancers. *Curr Opin Oncol*. 2009;21(4):369-373. doi:10.1097/CCO.0b013e32832c94bd

19. Chang L, Chang M, Chang HM, Chang F. Microsatellite Instability: A Predictive Biomarker for Cancer Immunotherapy. *Appl Immunohistochem Mol Morphol*. 2018;26(2):e15-e21. doi:10.1097/PAI.0000000000000575

20. Lynch HT, de la Chapelle A. Hereditary colorectal cancer. *Mol Basis Hum Cancer*. 2003;348(10):919-932. doi:10.1007/978-1-59745-458-2_25

21. Fishel R, Lescoe MK, Copeland NG, et al. The Human Mutator Gene Homolog MSH2 and Its Association with Hereditary Nonpolyposis Colon Cancer. 1993;75:1027-1038.

22. Peltomäki P, De La Chapelle A. Mutations predisposing to hereditary nonpolyposis colorectal cancer. *Adv Cancer Res*. 1997;71:93-119. doi:10.1016/s0065-230x(08)60097-4

23. Kolodner RD. Mismatch repair : mechanisms and relationship to cancer susceptibility. *Trends Biochem Sci*. 1995;20(10):397-401.

24. Dherin C, Gueneau E, Francin M, et al. Characterization of a Highly Conserved Binding Site of Mlh1 Required for Exonuclease I-Dependent Mismatch Repair. *Mol Cell Biol*. 2009;29(3):907-918. doi:10.1128/mcb.00945-08

25. Porro A, Mohiuddin M, Zurfluh C, et al. FAN1-MLH1 interaction affects repair of DNA interstrand cross-links and slipped-CAG/CTG repeats. *Sci Adv*. 2021;7(31):1-13. doi:10.1126/sciadv.abf7906

26. Goellner EM, Putnam CD, Graham WJ, Rahal CM, Li BZ, Kolodner RD. Identification of Exo1-Msh2 interaction motifs in DNA mismatch repair and new Msh2-binding partners. *Nat Struct Mol Biol*. 2018;25(8):650-659. doi:10.1038/s41594-018-0092-y

27. Calil FA, Li BZ, Torres KA, et al. Rad27 and Exo1 function in different excision pathways for mismatch repair in Saccharomyces cerevisiae. *Nat Commun*. 2021;12(1):1-10. doi:10.1038/s41467-021-25866-z

28. Goold R, Hamilton J, Menneteau T, et al. FAN1 controls mismatch repair complex assembly via MLH1 retention to stabilize CAG repeat expansion in Huntington's disease. *Cell Rep*. 2021;36(9). doi:10.1016/j.celrep.2021.109649

29. Oh J-M, Kang Y, Park J, et al. MSH2-MSH3 promotes DNA end resection during homologous recombination and blocks polymerase theta-mediated end-joining through interaction with SMARCAD1 and EXO1. *Nucleic Acids Res*. 2023;51(11):5584-5602. doi:10.1093/nar/gkad308

30. Wang TF, Kleckner N, Hunter N. Functional specificity of MutL homologs in yeast: Evidence for three Mlh1-based heterocomplexes with distinct roles during meiosis in recombination and mismatch correction. *Proc Natl Acad Sci U S A*. 1999;96(24):13914-13919. doi:10.1073/pnas.96.24.13914

31. Campbell CS, Hombauer H, Srivatsan A, et al. Mlh2 Is an Accessory Factor for DNA Mismatch Repair in Saccharomyces cerevisiae. *PLoS Genet*. 2014;10(5):e1004327. doi:10.1371/journal.pgen.1004327

32. Gellon L, Werner M, Boiteux S. Ntg2p , a Saccharomyces cerevisiae DNA N - Glycosylase / Apurinic or Apyrimidinic Lyase Involved in Base Excision Repair of Oxidative DNA Damage , Interacts with the DNA Mismatch Repair Protein Mlh1p. *J Biol Chem*. 2002;277(33):29963-29972. doi:10.1074/jbc.M202963200

33. Tran PT, Fey JP, Erdeniz N, Gellon L, Boiteux S, Liskay RM. A mutation in EXO1 defines separable roles in DNA mismatch repair and post-replication repair. *DNA Repair (Amst)*. 2007;6(11):1572-1583. doi:10.1016/j.dnarep.2007.05.004

34. Gueneau E, Dherin C, Legrand P, et al. Structure of the MutL α C-terminal domain reveals how Mlh1 contributes to Pms1 endonuclease site. *Nat Struct Mol Biol*. 2013;20(4):461-468. doi:10.1038/nsmb.2511

35. Sugawara N, Goldfarb T, Studamire B, Alani E, Haber JE. Heteroduplex rejection during single-strand annealing requires Sgs1 helicase and mismatch repair proteins Msh2 and Msh6 but not Pms1. *Proc Natl Acad Sci*. 2004;101(25):9315-9320. doi:10.1073/pnas.0305749101

36. Goldfarb T, Alani E. Distinct Roles for the Saccharomyces cerevisiae Mismatch Repair Proteins in Heteroduplex Rejection, Mismatch Repair and Nonhomologous Tail Removal. *Genetics*. 2005;169(2):563-574. doi:10.1534/genetics.104.035204

37. Gavin AC, Bösche M, Krause R, et al. Functional organization of the yeast proteome by systematic analysis of protein complexes. *Nature*. 2002;415(6868):141-147. doi:10.1038/415141a

38. Chakraborty U, George CM, Lyndaker AM, Alani E. A delicate balance between repair and replication factors regulates recombination between divergent DNA sequences in Saccharomyces cerevisiae. *Genetics*. 2016;202(2):525-540. doi:10.1534/genetics.115.184093

39. Tishkoff DX, Boerger AL, Bertrand P, et al. Identification and characterization of Saccharomyces cerevisiae EXO1, a gene encoding an exonuclease that interacts

with MSH2. *Proc Natl Acad Sci U S A*. 1997;94(14):7487-7492. doi:10.1073/pnas.94.14.7487

40. Terui R, Nagao K, Kawasoe Y, et al. Nucleosomes around a mismatched base pair are excluded via an Msh2-dependent reaction with the aid of SNF2 family ATPase Smarcad1. *Genes Dev*. 2018;32(11-12):806-821. doi:10.1101/gad.310995.117

41. Guervilly J, Blin M, Laureti L, Baudelet E, Audebert S, Gaillard P-H. SLX4 dampens MutSalpha-dependent mismatch repair. *Nucleic Acids Res*. 2022;50(5):2667-2680.

42. Bachrati CZ, Hickson ID. RecQ helicases: Suppressors of tumorigenesis and premature aging. *Biochem J*. 2003;374(3):577-606. doi:10.1042/BJ20030491

43. Doherty KM, Sharma S, Uzdilla LA, et al. RECQ1 helicase interacts with human mismatch repair factors that regulate genetic recombination. *J Biol Chem*. 2005;280(30):28085-28094. doi:10.1074/jbc.M500265200

44. Adra CN, Donato JL, Badovinac R, et al. SMARCAD1, a novel human helicase family-defining member associated with genetic instability: Cloning, expression, and mapping to 4q22-q23, a band rich in breakpoints and deletion mutants involved in several human diseases. *Genomics*. 2000;69(2):162-173. doi:10.1006/geno.2000.6281

45. Okazaki N, Ikeda S, Ohara R, et al. The Novel Protein Complex with SMARCAD1/KIAA1122 Binds to the Vicinity of TSS. *J Mol Biol*. 2008;382(2):257-265. doi:10.1016/j.jmb.2008.07.031

46. Takeishi Y, Fujikane R, Rikitake M, Obayashi Y, Sekiguchi M, Hidaka M. SMARCAD1-mediated recruitment of the DNA mismatch repair protein MutLα to MutSα on damaged chromatin induces apoptosis in human cells. *J Biol Chem*. 2020;295(4):1056-1065. doi:10.1074/jbc.RA119.008854

47. Burdova K, Mihaljevic B, Sturzenegger A, Chappidi N, Janscak P. The Mismatch-Binding Factor MutSβ Can Mediate ATR Activation in Response to DNA Double-Strand Breaks. *Mol Cell*. 2015;59(4):603-614. doi:10.1016/j.molcel.2015.06.026

48. Rong SB, Väliaho J, Vihinen M. Structural basis of Bloom syndrome (BS) causing mutations in the BLM helicase domain. *Mol Med*. 2000;6(3):155-164. doi:10.1007/bf03402111

49. Ellis NA, Groden J, Ye TZ, et al. The Bloom's syndrome gene product is homologous to RecQ helicases. *Cell*. 1995;83(4):655-666. doi:10.1016/0092-8674(95)90105-1

50. Pedrazzi G, Perrera C, Blaser H, et al. Direct association of Bloom's syndrome gene product with the human mismatch repair protein MLH1. *Nucleic Acids Res*. 2001;29(21):4378-4386. doi:10.1093/nar/29.21.4378

51. Langland G, Kordich J, Creaney J, et al. The Bloom's Syndrome Protein (BLM) Interacts with MLH1 but Is Not Required for DNA Mismatch Repair. *J Biol Chem*. 2001;276(32):30031-30035. doi:10.1074/jbc.M009664200

52. Evans E, Alani E. Roles for Mismatch Repair Factors in Regulating Genetic Recombination. *Mol Cell Biol*. 2000;20(21):7839-7844. doi:10.1128/mcb.20.21.7839-7844.2000

53. Karow JK, Constantinou A, Li JL, West SC, Hickson ID. The Bloom's syndrome gene product promotes branch migration of Holliday junctions. *Proc Natl Acad Sci U S A*. 2000;97(12):6504-6508. doi:10.1073/pnas.100448097

54. Pedrazzi G, Bachrati CZ, Selak N, et al. The bloom's syndrome helicase interacts directly with the human DNA mismatch repair protein hMSH6. *Biol Chem*. 2003;384(8):1155-1164. doi:10.1515/BC.2003.128

55. Yang Q, Zhang R, Wang XW, et al. The mismatch DNA repair heterodimer, hMSH2/6, regulates BLM helicase. *Oncogene*. 2004;23(21):3749-3756. doi:10.1038/sj.onc.1207462

56. Cannavo E, Gerrits B, Marra G, Schlapbach R, Jiricny J. Characterization of the interactome of the human MutL homologues MLH1, PMS1, and PMS2. *J Biol Chem*. 2007;282(5):2976-2986. doi:10.1074/jbc.M609989200

57. Rikitake M, Fujikane R, Obayashi Y, Oka K, Ozaki M, Hidaka M. MLH1-mediated recruitment of FAN1 to chromatin for the induction of apoptosis triggered by O6-methylguanine. *Genes to Cells*. 2020;25(3):175-186. doi:10.1111/gtc.12748

58. Guervilly JH, Gaillard PH. SLX4: multitasking to maintain genome stability. *Crit Rev Biochem Mol Biol*. 2018;53(5):475-514. doi:10.1080/10409238.2018.1488803

59. Svendsen JM, Smogorzewska A, Sowa ME, et al. Mammalian BTBD12/SLX4 Assembles A Holliday Junction Resolvase and Is Required for DNA Repair. *Cell*. 2009;138(1):63-77. doi:10.1016/j.cell.2009.06.030

60. González-Prieto R, Cuijpers SA, Luijsterburg MS, van Attikum H, Vertegaal AC. SUMO ylation and PAR ylation cooperate to recruit and stabilize SLX 4 at DNA damage sites . *EMBO Rep*. 2015;16(4):512-519. doi:10.15252/embr.201440017

61. Zhang H, Chen Z, Ye Y, et al. SLX4IP acts with SLX4 and XPF-ERCC1 to promote interstrand crosslink repair. *Nucleic Acids Res*. 2019;47(19):10181-10201. doi:10.1093/NAR/GKZ769

62. Young SJ, Sebald M, Shah Punatar R, et al. MutSβ Stimulates Holliday Junction Resolution by the SMX Complex. *Cell Rep*. 2020;33(3):108289. doi:10.1016/j.celrep.2020.108289

63. Young SJ, West SC. Coordinated roles of SLX4 and MutSβ in DNA repair and the maintenance of genome stability. *Crit Rev Biochem Mol Biol*. 2021;56(2):157-177. doi:10.1080/10409238.2021.1881433

64. Hombauer H, Srivatsan A, Putnam CD, Kolodner RD. Mismatch repair, but not heteroduplex rejection, is temporally coupled to DNA replication. *Science (80-)*. 2011;334(6063):1713-1716. doi:10.1126/science.1210770

65. Schroering AG, Edelbrock MA, Richards TJ, Williams KJ. The cell cycle and DNA

mismatch repair. *Exp Cell Res*. 2007;313(2):292-304. doi:10.1016/j.yexcr.2006.10.018

66. Edelbrock MA, Kaliyaperumal S, Williams KJ. DNA mismatch repair efficiency and fidelity are elevated during DNA synthesis in human cells. *Mutat Res - Fundam Mol Mech Mutagen*. 2009;662(1-2):59-66. doi:10.1016/j.mrfmmm.2008.12.006

67. Haye JE, Gammie AE. The Eukaryotic Mismatch Recognition Complexes Track with the Replisome during DNA Synthesis. *PLoS Genet*. 2015;11(12):1-27. doi:10.1371/journal.pgen.1005719

68. Goellner EM. Chromatin remodeling and mismatch repair: Access and excision. *DNA Repair (Amst)*. 2020;85(September 2019):102733. doi:10.1016/j.dnarep.2019.102733

69. Kadyrova LY, Blanko ER, Kadyrov FA. CAF-I-dependent control of degradation of the discontinuous strands during mismatch repair. *Proc Natl Acad Sci U S A*. 2011;108(7):2753-2758. doi:10.1073/pnas.1015914108

70. Schöpf B, Bregenhorn S, Quivy JP, Kadyrov FA, Almouzni G, Jiricny J. Interplay between mismatch repair and chromatin assembly. *Proc Natl Acad Sci U S A*. 2012;109(6):1895-1900. doi:10.1073/pnas.1106696109

71. Kadyrova LY, Dahal BK, Kadyrov FA. The major replicative histone chaperone CAF-1 suppresses the activity of the DNA mismatch repair system in the cytotoxic response to a DNA-methylating agent. *J Biol Chem*. 2016;291(53):27298-27312. doi:10.1074/jbc.M116.760561

72. Li F, Mao G, Tong D, et al. The histone mark H3K36me3 regulates human DNA mismatch repair through its interaction with MutSα. *Cell*. 2013;153(3):590-600. doi:10.1016/j.cell.2013.03.025

73. Labbé RM, Holowatyj A, Yang ZQ. Histone lysine demethylase (kdm) subfamily 4: Structures, functions and therapeutic potential. *Am J Transl Res*. 2014;6(1):1-15.

74. Awwad SW, Ayoub N. Overexpression of KDM4 lysine demethylases disrupts the integrity of the DNA mismatch repair pathway. Published online 2015:498-504. doi:10.1242/bio.201410991

75. Gibney ER, Nolan CM. Epigenetics and gene expression. *Heredity (Edinb)*. 2010;105(1):4-13. doi:10.1038/hdy.2010.54

76. Lin Y, Wilson JH. Diverse effects of individual mismatch repair components on transcription-induced CAG repeat instability in human cells. *DNA Repair (Amst)*. 2009;8(8):878-885. doi:10.1016/j.dnarep.2009.04.024

77. Guo G, Wang W, Bradley A. Mismatch repair genes identified using genetic screens in Blm-deficient embryonic stem cells. *Nature*. 2004;429(6994):891-895. doi:10.1038/nature02653

78. Wang KY, Shen CKJ. DNA methyltransferase Dnmt1 and mismatch repair. *Oncogene*. 2004;23(47):7898-7902. doi:10.1038/sj.onc.1208111

79. Loughery JEP, Dunne PD, O'Neill KM, Meehan RR, Mcdaid JR, Walsh CP. DNMT1 deficiency triggers mismatch repair defects in human cells through depletion of repair protein levels in a process involving the DNA damage response. *Hum Mol Genet*. 2011;20(16):3241-3255. doi:10.1093/hmg/ddr236

80. Ding N, Bonham EM, Hannon BE, Amick TR, Baylin SB, O'Hagan HM. Mismatch repair proteins recruit DNA methyltransferase 1 to sites of oxidative DNA damage. *J Mol Cell Biol*. 2016;8(3):244-254. doi:10.1093/jmcb/mjv050

81. Kane MF, Loda M, Gaida GM, et al. Methylation of the hMLH1 promoter correlates with lack of expression of hMLH1 in sporadic colon tumors and mismatch repair-defective human tumor cell lines. *Cancer Res*. 1997;57(5):808-811.

82. Hendrich B, Bird A. Identification and Characterization of a Family of Mammalian Methyl-CpG Binding Proteins. *Mol Cell Biol*. 1998;18(11):6538-6547. doi:10.1128/mcb.18.11.6538

83. Bellacosa A, Cicchillitti L, Schepis F, et al. MED1, a novel human methyl-CpG-binding endonuclease, interacts with DNA mismatch repair protein MLH1. *Proc Natl Acad Sci U S A*. 1999;96(7):3969-3974. doi:10.1073/pnas.96.7.3969

84. Sannai M, Doneddu V, Giri V, et al. Modification of the base excision repair enzyme MBD4 by the small ubiquitin-like molecule SUMO1. *DNA Repair (Amst)*. 2019;82(April). doi:10.1016/j.dnarep.2019.102687

85. Laget S, Miotto B, Chin HG, et al. MBD4 cooperates with DNMT1 to mediate methyl-DNA repression and protects mammalian cells from oxidative stress. *Epigenetics*. 2014;9(4):546-556. doi:10.4161/epi.27695

86. Ruzov A, Shorning B, Mortusewicz O, Dunican DS, Leonhardt H, Meehan RR. MBD4 and MLH1 are required for apoptotic induction in xDNMT1-depleted embryos. *Development*. 2009;136(13):2277-2286. doi:10.1242/dev.032227

87. Peng M, Litman R, Xie J, Sharma S, Brosh RM, Cantor SB. The FANCJ/MutLα interaction is required for correction of the cross-link response in FA-J cells. *EMBO J*. 2007;26(13):3238-3249. doi:10.1038/sj.emboj.7601754

88. Park J, Long DT, Lee KY, et al. The MCM8-MCM9 Complex Promotes RAD51 Recruitment at DNA Damage Sites To Facilitate Homologous Recombination. *Mol Cell Biol*. 2013;33(8):1632-1644. doi:10.1128/mcb.01503-12

89. Traver S, Coulombe P, Peiffer I, et al. MCM9 Is Required for Mammalian DNA Mismatch Repair. *Mol Cell*. 2015;59(5):831-839. doi:10.1016/j.molcel.2015.07.010

90. Vashee S, Cvetic C, Lu W, Simancek P, Kelly TJ, Walter JC. Sequence-independent DNA binding and replication initiation by the human origin recognition complex. *Genes Dev*. 2003;17(15):1894-1908. doi:10.1101/gad.1084203

91. Liu S, Balasov M, Wang H, Wu L, Chesnokov IN, Liu Y. Structural analysis of human Orc6 protein reveals a homology with transcription factor TFIIB. *Proc Natl Acad Sci U S A*. 2011;108(18):7373-7378. doi:10.1073/pnas.1013676108

92. Lin Y-C, Liu D, Chakraborty A, et al. Orc6 is a component of the replication fork and enables efficient mismatch repair. *Proc Natl Acad Sci U S A*. 2022;119(2). doi:10.1073/pnas

93. Štros M, Launholt D, Grasser KD. The HMG-box: A versatile protein domain occurring in a wide variety of DNA-binding proteins. *Cell Mol Life Sci*. 2007;64(19-20):2590-2606. doi:10.1007/s00018-007-7162-3

94. Yuan F, Gu L, Guo S, Wang C, Li GM. Evidence for involvement of HMGB1 protein in human DNA mismatch repair. *J Biol Chem*. 2004;279(20):20935-20940. doi:10.1074/jbc.M401931200

95. Chen Z, Tran M, Tang M, Wang W, Gong JCZ. Proteomic analysis reveals a novel mutator S (MutS) partner involved in mismatch repair pathway. *Mol Cell Proteomics*. 2016;15(4):1299-1308. doi:10.1074/mcp.M115.056093

96. Miller AK, Mao G, Knicely BG, et al. Rad5 and Its Human Homologs, HLTF and SHPRH, Are Novel Interactors of Mismatch Repair. *Front Cell Dev Biol*. 2022;10(June):1-17. doi:10.3389/fcell.2022.843121

97. Lynch HT, Snyder CL, Shaw TG, Heinen CD, Hitchins MP. Milestones of Lynch syndrome: 1985-2015. *Nat Rev*. 2015;15(March):181-194.

98. Durno CA, Sherman PM, Aronson M, et al. Phenotypic and genotypic characterisation of biallelic mismatch repair deficiency (BMMR-D) syndrome. *Eur J Cancer*. 2015;51:977-983. doi:10.1016/j.ejca.2015.02.008

99. de la Chapelle A. Genetic Predisposition to Colorectal Cancer. *Nat Rev Cancer*. 2004;4(October):11-13. doi:10.1038/nrc1453

100. Kastrinos F, Stoffel E. History, Genetics, and Strategies for Cancer Prevention in Lynch Syndrome Fay. 2014;12(5):715-727. doi:10.1016/j.cgh.2013.06.031.History

101. Borresen A-L, Lothe R, Melin GI, et al. Somatic mutations in the hMSH2 gene in microsatellite unstable colorectal carcinomas. *Hum Mol Genet*. 1995;4(11):2065-2072.

102. Gallo D, Kim TH, Szakal B, et al. Rad5 Recruits Error-Prone DNA Polymerases for Mutagenic Repair of ssDNA Gaps on Undamaged Templates. *Mol Cell*. 2019;73(5):900-914.e9. doi:10.1016/j.molcel.2019.01.001

103. Xu X, Lin A, Zhou C, et al. Involvement of budding yeast Rad5 in translesion DNA synthesis through physical interaction with Rev1. *Nucleic Acids Res*. 2016;44(11):5231-5245. doi:10.1093/nar/gkw183

104. Gallo D, Brown GW. Post-replication repair: Rad5/HLTF regulation, activity on undamaged templates, and relationship to cancer. *Crit Rev Biochem Mol Biol*. 2019;54(3):301-332. doi:10.1080/10409238.2019.1651817

105. Motegi A, Liaw HJ, Lee KY, et al. Polyubiquitination of proliferating cell nuclear antigen by HLTF and SHPRH prevents genomic instability from stalled replication forks. *Proc Natl Acad Sci U S A*. 2008;105(34):12411-12416.

doi:10.1073/pnas.0805685105

106. Putnam CD, Hayes TK, Kolodner RD. Post-replication repair suppresses duplication-mediated genome instability. *PLoS Genet*. 2010;6(5):33. doi:10.1371/journal.pgen.1000933

107. Unk I, Hajdú I, Blastyák A, Haracska L. Role of yeast Rad5 and its human orthologs, HLTF and SHPRH in DNA damage tolerance. *DNA Repair (Amst)*. 2010;9(3):257-267. doi:10.1016/j.dnarep.2009.12.013

108. Masuda Y, Suzuki M, Kawai H, et al. En bloc transfer of polyubiquitin chains to PCNA in vitro is mediated by two different human E2-E3 pairs. *Nucleic Acids Res*. 2012;40(20):10394-10407. doi:10.1093/nar/gks763

109. Unk I, Hajdú I, Fátyol K, et al. Human HLTF functions as a ubiquitin ligase for proliferating cell nuclear antigen polyubiquitination. *Proc Natl Acad Sci U S A*. 2008;105(10):3768-3773. doi:10.1073/pnas.0800563105

110. Unk I, Hajdú I, Fátyol K, et al. Human SHPRH is a ubiquitin ligase for Mms2-Ubc13-dependent polyubiquitylation of proliferating cell nuclear antigen. *Proc Natl Acad Sci U S A*. 2006;103(48):18107-18112. doi:10.1073/pnas.0608595103

111. Seelinger M, Søgaard CK, Otterlei M. The human RAD5 homologs, HLTF and SHPRH, have separate functions in DNA damage tolerance dependent on the DNA lesion type. *Biomolecules*. 2020;10(3):1-15. doi:10.3390/biom10030463

112. Lin J, Zeman MK, Chen J, Yee M, Cimprich KA. SHPRH and HLTF Act in a Damage-Specific Manner to Coordinate Different Forms of Postreplication Repair and Prevent Mutagenesis. *Mol Cell*. 2011;42:237-249. doi:10.1016/j.molcel.2011.02.026

113. Moinova HR, Chen WD, Shen L, et al. HLTF gene silencing in human colon cancer. *Proc Natl Acad Sci U S A*. 2002;99(7):4562-4567. doi:10.1073/pnas.062459899

114. Sood R, Makalowska I, Galdzicki M, et al. Cloning and characterization of a novel gene, SHPRH, encoding a conserved putative protein with SNF2/helicase and PHD-finger domains from the 6q24 region. *Genomics*. 2003;82(2):153-161. doi:10.1016/S0888-7543(03)00121-6

115. Begum S, Yiu A, Stebbing J, Castellano L. Novel tumour suppressive protein encoded by circular RNA, circ-SHPRH, in glioblastomas. *Oncogene*. 2018;37(30):4055-4057. doi:10.1038/s41388-018-0230-3

116. Zhang M, Huang N, Yang X, et al. A novel protein encoded by the circular form of the SHPRH gene suppresses glioma tumorigenesis. *Oncogene*. 2018;37(13):1805-1814. doi:10.1038/s41388-017-0019-9

117. Yan D, Jin Y. Regulation of DLK-1 Kinase Activity by Calcium-Mediated Dissociation from an Inhibitory Isoform. *Neuron*. 2012;76(3):534-548. doi:10.1016/j.neuron.2012.08.043

118. Dosztányi Z, Csizmok V, Tompa P, Simon I. IUPred: Web server for the prediction

of intrinsically unstructured regions of proteins based on estimated energy content. *Bioinformatics*. 2005;21(16):3433-3434. doi:10.1093/bioinformatics/bti541

119. Katoh K, Standley D. MAFFT: iterative refinement and additional methods. In: *Methods in Molecular Biology*. ; 2010:131-146. doi:10.1017/cbo9780511617829.007

120. Retief JD. Phylogenetic Analysis Using PHYLIP. In: *Methods in Molecular Biology (Clifton, N.J.)*. Vol 132. ; 2000:243-258. doi:10.1385/1-59259-192-2:313

121. Thomsen MCF, Nielsen M. Seq2Logo: A method for construction and visualization of amino acid binding motifs and sequence profiles including sequence weighting, pseudo counts and two-sided representation of amino acid enrichment and depletion. *Nucleic Acids Res*. 2012;40(W1):281-287. doi:10.1093/nar/gks469

122. Schroering AG, Williams KJ. Rapid induction of chromatin-associated DNA mismatch repair proteins after MNNG treatment. *DNA Repair (Amst)*. 2008;7(6):951-969. doi:10.1016/j.dnarep.2008.03.023

123. Stormo GD, Schneider TD, Gold L, Ehrenfeucht A. Use of the "Perceptron" algorith to distinguish translational initiation site in E. voli. *Nucleic Acids Res*. 1982;10(9):2997-3011.

124. Flores-Rozas H, Kolodner RD. The Saccharomyces cerevisiae MLH3 gene functions in MSH3-dependent suppression of frameshift mutations. *Proc Natl Acad Sci U S A*. 1998;95(21):12404-12409. doi:10.1073/pnas.95.21.12404

125. Tishkoff DX, Filosi N, Gaida GM, Kolodner RD, Dana CA. *A Novel Mutation Avoidance Mechanism Dependent on S. Cerevisiae RAD27 Is Distinct from DNA Mismatch Repair*. Vol 88.; 1997.

126. Johnson RE, Henderson ST, Petes TD, Prakash S, Bankmann M, Prakash L. Saccharomyces cerevisiae RAD5-encoded DNA repair protein contains DNA helicase and zinc-binding sequence motifs and affects the stability of simple repetitive sequences in the genome. *Mol Cell Biol*. 1992;12(9):3807-3818. doi:10.1128/mcb.12.9.3807

127. Meikrantz W, Bergom MA, Memisoglu A, Samson L. SHORT COMMUNICATION O 6 -Alkylguanine DNA lesions trigger apoptosis. *Carcinogenesis*. 1998;19(2):369-372.

128. Huang ME, Riot AG, Nicolas A, Kolodner RD. A genomewide screen in Saccharomyces cerevisiae for genes that suppress the accumulation of mutations. *Proc Natl Acad Sci U S A*. 2003;100(20):11529-11534. doi:10.1073/pnas.2035018100

129. Schmidt TT, Reyes G, Gries K, et al. Alterations in cellular metabolism triggered by URA7 or GLN3 inactivation cause imbalanced dNTP pools and increased mutagenesis. *Proc Natl Acad Sci U S A*. 2017;114(22):E4442-E4451. doi:10.1073/pnas.1618714114

130. Harfe BD, Jinks-Robertson S. Removal of Frameshift Intermediates by Mismatch

Repair Proteins in Saccharomyces cerevisiae . *Mol Cell Biol*. 1999;19(7):4766-4773. doi:10.1128/mcb.19.7.4766

131. Marsischky GT, Filosi N, Kane MF, Kolodner RD. Redundancy of Saccharomyces cerevisiae. *Genes Dev*. 1996;10:407-420.

132. Cejka P, Mojas N, Gillet L, Schär P, Jiricny J. Homologous recombination rescues mismatch-repair-dependent cytotoxicity of SN1-type methylating agents in S. cerevisiae. *Curr Biol*. 2005;15(15):1395-1400. doi:10.1016/j.cub.2005.07.032

133. Cejka P, Jiricny J. Interplay of DNA repair pathways controls methylation damage toxicity in Saccharomyces cerevisiae. *Genetics*. 2008;179(4):1835-1844. doi:10.1534/genetics.108.089979

134. Elserafy M, Abugable AA, Atteya R, El-Khamisy SF. Rad5, HLTF, and SHPRH: A Fresh View of an Old Story. *Trends Genet*. 2018;34(8):574-577. doi:10.1016/j.tig.2018.04.006

135. Ohno S. Evolution by Gene Duplication. *Population (Paris)*. 1971;26(6):1176.

136. Tham KC, Kanaar R, Lebbink JHG. Mismatch repair and homeologous recombination. *DNA Repair (Amst)*. 2016;38(Muller 1916):75-83. doi:10.1016/j.dnarep.2015.11.010

137. Jumper J, Evans R, Pritzel A, et al. Highly accurate protein structure prediction with AlphaFold. *Nature*. 2021;596(7873):583-589. doi:10.1038/s41586-021-03819-2

138. Varadi M, Anyango S, Deshpande M, et al. AlphaFold Protein Structure Database: Massively expanding the structural coverage of protein-sequence space with high-accuracy models. *Nucleic Acids Res*. 2022;50(D1):D439-D444. doi:10.1093/nar/gkab1061

139. Broomfield S, Hryciw T, Xiao W. DNA postreplication repair and mutagenesis in Saccharomyces cerevisiae. *Mutat Res - DNA Repair*. 2001;486(3):167-184. doi:10.1016/S0921-8777(01)00091-X

140. Gangavarapu V, Haracska L, Unk I, Johnson RE, Prakash S, Prakash L. Mms2-Ubc13-Dependent and -Independent Roles of Rad5 Ubiquitin Ligase in Postreplication Repair and Translesion DNA Synthesis in Saccharomyces cerevisiae. *Mol Cell Biol*. 2006;26(20):7783-7790. doi:10.1128/mcb.01260-06

141. Motegi A, Sood R, Moinova H, Markowitz SD, Liu PP, Myung K. Human SHPRH suppresses genomic instability through proliferating cell nuclear antigen polyubiquitination. *J Cell Biol*. 2006;175(5):703-708. doi:10.1083/jcb.200606145

142. Pagès V, Bresson A, Acharya N, Prakash S, Fuchs RP, Prakash L. Requirement of Rad5 for DNA polymerase ζ-dependent translesion synthesis in Saccharomyces cerevisiae. *Genetics*. 2008;180(1):73-82. doi:10.1534/genetics.108.091066

143. Ulrich HD, Jentsch S. Two RING finger proteins mediate cooperation between ubiquitin-conjugating enzymes in DNA repair. *EMBO J*. 2000;19(13):3388-3397. doi:10.1093/emboj/19.13.3388

144. Iyer LM, Babu MM, Aravind L. The HIRAN domain and recruitment of chromatin remodeling and repair activities to damaged DNA. *Cell Cycle*. 2006;5(7):775-782. doi:10.4161/cc.5.7.2629

145. Chavez DA, Greer BH, Eichman BF. The HIRAN domain of helicase-like transcription factor positions the DNA translocase motor to drive efficient DNA fork regression. *J Biol Chem*. 2018;293(22):8484-8494. doi:10.1074/jbc.RA118.002905

146. Kile AC, Chavez DA, Bacal J, et al. HLTF's Ancient HIRAN Domain Binds 3' DNA Ends to Drive Replication Fork Reversal. *Mol Cell*. 2015;58(6):1090-1100. doi:10.1016/j.molcel.2015.05.013

147. Achar YJ, Balogh D, Neculai D, et al. Human HLTF mediates postreplication repair by its HIRAN domain-dependent replication fork remodelling. *Nucleic Acids Res*. 2015;43(21):10277-10291. doi:10.1093/nar/gkv896

148. Hishiki A, Hara K, Ikegaya Y, et al. Structure of a novel DNA-binding domain of Helicase-like Transcription Factor (HLTF) and its functional implication in DNA damage tolerance. *J Biol Chem*. 2015;290(21):13215-13223. doi:10.1074/jbc.M115.643643

149. Berg IL, Persson JO, Åström SU. MutSα deficiency increases tolerance to DNA damage in yeast lacking postreplication repair. *DNA Repair (Amst)*. 2020;91-92(January). doi:10.1016/j.dnarep.2020.102870

150. Huang D, Piening BD, Paulovich AG. The Preference for Error-Free or Error-Prone Postreplication Repair in Saccharomyces cerevisiae Exposed to Low-Dose Methyl Methanesulfonate Is Cell Cycle Dependent . *Mol Cell Biol*. 2013;33(8):1515-1527. doi:10.1128/mcb.01392-12

151. Quinet A, Martins DJ, Vessoni AT, et al. Translesion synthesis mechanisms depend on the nature of DNA damage in UV-irradiated human cells. *Nucleic Acids Res*. 2016;44(12):5717-5731. doi:10.1093/nar/gkw280

152. Park S, Yang JS, Shin YE, Park J, Jang SK, Kim S. Protein localization as a principal feature of the etiology and comorbidity of genetic diseases. *Mol Syst Biol*. 2011;7(494):1-11. doi:10.1038/msb.2011.29

153. Kelley JB, Paschal BM. Fluorescence-based quantification of nucleocytoplasmic transport. *Methods*. 2019;157(July 2018):106-114. doi:10.1016/j.ymeth.2018.11.002

154. MacDonald L, Baldini G, Storrie B. Does Super Resolution Fluorescence Microscopy Obsolete Previous Microscopic Approaches to Protein Co-localization? In: *Membrane Trafficking: Second Edition*. ; 2015:255-275. doi:10.1007/978-1-4939-2309-0

155. Alam MS. Proximity Ligation Assay (PLA). *Curr Protoc Immunol*. 2018;123(1):e58. doi:10.1002/cpim.58.Proximity

156. Wu X, Platt JL, Cascalho M. Dimerization of MLH1 and PMS2 Limits Nuclear Localization of MutLα. *Mol Cell Biol*. 2003;23(9):3320-3328.

doi:10.1128/mcb.23.9.3320-3328.2003

157.   Lin DP, Wang Y, Scherer SJ, et al. An Msh2 Point Mutation Uncouples DNA Mismatch Repair and Apoptosis. *Cancer Res*. 2004;64(2):517-522. doi:10.1158/0008-5472.CAN-03-2957

158.   Graham WJ, Putnam CD, Kolodner RD. The properties of Msh2–Msh6 ATP binding mutants suggest a signal amplification mechanism in DNA mismatch repair. *J Biol Chem*. 2018;293(47):18055-18070. doi:10.1074/jbc.RA118.005439

159.   Studamire B, Quach T, Alani E. Saccharomyces cerevisiae Msh2p and Msh6p ATPase Activities Are Both Required during Mismatch Repair . *Mol Cell Biol*. 1998;18(12):7590-7601. doi:10.1128/mcb.18.12.7590

160.   Lee S. MOLECULAR MECHANISM OF HUMAN MISMATCH REPAIR INITIATION. Published online 2014.

161.   Gammie AE, Erdeniz N, Beaver J, Devlin B, Nanji A, Rose MD. Functional characterization of pathogenic human MSH2 missense mutations in Saccharomyces cerevisiae. *Genetics*. 2007;177(2):707-721. doi:10.1534/genetics.107.071084

162.   Hayashida G, Shioi S, Hidaka K, et al. Differential genomic destabilisation in human cells with pathogenic MSH2 mutations introduced by genome editing. *Exp Cell Res*. 2019;377(1-2):24-35. doi:10.1016/j.yexcr.2019.02.020

163.   Tomé S, Holt I, Edelmann W, et al. MSH2 ATPase domain mutation affects CTG•CAG repeat instability in transgenic mice. *PLoS Genet*. 2009;5(5). doi:10.1371/journal.pgen.1000482

164.   Martin A, Li Z, Lin DP, et al. Msh2 ATPase Activity Is Essential for Somatic Hypermutation at A-T Basepairs and for Efficient Class Switch Recombination. *J Exp Med*. 2003;198(8):1171-1178. doi:10.1084/jem.20030880

165.   Drost M, Zonneveld JBM, van Hees S, Rasmussen LJ, Hofstra RMW, de Wind N. A rapid and cell-free assay to test the activity of lynch syndrome-associated MSH2 and MSH6 missense variants. *Hum Mutat*. 2012;33(3):488-494. doi:10.1002/humu.22000

166.   Lützen A, de Wind N, Georgijevic D, Nielsen FC, Rasmussen LJ. Functional analysis of HNPCC-related missense mutations in MSH2. *Mutat Res - Fundam Mol Mech Mutagen*. 2008;645(1-2):44-55. doi:10.1016/j.mrfmmm.2008.08.015

167.   Amin NS, Nguyen M-N, Oh S, Kolodner RD. exo1 -Dependent Mutator Mutations: Model System for Studying Functional Interactions in Mismatch Repair . *Mol Cell Biol*. 2001;21(15):5142-5155. doi:10.1128/mcb.21.15.5142-5155.2001

168.   Mastrocola AS, Heinen CD. Lynch syndrome-associated mutations in MSH2 alter DNA repair and checkpoint response functions in vivo. *Hum Mutat*. 2010;31(10):1699-1708. doi:10.1002/humu.21333

169.   Lee D, An J, Park YU, et al. SHPRH regulates rRNA transcription by recognizing the histone code in an mTOR-dependent manner. *Proc Natl Acad Sci U S A*.

2017;114(17):E3424-E3433. doi:10.1073/pnas.1701978114

170. Seelinger M, Otterlei M. Helicase-Like Transcription Factor HLTF and E3 Ubiquitin Ligase SHPRH Confer DNA Damage Tolerance through Direct Interactions with Proliferating Cell Nuclear Antigen (PCNA). *Int J Mol Sci*. 2020;21(693):1-14.

171. Bonneville R, Krook MA, Kautto EA, et al. Landscape of Microsatellite Instability Across 39 Cancer Types. *JCO Precis Oncol*. 2017;(1):1-15. doi:10.1200/po.17.00073

172. Kubecek O, Trojanova P, Molnarova V, Kopecky J. Microsatellite instability as a predictive factor for immunotherapy in malignant melanoma. *Med Hypotheses*. 2016;93(2016):74-76. doi:10.1016/j.mehy.2016.05.023

173. Zhao P, Li L, Jiang X, Li Q. Mismatch repair deficiency/microsatellite instability-high as a predictor for anti-PD-1/PD-L1 immunotherapy efficacy. *J Hematol Oncol*. 2019;12(1):1-14. doi:10.1186/s13045-019-0738-1

174. Le DT, Uram JN, Wang H, et al. PD-1 Blockade in Tumors with Mismatch-Repair Deficiency. *N Engl J Med*. 2015;372(26):2509-2520. doi:10.1056/nejmoa1500596

175. Buckley AR, Ideker T, Carter H, Harismendy O, Schork NJ. Exome-wide analysis of bi-allelic alterations identifies a Lynch phenotype in The Cancer Genome Atlas. *Genome Med*. 2018;10(1):10-12. doi:10.1186/s13073-018-0579-5

176. Liu B, Nicolaides NC, Markowitz S, et al. Mismatch repair gene defects in sporadic colorectal cancers with microsatellite instability. *1Nature Genet*. 95AD;9:48-55. doi:10.1016/s0764-4469(99)00102-x

177. Mosammaparast N, Ewart CS, Pemberton LF. A role for nucleosome assembly protein 1 in the nuclear transport of histones H2A and H2B. *EMBO J*. 2002;21(23):6527-6538. doi:10.1093/emboj/cdf647

178. Brühl J, Trautwein J, Schäfer A, Linne U, Bouazoune K. The DNA repair protein SHPRH is a nucleosome-stimulated ATPase and a nucleosome-E3 ubiquitin ligase. *Epigenetics Chromatin*. Published online 2019:1-16. doi:10.1186/s13072-019-0294-5

VITA

<u>ANNA KRISTIN MILLER</u>

EDUCATION

Bachelor of Science, University of Kentucky   2015 – 2019

Agricultural and Medical Biotechnology, Minor in Biology, Honors Program

Certificate in Undergraduate Research in Human Health Sciences

GPA: 3.776

PROFESSIONAL EXPERIENCE

PhD Intern	May 2023 – August 2023
Graduate Research Assistant	July 2019 – Present
Undergraduate Lab Technician	August 2016 – August 2019
Cancer Training in Oncology Program Participant	August 2016 – June 2018
Research Assistant	June 2017 – January 2018

HONORS AND AWARDS

UK Women in Medicine and Science Rising Star Award	2022
UK Department of Toxicology and Cancer Biology Retreat Poster Award	2022
UK Department of Toxicology and Cancer Biology Early Publication Award	2022
UK Department of Toxicology and Cancer Biology Research Fellowship	2022
Markey Cancer Center Research Day – 3rd Place Poster Presentation	2022
Markey Cancer Center Scientist in Training Travel Award	2022
UK Department of Toxicology and Cancer Biology Excellent Research Fellowship	2021
UK IBS Program Incentive Award	2019-2020
CHS Office of Undergraduate Research Travel Award	2017
CEDIK Appalachian Health Career Scholarship	2017

William and Elizabeth Hamilton Scholarship	2017 – May 2019
Mammoth Cave Area Alumni Scholarship	2015 – 2016, 2017 – May 2019
Farmers RECC Scholarship	2016
Governor's Scholars Program Presidential Scholarship	2015 – May 2019
Kentucky Educational Excellence Scholarship	2015 – May 2019
University of Kentucky Dean's List	December 2015 – May 2019
Metcalfe County Schools Improving Lives Scholarship	2015

PEER-REVIEWED MANUSCRIPTS

1. Miller, A.K., Mao, G., Knicely, B.K., Daniels, H.G., Rahal, C., Putnam, C., Kolodner, R., Goellner, E.M. "Rad5 and its Human Homologs, HLTF and SHPRH, are Novel Interactors of Mismatch Repair." Frontiers in Cell and Developmental Biology – Mechanistic Studies of Genome Integrity, Environmental Health and Cancer Etiology. June 16, 2022.
2. Daniels, H.G, Knicely, B.K., Miller, A.K., Thompson, A., Plattner, R., Goellner, E.M. "Inhibition of ABL1 by Tyrosine Kinase Inhibitors Leads to a Downregulation of MLH1 by Hsp70-mediated Lysosomal Protein Degradation." Frontiers in Genetics – Cancer Genetics and Oncogenomics. October 20, 2022.